Gr th of Erbium-Doped Si/SiGe Double Heterostructures by Ultra-High Vacuum Chemical Vapor Deposition

by

Michael Ty Morse

B.S., The Ohio State University (1991)

Submitted to the Department of Materials Science and Engineering
in partial fulfillment of the requirements for the degree of

Doctor of Philosophy

at the

MASSACHUSETTS INSTITUTE OF TECHNOLOGY

June 1997

© Massachusetts Institute of Technology 1997

Signature of Author ....
Department of Materials Science and Engineering
May 2, 1997

Certified by ....
Lionel C. Kimerling
Thomas Lord Professor of Materials Science and Engineering
Thesis Supervisor

Accepted by ....
Linn Hobbs
John F. Elliot Professor of Materials
Chairman, Department Committee on Graduate Students

MASSACHUSETTS INSTITUTE
OF TECHNOLOGY

JUN 16 1997

LIBRARIES

ARCHIVES

Growth of Erbium-Doped Si/SiGe Double Heterostructures by Ultra-High Vacuum Chemical Vapor Deposition

by

Michael Ty Morse

Submitted to the Department of Materials Science and Engineering
on May 2, 1997, in partial fulfillment of the
requirements for the degree of
Doctor of Philosophy

Abstract

This thesis explores a new low temperature technique for the incorporation of erbium into silicon-based thin films with applications for novel optoelectronic devices. Growth of erbium-doped Si and $Si_{1-x}Ge_x$ films at temperatures between 520° and 610°C occurred in a hot-wall, ultra-high vacuum metallorganic chemical vapor deposition (UHV-MOCVD) reactor especially designed and built for this work.

Three metallorganic erbium precursors, each chosen for the bonding of erbium to ligands known to enhance the luminescence of erbium, were studied to determined which resulted in films with the srongest luminescence and highest crystal quality. Photoluminescence and glancing angle x-ray diffraction studies of erbium-doped silicon films using $Er(tmhd)_3$, $Er(fod)_3$, and $Er(tmsa)_3$ as erbium sources showed conclusively that the $Er(tmsa)_3$ gave films with the strongest erbium luminescence and highest crystal quality. As a result, only this precursor was used in the remaining work.

Non-uniformities in precursor incorporation, caused by precursor fragmentation in the hot-wall environment, were observed from wafer to wafer, and across the surface of the wafer. The ratio of ligand to erbium, which determines the optical activity of the erbium, increased the further downstream in the reactor the wafer was located. The effective optical cross-section increased from $9x10^{-19}/cm^2$ to $4x10^{-16}/cm^2$, as the ligand ratio went from 3 to 400, in going from the most upstream wafer to the wafer located just behind it.

The internal quantum efficiency of these films was found to be twice as high as silicon implanted with erbium at 400 keV. Although the photoluminescence of silicon implanted with erbium to a concentration of $5\times10^{17}/cm^3$ saturated at a pump power below 0.1 W, CVD grown Si:Er with only a slightly higher erbium concentration did not saturate at the maximum pump power of 1.5 W. This indicates that a larger fraction of the erbium concentration is optically active in the CVD samples, which confirms the quantum efficiency measurement.

The first $Si/Si_{1-x}Ge_x$:Er double heterostructures were grown to take advantage of electrical and optical confinement in the $Si_{1-x}Ge_x$ and improve the external quantum efficiency of the erbium. Stronger room temperature luminescence was observed in this films than in erbium-implanted silicon.

Thesis Supervisor: Lionel C. Kimerling

Title: Thomas Lord Professor of Materials Science and Engineering

Contents

Acknowledgments **11**

1 Introduction **12**

1.1 Motivation 12

1.2 Thesis Organization 15

2 Erbium Doping of Si **16**

2.1 Theory 16

2.2 Excitation and De-excitation Mechanisms 19

2.2.1 Auger Excitation and Back Transfer 20

2.2.2 Impact Ionization 21

2.3 Methods of Growth 22

2.3.1 Ion Implantation 23

2.3.2 Solid Phase Epitaxy (SPE) 25

2.3.3 Molecular Beam Epitaxy (MBE) 27

2.3.4 Ion-Beam Epitaxy (IBE) 28

2.3.5 Chemical Vapor Deposition (CVD) 29

3 UHV-CVD Reactor **32**

3.1 Description of System 37

3.2 Safety Features 40

3.3 Summary 43

4 Silicon-Germanium Heterostructures **44**

4.1 Introduction 44

4.2 Band Structure and Electrical Confinement 44

4.3 Growth Morphology 48

4.4 Film Quality 48

4.5 Growth Rates 53

4.6 Summary 55

5 Growth of Erbium-Doped Films **58**

5.1 Erbium in Silicon 58

5.1.1 Precursors 58

5.1.2 Growth Procedure 60

5.1.3 Comparison of precursors 61

5.1.4 Uniformity of Luminescence 68

5.1.5 Glancing Angle X-ray Diffraction 73

5.1.6 Electrical Activity 74

5.2 Erbium in $Si_{1-x}Ge_x$ 77

5.2.1 Luminescence 77

5.2.2 Lattice Position of Er 80

5.2.3 Segregation of Ge 81

5.3 Summary 86

6 Excitation and De-excitation of Erbium in Si and $Si_{1-x}Ge_x$ **88**

6.1 Optically Active Sites 88

6.2 Quantum Efficiencies 94

6.3 Lifetime Measurements 98

6.4 Effective Optical Cross-Section 101

6.5 Temperature Quenching 103

6.6 Summary 106

7 Achievements and Future Work **108**

List of Tables

5.1 Composition of film deposited by Er(tmsa) 59
5.2 Calculated sticking coefficients as a function of position on the wafer 73
6.1 Comparison of the ratio between erbium and possible ligands. Data from a sample grown with the same precursor by ECR-PECVD is also included 91
6.2 Effective Optical Cross-Section of Erbium. The data was taken at 1.5W 102

List of Figures

1-1 Light emission process in erbium-doped silicon. 14

2-1 Splitting of the $4f$ states of erbium in a crystal field. 17

2-2 Effect of co-implanted species on erbium luminescence at 4 K. 20

2-3 Effect of annealing on the luminescence of erbium implanted silicon. All annealing was done for 30 minutes in an argon atmosphere. 24

3-1 Oxide-free silicon stability diagram as a function of the partial pressures of water and oxygen. 34

3-2 Diagram of the gas lines used for the UHV-CVD reactor. 38

3-3 Diagram of the UHV-CVD reactor. 41

3-4 Growth temperature calibration based on the temperature reported by the furnace thermocouples. 42

4-1 Theoretical bandgap and valence band offset for strained $Si_{1-x}Ge_x$ on Si. 45

4-2 Model of the band structure of strained $Si_{1-x}Ge_x$ on Si. 46

4-3 Index difference between strained $Si_{1-x}Ge_x$ and Si. The curve labeled Soref is a model based on a red-shift effect while the de Sande curve is based on an empirical fit to data. 47

4-4 Critical thickness in the $Si_{1-x}Ge_x$ system as a function of the growth temperature. 49

4-5 SEM image of a $Si_{0.7}Ge_{0.3}$ film which relaxed by roughening. 50

4-6 Photoluminescence taken at 4 K of a multiple quantum well structure grown at $560°C$. The sample consisted of 30 periods of $Si_{0.75}Ge_{0.25}$/Si layers. 51

4-7 X-ray diffraction rocking curves of $Si_{1-x}Ge_x$ films. 52

4-8 Germanium concentration as a function of GeH_4 flow at 530°C with 20 sccm SiH_4 used for all growth runs. 54
4-9 Growth rate calibration for $Si_{1-x}Ge_x$ at 530°C. 55
4-10 Growth rate calibration for $Si_{1-x}Ge_x$at 560°C. The line is a linear best fit to the data. 56

5-1 Structure of the three precursors used in this study; (a) $Er(tmhd)_3$, (b) $Er(fod)_3$, (c) $Er(tmsa)_3$. 59
5-2 Photomuniescence at 4 K of Si:Er doped with three different precursors. All growths were done at 560°C. 63
5-3 SIMS of Si:Er grown at 560°C using the precursor $Er(tmhd)_3$. 64
5-4 SIMS of Si:Er grown at 560°C with the precursor $Er(fod)_3$. 65
5-5 Glancing angle x-ray diffraction of Si:Er doped with three different precursors. All growth were at 560°C. A scan from a silicon substrate is included for reference. 67
5-6 Photoluminescence at 4 K of Si:Er from three sample scribed from the center of wafers in the same growth run. 69
5-7 Photoluminescence at 4 K from three different samples from the last substrate in the growth run. The samples were scribed from the center, top and a point mid-way in between. 70
5-8 Dependence of PL intensity at 4 K as a function of the position across the wafer and from wafer to wafer. In (a), the intensities were divided by the erbium dose at that location. This shows that the liminescence efficiency of erbium is increasing closer to the center of the wafer. In (b), the relationship between the bound excition (BE) line and the C-O defect (C-O) line is shown. No C-O line was observed in the second wafer at this power and temperature. 71
5-9 Glancing angle x-ray diffractions scans of Si:Er from samples scribed from substrates in different positions over several runs. 74
5-10 Spreading resistance of Si:Er with an undoped Si capping layer. The erbium concentration was determined to be $3x10^{20}/cm^3$ by RBS. 75
5-11 Spreading resistance of a Si:Er film grow on top of an epi-p^+ layer. An undoped capping layer is also present. The erbium concentration is $7x10^{20}/cm^3$. 76

5-12 PL at 4 K of $Si_{1-x}Ge_x$ grown at $530°C$. The increasity increases with increasing erbium concentration upto $3\times10^{18}/cm^3$, the highest value measured in the second wafer of a growht run. 78
5-13 XTEM of $Si_{0.9}Ge_{0.1}$:Er. The erbium-doped region is the dark area, with a lighter silicon capping layer above it. This was taken under a weak beam (220) condition in an attempt to reveal any defects. None could be seen though. The space bar is 100 nm. 79
5-14 Room temperature photoluminescence of $Si_{1-x}Ge_x$:Er. 80
5-15 RBS channeling and random spectra of $Si_{1-x}Ge_x$:Er grown at $530°C$. The inset is of the erbium peak. 81
5-16 RBS spectra of $Si_{1-x}Ge_x$ growth runs with and without erbium doping. All films were grown at $540°C$ and the same pressure. 83
5-17 Dependence of peak germanium and erbium concentrations on the integrated area of germanium in the low content $Si_{1-x}Ge_x$ film. Integration was carried out over channels, not depth. 85
5-18 Correlation of erbium concentration to the germanium concentration in the segregated $Si_{1-x}Ge_x$ film. 86

6-1 High-resolution photoluminescence measurements at 4 K of Si:Er and $Si_{1-x}Ge_x$:Er samples. Spectra from float zone silicon implanted with Er/O and Er/N are shown for comparison. 89
6-2 SIMS of $Si_{1-x}Ge_x$:Er grown at $540°C$. Besides the species in the precursor, oxygen and fluorine were also monitored since they could be contaminants. . . . 92
6-3 SIMS of $Si_{1-x}Ge_x$:Er. This sample was scribed from the wafer directly located behind the wafer (during growth) for which SIMS was reported above. 93
6-4 Raw power dependence dependence of the Si:Er and $Si_{1-x}Ge_x$:Er samples with the highest 4 K luminescence. 97
6-5 Normalized PL dependence of erbium luminescence at 4 K of implanted and CVD-grown material. 97
6-6 PL decay curves at 4 K of Si implanted with erbium at 400 keV. Fits to the curves are shown. 99

6-7 PL decay curves at 4 K of Si:Er grown by CVD at 560°C. A double exponential equation was used to fit the data (as shown). 99

6-8 PL decay curves at 4 K of $Si_{0.92}Ge_{0.08}$:Er grown by CVD at 560°C. A double exponential equation was used to fit the data. 100

6-9 PL decay lifetimes at 4 K of implanted and CVD grown material; (a) long lifetimes, (b) short lifetimes. 100

6-10 Normalized temperature dependence of erbium luminescence in Si:Er and $Si_{1-x}Ge_x$:Er. The pump power was 1.0 W for all measurements. 104

6-11 Temperature dependence of erbium luminescence plotted against recipirical temperature. 105

Acknowledgments

As this is the last thing that is being written in this thesis, I feel the need to keep it very short. This 'monsterously conceived' project could not have been possible without the help, support, and counseling of my advisor and peers. To all of those who helped me through my seemingly forty years wandering in the wilderness, especially the post-docs, I want to express my deepest gratitude. Even more important than the thesis work, however, is the 'work' that has gone on outside of MIT. The years spent here represent the period of greatest personal changes in my life, and for that I'm even more appreciative (I think). As 95% of the people who have contributed to this change have already left MIT and will never see this, I won't list the names. For the small band of people still around, and you know who you are, thanks and good luck getting out. Last but not least, I want to thank my family for supporting me through this, and every other part of my life.

Chapter 1

Introduction

1.1 Motivation

With each new generation of integrated silicon devices, characteristic dimensions such as gate width and interconnect pitch are decreasing. While this miniaturization is increasing the speed of the devices due to lower transit times, it is also increasing the delays in signal transmission. This is due to increasing capacitance effects felt by the closely spaced aluminum interconnect lines. Indeed, the RC time delay from the interconnects is expected to be the limiting factor in determining the speed of integrated circuits within the next few generations.

The most conventional approach to reduce the interconnect delay is to reduce the resistivity of the interconnects by switching to copper or decrease the dielectric constant of the material between the metal lines. Although research into the use of copper interconnections has been well underway for more than a decade, complex processing issues and lower than expected conductivities make it unlikely to be used in the future. However, materials with lower dielectric constants than SiO_2 (k=3.9-4.5), such as fluorinated SiO_2 ($k \simeq$3.5), will be included into standard device processes no later than the 0.18 μm generation. The fluorine doped oxide is only an incremental improvement, with a longer term solution still required. Polymers are also being considered seriously for a long-term solution to the problem since the reduction in the dielectric constant is very large ($\Delta k > 1$)[1]. The thermal stability of these materials is problematic and could prevent their use however.

A more radical approach to the delay problem is using light instead of electrons to transmit

data. Due to the indirect nature of silicon's bandgap, however, it cannot be an efficient emitter of light. Several solutions to overcome the problem of integrating the electronic and optical devices are currently under heavy research. Some work has already been done in making optoelectronic integrated circuits(OEIC) on GaAs at medium level integration (MLI). While light emitting diodes (LED), lasers and faster electronic devices can easily be made from GaAs, the processing complexity and cost make this solution commercially unsuitable in the foreseeable future. Other research is focussing on combining silicon's electronic devices with optical devices of the III-V's. This can be done through monolithic integration on a silicon substrate by epitaxial growth or bonding, or by packaging silicon and GaAs devices in a multichip module (MCM). Problems such as lattice mismatch, different thermal expansion coefficients, device alignment and signal distortion or loss in traveling from Si to GaAs must be solved before either of these options is viable. These difficulties in interfacing make a silicon-based OEIC more desirable.

Several silicon-compatible materials are being considered for light emitting applications. Some theorists have argued that zone folding in SiGe/Si superlattices will create a direct bandgap material that would be an efficient light emitter. Although experimental evidence has not yet bourn this out, other quantum effects in this system have yielded broad, weak room temperature luminescence. Quantum confinement in nanocrystalline or porous silicon is also a possibility for room temperature devices. The large tunability of emission in this materials based on variations in processing are especially attractive, but serious contact and reliability issues, coupled with a lack of fundamental understanding of the light emission process, hamper the application of this material. Point-defects in silicon have also attracted attention recently as well, and include beryllium pairs, sulfur, and erbium. Of these, erbium is the most promising because it has shown room temperature luminescence which does not shift wavelengths with variations in temperature.

Fundamental understanding of erbium-doped silicon fabricated by ion-implantation has been achieved in the last 5 years. One of the most important discoveries has been the excitation and de-excitation pathways in this system, shown in figure 1-1. The process begins with the introduction of electrons and holes either through optical excitation, as in photoluminenscence measurements, or carrier injection through an external circuit. Optically active erbium and other recombination centers then compete for the capture of these carriers (or excitons). Erbium

Figure 1-1: Light emission process in erbium-doped silicon.

centers which are successful in capturing the carriers become excited, with relaxation occurring through two paths. Competition between a radiative transition ($\tau_{sp} \approx 1ms$) and non-radiative transitions (τ_{bt}) determines the intensity and the effective lifetime of the erbium luminescence. As will be discussed in chapter 2, the requirement of high erbium luminescence intensity for device applications is not well served through fabrication by ion implantation.

The goal of this thesis was to develop a low temperature, low damage alternative to ion implantation for the fabrication of erbium-doped materials. Ultra-high vacuum chemical vapor deposition (UHV-CVD), a low-temperature technique previously used exclusively for Si or $Si_{1-x}Ge_x$ growth, was modified for this purpose. This growth method should improve the performance of the light emission process in several ways. Higher quality material will hinder electron-hole recombination at other defect centers, thereby increasing the pumping efficiency of erbium. Additionally, the concentration of optically active erbium can possibly be increased by up to 3 orders of magnitude, resulting in an increase of erbium luminescence. A novel $Si/Si_{1-x}Ge_x$ double heterostructure design was also used to take advantage of optical and electrical confinement to further increase the quantum efficiency of pumping and power collection.

1.2 Thesis Organization

This thesis is organized into seven chapters. After a review of erbium's properties in silicon in Chapter 2, the theory of UHV-CVD will be presented in Chapter 3. There the reasons for UHV-CVD advantages with respect to ion implantation will be more fully discussed. Chapter 4 will cover the properties of the $Si_{1-x}Ge_x/Si$, which are fundamental to understanding the behavior of erbium in that system. Chapters 5 and 6 cover the results of growth of erbium-doped films and the physics of the excitation and de-excitation of erbium in the CVD films. The last chapter will summarize the accomplishment of this work and discuss possible directions for future work

Chapter 2

Erbium Doping of Si

Although rare-earth luminescence in ionic materials had been studied for decades, no reports of rare-earths in silicon or III-Vs were published until 1983 by Ennen *et al*[2]. In that initial report, the potential of erbium in semiconductor diodes for optical communication was speculated on. Much research has occurred since then leading to erbium-doped silicon light emitting diodes (LEDs) operating at room temperature. However, serious barriers need to be overcome if these devices are to become commercially viable. These problems arise from both the physics and the processing of the material, and will be discussed in the next sections.

2.1 Theory

The 1.54 μm transition of erbium is due to an intra $4f$ -shell transition, as shown in figure 2-1. In this picture, the $Er^{+3}(4f^{11})$ ion's ground state energy level is the multiplet ^4I. This multiplet allows for 4 different **J** (angular momentum quantum number) values of 15/2, 13/2, 11/2 and 9/2. Transitions between these states in a free ion is parity forbidden since they all have f character. When Er^{+3} is placed in a semiconductor, however, the crystal field admixes the f-state character with s,p, and d character and relaxes the restriction on the transition. This gives rise to the crystal split states to the right of the figure, shown only for the transitions of interest. The crystal field splitting is usually small, however, due to the fact the f-shell is shielded from the host by 5p and 6s electrons, so the states remain primarily f-like in nature. This causes the long excited state lifetime and relatively weak emission seen for the $^4I_{13/2}$

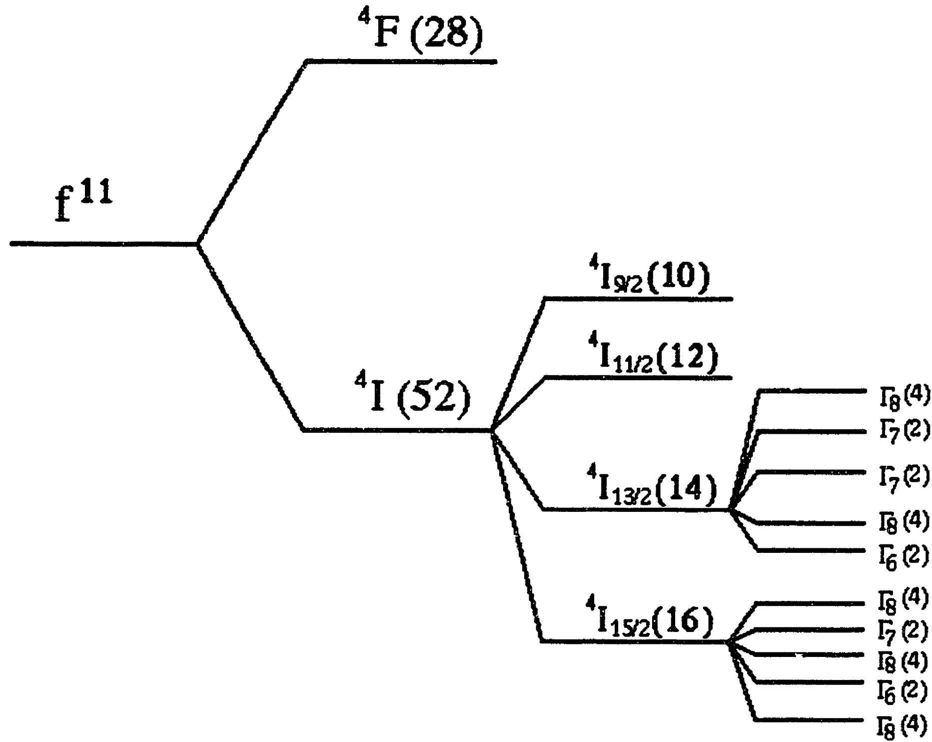

Figure 2-1: Splitting of the $4f$ states of erbium in a crystal field.

$\rightarrow$ $^4I_{15/2}$ transition occurring at 1.54 μm. The fact that the $4f$ electrons are isolated from the surrounding crystal also causes the radiative lifetime (τ_{sp}) and emission wavelength of erbium to be relatively independent of the host, with values of approximately 1 ms and 1.537 μm respectively. Due to the long τ_{sp}, the erbium transitions have a very small energy (or wavelength) width. The 1.54 μm transition has a sharp linewidth of 100 Å at 77 K compared to the band edge luminescence of GaAs which is 1000 Å at that temperature[3].

Although erbium luminescence is independent of host, changes in the ligand environment of erbium have produced dramatic effects in intensity. Favennec[4] first reported an enhancement of luminescence in Cz-Si with respect to FZ-Si which was attributed to the increase of oxygen concentration by two orders of magnitude in Cz-Si. Later results by Michel confirmed this when erbium luminescence in FZ-Si was increased to a level comparable to Cz-Si after it received an additional oxygen implantation[5]. More recent work has also shown that temperature

quenching can be reduced when the oxygen concentration is increased. Co-implantations of other ligands in Cz and FZ-Si have also improved the luminescence by varying degrees as shown in figure 2-2. At least two theories have been proposed for the origin of this enhancement.

Jantsch[6] reports that the ligands serve two purposes; passivation of deep level states in the bandgap and facilitation of erbium incorporation into optically active sites. While DLTS studies have clearly shown that oxygen reduces the deep level states caused by implantation, the second proposed role of the ligand is controversial, bordering on heretical. In this theory, the most important optically active erbium site is the isolated, interstitial erbium in cubic (T_d) symmetry as found in FZ-Si. This group did attribute some luminescence lines to Er/O and Er/defect interactions, but they were quenched much sooner than the cubic lines. The difficulty with this interpretation is that the foundation assumes that the lines seen in implanted FZ-Si samples are not caused by Er/O interaction, even though such structures could exist in concentrations high enough to cause the relatively weak luminescence. No evidence for the mechanism by which the ligands shepherd the erbium into isolated interstitial sites is presented either. The well known affinity of erbium for oxygen would suggest that the two species would be drawn together, not apart when governed by thermodynamic laws as found during annealing. Finally, they reported seeing no new spectral features when erbium was co-implanted with ligands other than oxygen. While this observation is consistent with their proposed theory, it is contradictory with results from other groups.

All other theories are based on the premise that the ligands somehow modify the electronic state of the erbium into a center which is more optically active than the isolated erbium atoms. Data from extended x-ray absorption fine structure (EXAFS) of erbium implanted silicon clearly show that a strong interaction between erbium and oxygen is present[7][8]. Terrasi[7] followed the Er L_{III} edge in samples which had been annealed at various temperatures and times. Samples implanted with erbium and oxygen which were annealed at $900°C$ had EXAFS signals resembling an Er_2O_3 reference while those samples not annealed were similar to a $ErSi_2$ film. The extracted radial distribution functions could be fit by a first-shell consisting of 5 oxygen atoms at a distance of 2.27 Å from the erbium. A similar study by Adler[8] reported a first-shell environment of 6 oxygen atoms, with the same annealing behavior. Exactly how this interaction increases of luminescence is still under debate however. X-α calculations predict

that the major effect of oxygen is to enable the erbium to hybridize the $4f$ electrons allow for less restricted transitions[9]. Other groups believe that the role of ligands is to introduce and gateway state into the bandgap, associated with the erbium/ligand cluster, which enables for electronic pumping.

Deep level transient spectroscopy (DLTS) studies confirm some of some of each theory. Defect states present after only an erbium implantation are strongly reduced when erbium is co-implanted with oxygen[10], meaning that passivation of defects is important for longer exciton lifetimes and efficient excitation of erbium. This same study also emphasized the role of ligands in forming a defect state 0.15 meV from the conduction band (E_c- 0.15). Although earlier work by Benton[11] did not show a correlation between PL intensity and the concentration of this state, more recent evidence is increasingly favoring this theory[12]. The most convincing is a temperature dependent junction photocurrent spectroscopy (JPCS) study done by Palm[13]. Above 100 K, light directly absorbed by the erbium at 0.81 eV caused an increase in current, which was attributed to thermalized carriers from a state approximately 0.17 eV from a band. Other species were also co-implanted with erbium to determine which had the greatest effect on intensity (see figure 2-2). In general, the lighter elements with higher electronegativities tend to result in the best erbium luminescence intensity.

2.2 Excitation and De-excitation Mechanisms

In order to optimize erbium-doped material, it is crucial to understand how it is excited and de-excited by nonradiative processes. In the previous three years several studies have tried to identify these mechanisms with some success. Two excitation mechanisms have been found which operate under different biasing conditions. Auger excitation is responsible for photoluminescence and electroluminescence (EL) when the diodes are operated in forward bias. If diodes are so strongly in reverse bias that they breakdown, impact ionization can excite the erbium. Since the de-excitation processes are dependent upon the biasing regime, each will be briefly considered.

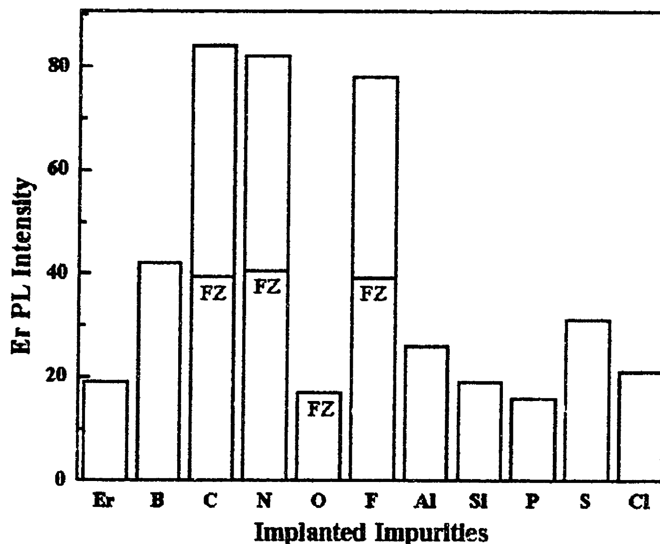

Figure 2-2: Effect of co-implanted species on erbium luminescence at 4 K.

2.2.1 Auger Excitation and Back Transfer

Erbium is believed to be excited after an exciton, which has been trapped near it, recombines and transfers the energy into the $4f$ shell of erbium. Efficient pumping of erbium, therefore, requires high quality material for longer carrier lifetimes to allow for the exciton to find the erbium. If erbium creates a state in the bandgap, a coulombic interaction between it the exciton would also make the trapping and hence excitation more likely. The position of such a state in the gap could be modified by changing the environment around the erbium.

Erbium luminescence excited by this process exhibits two different temperature quenching regimes in samples without amorphization. From 4 to 100 K, an impurity auger effect with an activation energy of 20 meV cause a slight decline in luminescence. In this process, the excited erbium decays to the ground state, transferring its energy to carriers in shallow donor states or the bottom of the conduction band. Above 100 K, Palm[14] and Polman[15] report that a multiphonon process with an activation energy of approximately 160 meV strongly quenches the luminescence. The model proposed by Palm is similar to one put forward by Taguchi[16]

for Ytterbium in InP. In this process, the excited erbium relaxes back to the ground state and promotes an electron from the valence band into a virtual state in the band gap. Energy absorbed from phonons provide the extra energy needed for the electron to reach the ErO_x donor state located approximately 160 meV below E_c, from which the electron can then thermalize into the conduction band. Since the amount of phonon energy required, about 150 meV, is very similar to the energy difference between the ErO_x state and the conduction band, there is some speculation about which step is determining the temperature quenching. Studies of erbium in $Si_{1-x}Ge_x$ can aid in the solution to this problem since the phonon energy required for the process can be tuned by the germanium fraction.

2.2.2 Impact Ionization

Erbium can also be excited into the $I_{13/2}$ state if a hot carrier with sufficient energy strikes it. Several groups have seen this when diodes were operated in the breakdown regime. In their structures, breakdown would occur at -5.5 V (avalanche breakdown) and some hot electrons would have enough energy to excite the erbium. Luminescence excited in reverse breakdown is relatively equal to that under forward bias at 4 K at high current densities (2.5 A/cm^2). However, instead of a reduction of luminescence by as much as three orders of magnitude in going to room temperature, only a 4 fold reduction is seen. Little research has been done to understand the reason of the persistence of the luminescence. The only report on this subject suggests the principle reason for the reduced quenching is that different erbium is participating in luminescence in forward and reverse biases. Franzò[17] has suggested that erbium which is not normally excited in forward bias becomes optically active when excited by impact ionization. This could be the case if some of the erbium did not have an associated state in the bandgap through which exciton localization and pumping would occur. DLTS and SRP measurements taken by the same group confirm that only 1% of erbium ions introduce the $E_c-0.15$ eV state, which is similar to the number that can be pumped in forward bias. Since no associated level exists in the gap to which electrons can be transferred upon relaxation of the erbium, quenching would be much more difficult.

Another possible explanation for the high temperature luminescence is that erbium which luminescences in reverse bias is effectively in an insulating material, possibly a localized environ-

ment resembling an oxide, which cannot be pumped in forward bias. The increase in bandgap energy would reduce the free carriers available for Auger backtranfer and make it harder for non-radiative recombination of the erbium to effectively pump the host. It is unclear if this is different from the theory of Franzo however. Since increasing the oxygen concentration not only increases the concentration of the $E_c - 0.15$ eV state thought responsible for luminescence in forward bias but also the probability that erbium would be trapped in an oxide, it is unlikely that the models are the same.

Exciting the erbium by impact ionization has not been favored due to the unacceptably high voltages required. If structures with breakdown voltages lower than -5 V could be fabricated, this could alleviate the need to use forward bias LED's with their accompanying temperature quenching. High drive currents would be required however, so heat dissipation would become an issue. The two easiest ways to do this are to increase the doping in the diode or to build an internal electric field into the device. This technique has already been used in SiGe HBT's to increase the speed by grading the germanium fraction in the base. Unfortunately, due the band offsets in the $Si/Si_{1-x}Ge_x$ system, the built-in field would be mostly effective only for the holes. The electric field for the holes would still be an improvement to the silicon homojunctions now being used.

2.3 Methods of Growth

Since the first report of luminescence from erbium-doped silicon in 1983[2], several constraints on the luminescence of erbium in silicon have been discovered. The equilibrium solid solubility of erbium in silicon of $\leq 1 \times 10^{18}/cm^3$ (at $900°C$) is 1-2 orders of magnitude below the concentration estimated to be needed for light emitting devices[18]. Above this concentration, optically inactive precipitates of $ErSi_{2-x}$ form on [111] planes[19]. High temperature processing can also be limited by the need to keep the erbium-ligand complex together in order to see enhancement of the luminescence. The other critical issue in the growth of erbium-doped silicon is to minimize damage caused during the incorporation of erbium. These defects can act as non-radiative recombination centers which decrease the pumping efficiency of the erbium. Any growth technique useful for production of commercial devices must address these issues.

Several methods have been used to incorporate erbium into silicon including ion implantation [2][4][19][20], solid phase epitaxy (SPE)[21][22][23], molecular beam epitaxy (MBE)[24][25][26], chemical vapor deposition (CVD)[27][28], ion-beam epitaxy[29], diffusion[30], pulsed laser ablation [31], laser irradiation[32] and sputtering[33]. Since the use of UHV-CVD is potentially critical is erbium doping, the work with other methods will be briefly described into order to examine the differences. I will focus on the first five since they are processes most easily compatible with integrated circuits and have the highest crystalline quality.

2.3.1 Ion Implantation

Most of the research done on erbium-doped silicon has used ion implantation to incorporate the erbium. The implants were typically done with ^{166}Er at ion energies ranging from 200 keV to 5.25 MeV. Doses normally were between $10^{12}/cm^2$ and $10^{16}/cm^2$ with appropriate substrate temperatures to avoid amorphization. Annealing is always done after the implantation to improve the crystalline quality and optically activate the erbium. Studies have shown that luminescence is affected by the temperature and environment during annealing through changes in the defect concentration[5][34]. For samples implanted at high energies (MeV), annealing at $900°C$ maximized the intensity at 1.54 μm[5] (figure 2-3). This has been attributed to the competition of two processes. At lower annealing temperatures the crystallinity has not yet recovered from the implantation and nonradiative recombination pathways hinder Er luminescence. Additionally, the ligand species have not diffused to the erbium to form optically active centers. At temperatures above $900°C$, the dissociation of the erbium-ligand complexes is responsible for the reduction of erbium luminescence. This behavior is seen in lower energy implants (400 keV) as well, although the optimum annealing temperature shifts downward to $800°C$ or below (figure 2-3). The reduction in the optimal annealing temperature is a result of the difference in implant conditions. The lower energy and dose ($3.5\text{x}10^{12}/cm^2$ versus $3.8\text{x}10^{13}/cm^2$) of the 400 keV implant causes less damage in the substrate, which in turn reduces the thermal budget needed for lattice recovery. Since the dissociation of the erbium-ligand complex is thermally activated, the lower annealing temperature maintains a larger concentration of optically active erbium. This was demonstrated by a ten-fold improvement in optically active erbium (0.78% to 7.4%) in the 400 keV implant compared to the 4.5 MeV implant[12]. This strongly suggests

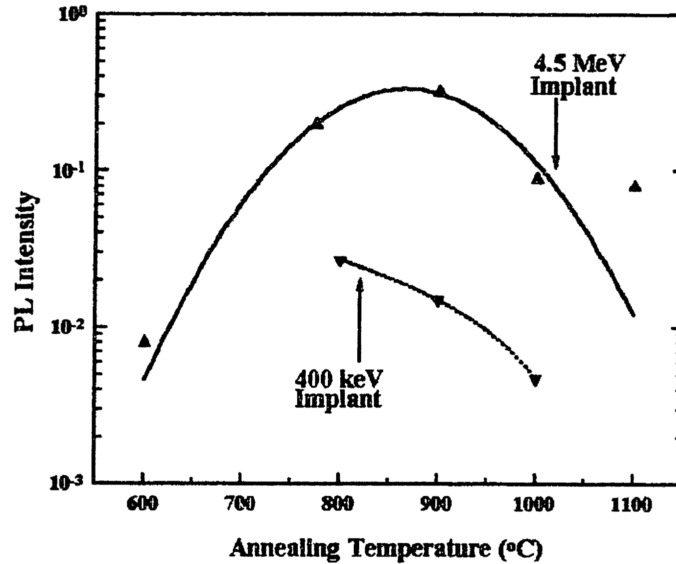

Figure 2-3: Effect of annealing on the luminescence of erbium implanted silicon. All annealing was done for 30 minutes in an argon atmosphere.

that lower temperature processes will be preferable to higher temperature ones if the erbium doses are comparable. In the implantation case cited above, the lower dose of the 400 keV implant nearly offset the gain in optical activity.

The microstructure of silicon implanted with erbium at various energies and concentrations has been extensively studied[19][35]. Eaglesham[19] found a threshold erbium concentration for precipitation of $1.3 \times 10^{18}/cm^3$ in 500 keV implanted silicon annealed at $900°C$ for 30 minutes. Above this concentration, erbium-rich platelets (tentatively identified as $ErSi_2$) formed on [111] planes near the peak concentration of erbium during annealing. The precipitate density increases rapidly as the erbium concentration rises above the threshold value. Implantation energy can affect the onset of precipitation however. Silicon implanted with erbium at 400 keV to achieve a peak concentration of $5 \times 10^{17}/cm^3$, and oxygen to a peak concentration of $3 \times 10^{18}/cm^3$ at the same depth, did not have precipitates after annealing[35]. When the erbium implantation was done at 4.5 MeV for the same concentrations, precipitates did form. Cross-sectional transmission electron microscopy (XTEM) was used to record the evolution of

microstructure for this sample as a function of annealing temperature[35]. Small dislocation loops at the end of range have formed after an $800°C$ anneal for 30 minutes which continue to grow in size as the annealing temperature is increased. Much longer anneals on this material show a second band of dislocation loops forming deeper into the substrate. A strong interaction between oxygen and both bands of defects can be seen by Secondary Ion Mass Spectroscopy (SIMS), suggesting that the oxygen segregates to the dislocation loops.

Light emitting diodes (LED's) operating at room temperature have been made from both the high energy (4.5 MeV) and low energy (400 keV) erbium implanted samples[36][12]. Oxygen was co-implanted in these samples to overlap the erbium profile at a concentration of $2\times10^{18}/cm^3$. Luminescence was seen only in forward bias. For low drive current densities, the internal quantum efficiency of the high energy implanted LED was 4×10^{-4} at 100 K. The total light output power at 100 K was estimated at 3.4 μwatts. The low energy implanted samples produced 2.5 times more light per erbium atom than the high energy implants at a tenth of the dose. Cross-sectional TEM revealed end of range defects in the high energy implants which were not present in the 400 keV implanted diodes. This difference in crystal quality, as well as the lower annealing temperatures which enhance the stability of erbium complexes, is the reason for the improvement for the low energy implants.

To summarize, ion implantation negatively impacts the light emission of erbium in several ways . The damage caused by the implantation process creates defects which can act as recombination centers, natural competitors with erbium for the capture of electron-hole pairs. The high temperature anneal which is required to minimize these defects, reduces the concentration of optically active erbium through the dissociation of the erbium-ligand complex(figure 1-1). Lowering the maximum temperature of the process from 900° to $800°C$ resulted is an order of magnitude improvement in the optically active erbium concentration. Even lower temperature processes should be able to better this as the limiting factor of complex dissociation will be suppressed further.

2.3.2 Solid Phase Epitaxy (SPE)

In an effort to improve the crystal quality of high-dose erbium implants and to increase the amount of erbium incorporated into the silicon, some research has been focussed on solid phase

epitaxy. The earliest work done implanted with high doses at room temperature to amorphize the surface[19]. The same annealing that was typically used for implantation, $900°C$ for 30 minutes, was used to regrow the crystalline silicon from the single crystal/amorphous interface. Erbium segregated with the moving interface, reaching a maximum concentration of $8.5\times10^{19}/cm^3$ before precipitation occurred and regrowth broke down. Above this point the erbium concentration fell to pre-regrowth values and the subsequent growth was highly defective. TEM revealed stacking faults and twinning extending to the surface. Later work on SPE modified the annealing procedure to optimize it for regrowth. In these studies, implanted erbium at 250 keV into crystalline(c-Si) or pre-amorphized silicon (a-Si) at 77 K[21]. Post-implantation anneals at $600\text{-}650°C$ for 3 hours were done to regrow single crystal silicon through the erbium-doped amorphous silicon. The erbium again segregated in front of the a-Si/c-Si interface until it reached high concentration, where it became trapped in c-Si. Erbium concentrations as high as $2\times10^{20}/cm^3$ have been achieved in very thin regions (approximately 20 nm). The minimum channeling yield (χ_{min}), which is the ratio between the backscattered intensity of channeled and random sample orientation, was <5% indicating 'high quality' material. This is a qualitative measure of film perfection, however, and is not sensitive to differences in structure when χ_{min} is near 5%. Cross-sectional TEM of this sample did show a thin disordered region near the surface. A final rapid thermal anneal at temperatures $\geq 900°C$ for 15 seconds was done in an attempt to optically activate the erbium. No evidence of optical or electrical activation was reported however.

More recent work has used multiple erbium implants (77 K) at energies from 0.5 to 5 MeV with corresponding oxygen co-implants for spatial overlap to increase the thickness of the highly doped material[37]. Regrowth in samples without oxygen only preceded for 800 nm before breaking down leaving large amounts of twins. The presence of oxygen ($\sim 10^{20}/cm^3$) during the anneal stabilized the regrowth over the entire amorphous thickness leaving a 2 μm region with an erbium concentration of $10^{19}/cm^3$. End of range defects and threading dislocations with concentrations of approximately $1\text{x}10^7/cm^3$ were still evident in TEM though. Spreading resistance measurements showed a donor concentration of $8\times10^{18}/cm^3$, similar to values reported by Priolo[10] by ion implantation. The PL intensity at 3 K of the SPE sample was approximately 4 times that of the ion implanted sample with similar concentrations of er-

bium, oxygen and donors. Electroluminescence from diodes made of this material was reported at room temperature in forward and reverse bias[38] with a reduction in intensity of only 15 times from 110 K to 300 K in forward bias. Samples made by ion implantation of erbium at 400 keV, as described in the last section, had a reduction in intensity by 100 times in the same temperature range.

Significant progress in the material quality of Si:Er film grown by SPE have occurred in the last 5 years, although the defect concentrations are still higher than those in ion implantation. As the output power and quantum efficiencies of this material are 1-2 orders of magnitude higher than similar implanted samples, however, it is clear that this quasi-low temperature technique has distinct advantages over implantation. Among these are higher erbium concentrations and reduced erbium complex dissociation due to the lower thermal budget for annealing. The increase in the ligand to erbium ratio also is important in erbium luminescence, and will be discussed in more detail in chapter 6.

2.3.3 Molecular Beam Epitaxy (MBE)

The previous two methods have been able to incorporate large amounts of erbium while simultaneously degrading crystalline quality. High temperature anneals can remove the implantation damage at the cost of precipitation of metastable erbium concentrations. To avoid the problem of damage, research into the non-equilibrium growth process of MBE is being done. Initial work used a metallic erbium source in a standard MBE system[24] at growth temperatures of 500° or $700°C$. Cross-sectional TEM showed precipitates at an erbium concentration of $2\times10^{18}/cm^3$ even at these low processing temperatures. After growth, the samples were implanted with oxygen to achieve a constant concentration ($10^{19}/cm^3$) throughout the erbium profile, then annealed at $800°C$ to remove the implantation damage. The photoluminescence of this material was comparable to implanted erbium standards at very low temperatures, but it was quenched near 150 K.

A more promising method which incorporates both erbium and oxygen during the growth of silicon has been reported[25][39]. When oxygen is not present during growth on (100) silicon, erbium segregates to the surface, possibly forming precipitates above areal densities of $2\times10^{14}/cm^2$. With the introduction of oxygen though a leak valve during growth, erbium segre-

gation was suppressed due to a reduction in erbium mobility or the formation of erbium/oxygen complexes. Four times the amount of erbium was incorporated in the presence of oxygen by this method. An oxygen partial pressure of 4×10^{-10} mbar resulted in a $4\pm1\times10^{19}/cm^3$ oxygen concentration in the film. A maximum erbium concentration of $2\times10^{19}/cm^3$ before precipitation was reported based on Rutherford backscattering spectroscopy. Light emitting diodes have been made with similar material grown at $500°C$[41]. Maximum photoluminescence intensity occurred in samples grown at $500°C$ with an erbium concentration of $4\times10^{19}/cm^3$. Oxygen incorporation was limited to pressures below 4×10^{-9} mbar due to the emergence of 3-D growth, but a concentration of $8\times10^{20}/cm^3$ was reported in that regime. This resulted in a oxygen to erbium ratio of 20. Both forward and reverse electroluminescence was observed, although the reverse bias intensity was over 30 times that of forward bias. Reverse biased electroluminescence exhibited no temperature quenching to 293 K and the forward bias luminescence only decreased by a factor of five[42]. The estimated power output was several microwatts at room temperature with a quantum efficiency greater than 10^{-5}.

This low temperature growth process has demonstrated high erbium and oxygen incorporation into silicon with relatively strong room temperature luminescence. Although little data has been reported about the crystal quality, it is likely the material is far superior to the material made by SPE. The process also seemingly offers good control of growth parameters which makes it a viable technique. The only disadvantage is the potential precipitation in the 10^{19} range of erbium concentration which is due to the high surface diffusivities of adatoms in this technique.

2.3.4 Ion-Beam Epitaxy (IBE)

IBE is an ultra-high vacuum sputtering process with a plasma beam in which single crystal silicon can be grown at temperatures as low as $320°C$[43]. Matsuoka[29][44] has grown erbium-doped silicon films with low energy ions ($\sim$ 10eV) at $500°C$ with erbium concentrations as high as $6\times10^{20}/cm^3$. Oxygen was incorporated into the film by flowing argon with trace amounts of oxygen during growth. The incorporation of erbium was strongly dependent on the amount of oxygen in the argon gas, suggesting that the oxygen is increasing the sticking coefficient of erbium and selectively oxidizing it. As with MBE, the presence of oxygen suppressed segregation

of erbium during growth.

The crystal quality of IBE films has been characterized by TEM, SEM, reflective high energy electron diffraction (RHEED), SIMS and PL. No dislocations or extended defects were seen by TEM, although high concentrations of point defects almost certainly exist. This was also confirmed by the more sensitive technique of etch pitting with examination in the SEM. RHEED patterns of the surface show a typical silicon 2×1 reconstruction for films with an erbium concentration below $3\times10^{19}/cm^3$, after which a diffuse pattern is observed, indicating poor crystallinity. Metal contamination, a common problem for sputtering, was below the detection limits of SIMS for growth temperatures above $400°C$. Maximum intensity occurred for samples with a erbium concentration of $2\times10^{18}/cm^3$at 4 K. Weak room temperature PL has also been seen in samples with $5\times10^{18}Er/cm^3$ and $3\times10^{18}O/cm^3$.

This technique does not look promising for the growth of Si:Er films due to several reasons. The low erbium concentrations and low ligand to erbium ratios, inherent in this process, will ultimately limit the potential of erbium luminescence well below that of other methods. Lack of dopant (n or p) control makes the growth of junctions for lasers and LEDs difficult as well. As the silicon target cannot be changed during growth the only junction that can be made would include the substrate which forces the original wafer surface to be in the active region. Since this would be of low quality than the film or substrate, device performance would suffer.

2.3.5 Chemical Vapor Deposition (CVD)

Like molecular beam epitaxy, CVD of erbium-doped silicon offers metastable erbium concentrations due to low processing temperatures without lattice damage. Electron cyclotron resonance plasma enhanced CVD (ECR-PECVD) and ultra-high vacuum CVD (UHV-CVD) have grown erbium-doped silicon at temperatures from 400° to $610°C$ [27][28][45][46]. Both types of systems used organometallic compounds which contained both the erbium and the ligands needed for optically activation. An inherent problem with these sources is the incorporation of large concentrations of carbon coming from the precursor which can degrade the crystal quality of the film. Control of the decomposition of the precursor through processing parameters is crucial to suppress this problem. While the difficulties associated with precursor cracking are common to both systems, the method of film growth is different.

ECR-PECVD uses a high-density plasma to excite the gas molecules to a reactive state which are then accelerated toward the silicon surface with energies $\geq$ 10 eV, hence thermal energy is not required for decomposition and growth. Since energetic particles impinge on the surface, however, damage can occur above the energy necessary to displace a silicon atom from a lattice site, estimated to be 13 eV from Monte Carlo simulations[47]. Threading dislocations were observed by cross-sectional TEM in undoped silicon films grown at $430°C$ with radicals of approximately 11 eV, but not in films grown at $500°C$, where only a slightly disordered interface was seen[48]. The silicon device community has not yet accepted this technique for production of single crystal silicon due to the susceptibility to point and line defects, but further refinement might produce integrated circuit device quality material. Maximum photoluminescence was seen in films grown at $430°C$ containing an erbium concentration of $6\times10^{18}/cm^3$ and a χ_{min} of 6%, indicating fairly high crystal quality[45]. Nitrogen was the ligand in the precursor and had concentrations of approximately $2\times10^{19}/cm^3$ in the film. High levels of carbon contamination were reported (15 times that of the erbium), but it is possible that the carbon is also complexing with erbium, forming optically active centers. Rocking curve analysis of the Si (044) shows a narrow FWHM of 71 arcsec for the film. The photoluminescence intensity decreased by a factor of 40 from 4 K to room temperature.

UHV-CVD is low-temperature ($500° - 650°C$) epitaxial growth method, described in full detail the next chapter. Undoped silicon growth rates still tend to be smaller than growth rates for ECR-PECVD (10 Å/min vs. 40Å/min), but over 20 wafers can be deposited on at a time in UHV-CVD as compared to one wafer in ECR-PECVD. It is still unclear, however, if the large batch sizes quoted for silicon growth in UHV-CVD can be extrapolated to erbium-doped films, since the precursor could be depleted at the end of the batch. Erbium concentrations have been $>10^{20}/cm^3$ in UHV-CVD grown films, but contamination from other species in the precursor can be large, exceeding $10^{21}/cm^3$ in some cases. Beach[27] reported high concentrations of threading defects in the erbium-doped films from TEM, most likely due to the high concentration of carbon ($10^{20}/cm^3$) in the film. The work done in this thesis shows that threading defect problems have been eliminated however.

In conclusion, CVD processes have several advantages over ion implantation and SPE. The low growth temperatures will allow for higher erbium concentrations since lethargic kinetics

prevent precipitation above the solubility limit. The dissociation of erbium-ligand complexes will also be suppressed at growth temperatures. An improvement in crystal quality, especially in UHV-CVD, is expected since the low energy of the impinging molecules is unlikely to displace atoms at the surface which ultimately lead to defect clusters. The control of the CVD process, as compared to MBE, is limited though since the fragmentation of the precursor is not well understood. The advantage of CVD over MBE is a reduction in surface diffusivity with a potentially higher erbium concentration.

Chapter 3

UHV-CVD Reactor

In order to fabricate erbium-doped silicon based optoelectronic devices, several thermodynamic and kinetic issues have to be resolved. The most important of these are the concentration of optically active erbium which can be achieved in silicon and an improved quantum efficiency. For the erbium to be optically active, it has to have co-dopants such as oxygen or fluorine surrounding it. The difficulty is introducing these co-dopants so that they are only localized around the erbium and not forming defects in other parts of the device. We have designed and built an ultra-high vacuum chemical vapor deposition (UHV-CVD) reactor which addresses both of these issues. Before this is discussed, however, the fundamentals of the system will be addressed.

UHV-CVD was developed at IBM in the mid-1980's as a way of growing single crystal silicon at lower temperatures than the conventional low pressure chemical vapor deposition (LP-CVD)[50][51]. Until that time, silicon was typically grown between 850° and 1000°C at pressures near 80 torr. While this produced very high quality silicon, the growth temperatures hindered sharp dopant profiles. As faster devices required smaller dimensions, the thermal budget of production had to be decreased. UHV-CVD is able to do this by modifying two aspects of conventional CVD; wafer cleaning and vacuum.

The necessity of growing single crystal silicon at high temperatures was caused by the presence of approximately 10-20 Å of oxide at the wafer surface. This layer prevents the Si adatoms from sensing the underlying crystalline structure and promotes polycrystalline or amphorous film growth. Under certain processing conditions, however, the oxide becomes

unstable and desorbs as:

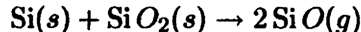

$$\mathrm{Si}(s) + \mathrm{Si}\,O_2(s) \rightarrow 2\,\mathrm{Si}\,O(g)$$

Lander and Morrison[52] systematically studied the stability of SiO_2 on Si (100) with respect to temperature and the partial pressure of oxygen (Figure 3-1). Ghidini and Smith [53][54] extended this work to higher temperatures and included the effect of water vapor (also Figure 3-1). Both groups reported a sharp transition from a clean to oxidized silicon surface in the presence of O_2. However, an intermediate region where the surface was speculated to be passivated by $Si_xO_yH_z$(s) occurs in the presence of H_2O [53]. This region exists between the two lines for H_2O pressure. Conventional LP-CVD operated at temperatures high enough to desorb the oxide for typical system partial pressures of oxygen and water and to keep a clean surface stable during growth. UHV-CVD reduces the partial pressures of these species to 10^{-10} torr and therefore allows for a clean, stable silicon surface at temperatures as low as $500°C$. Due to the lethargic kinetics at these temperatures, however, an hydrofluoric dip immediately prior to growth is used to remove the native oxide for an initially clean surface which is hydrogen passivated. This last cleaning step is crucial in obtaining high quality films. The wafers need to be pulled slowly from the 10:1 DI H_2O-HF bath to allow the water to roll off the surface. Blowing water off with nitrogen should be avoided if possible because it can introduce particles onto the surface. Even with this drawback, blow drying is preferable to redipping in the HF bath. Almost without exception, wafers that were redipped exhibited rough surface morphology. On one occasion, wafers which were only immersed halfway in the bath resulted in films that were rough on the bottom half and mirror-like on the top. The cause of this phenomenon is not yet understood. After the HF dip is completed, the wafers are immediately loading into the loadlock to prevent excessive absorption of contaminants and attack on the hydrogen passivation. As the wafers are heated past $400°C$ during the initiation of growth, the hydrogen begins to desorb and the surface again becomes reactive. Growth should begin simultaneously with the desorption to prevent the surface from reacting with other background species.

The lower temperature growth that can be achieved by UHV-CVD is critical in obtaining high concentrations of erbium. The limiting factor for the optically active concentration of

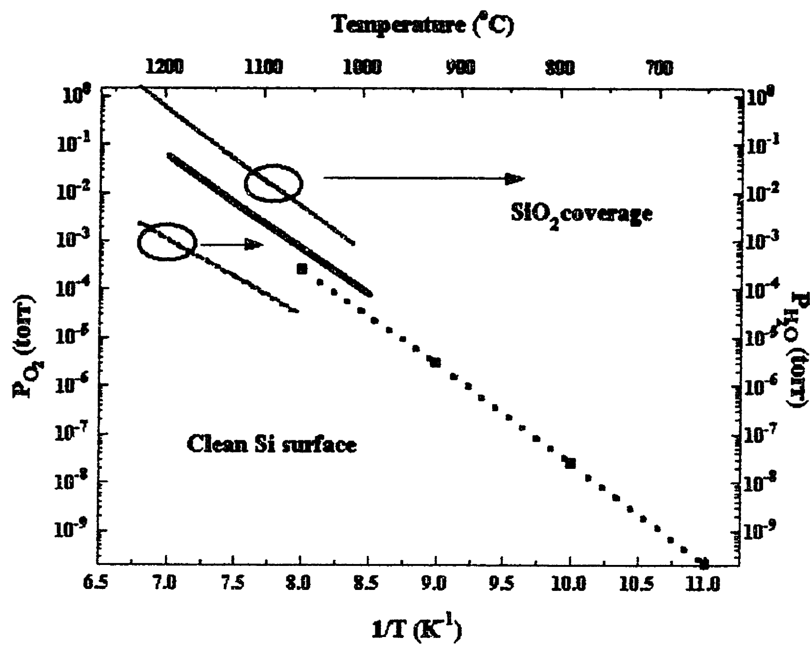

Figure 3-1: Oxide-free silicon stability diagram as a function of the partial pressures of water and oxygen.

erbium in ion implantation is the solubility limit, as the high temperature annealing for implant recovery drives the system into thermodynamic equilibrium. At the lower temperatures used in UHV-CVD, the system will be governed by kinetics and not thermodynamics and higher erbium concentrations should be possible. Although diffusion data has not been taken at typical UHV-CVD growth temperatures, extrapolation of higher temperature data has been done to predict the behavior of erbium. The diffusivity and migration enthalpy of erbium at $900°C$ for been determined to be $10^{-15} cm^2/s$ and 4.6 eV. Extrapolating to a typical growth temperature of $600°C$ gives a diffusivity of $1 \times 10^{-22} cm^2/s$, which is too low for segregation in the bulk to occur. Surface diffusion, which is typically much higher than bulk diffusion, is harder to predict. Since the growth surface is covered with hydrogen and other molecular fragments, it is reasonable to assume that surface diffusion of a precursor fragment will be difficult before it gets buried by the next monolayer. Indeed, studies made on Si:Er by MBE have shown that surface segregation is eliminated when both erbium and a ligand are being deposited. Since the source of erbium in this reactor is a metallorganic compound which already has the other ligands (such as oxygen or fluorine) bonded to the erbium, no surface segregation or significant diffusion is expected.

The second advantage of UHV-CVD is film uniformity, which arises from two factors; hot-wall growth and low operating pressures. Although hot-wall growth is not a requirement for UHV-CVD, it is the most common application of it. This is due to the very uniform temperature distribution in the three-zone furnace, as opposed to susceptor heating in cold-wall systems which has notoriously poor temperature control. As growth rates are thermally activated, temperature uniformity results in thickness uniformity. At the low growth pressures, typically 5-10 mtorr in UHV-CVD, heat transport occurs predominantly through radiation. However, the wafers in our reactor are sitting on quartz rods directly in contact with the tube, allowing for some heat conduction to occur. The quartz boat does not center the wafers in the tube either, shifting them torwards the bottom by approximately 1 cm instead. This shows up in growth rates being slightly higher growth rates at the bottom of the wafer than elsewhere.

The low operating pressures are also beneficial because gas flow is simplified. The mean free path of a gas molecule (in cm) is

$$\lambda_{mfp} = \frac{5 \times 10^{-3}}{p} \tag{3.1}$$

where p is the system pressure (in torr). Gas flow regimes are differentiated by their characteristic Knudsen number, Kn, which is defined by

$$Kn = \frac{D_p}{\lambda_{mfp}} \tag{3.2}$$

where D_p is an upper bound on the scattering length determined by the geometry of the system. If D_p is set equal to the inter-wafer spacing, approximately 0.5 cm, then $Kn \simeq 0.5$ and the system is in the molecular flow regime between the wafers. This means that the molecules collide with the wafer before they can be scattered by other gas molecules. As a result, no stagnant boundary is formed through which diffusion must occur, and the non-uniformities associated with different gas diffusivities are avoided. While deposition of Si and $Si_{1-x}Ge_x$ in our reactor occurs in the molecular flow regime, the introduction of large flows of hydrogen carrying erbium increase the pressure so much that the intermediate flow regime is entered. Since modeling of this regime has not been done, the effect of this shift on the deposition of erbium-doped films is unknown.

This cleaning procedure is still controversial due to some problems with interfacial contamination. Secondary Ion Mass Spectroscopy (SIMS) analysis done on films grown by UHV-CVD show carbon and oxygen doses at the wafer surface can be as high as $10^{14}/cm^2$. This can come from the wet cleaning, exposure to the atmosphere in transit to the reactor, or contamination from the load lock during sample transfer into the reactor. Studies of carrier surface lifetime have shown that surface quality degrades within seconds of removal from the HF dip[55], even though Meyerson[56] did not see peaks corresponding to SiO_2 in XPS after longer time intervals. However, it is likely that the absorbed oxygen and carbon bearing species do not react at low temperatures so no peaks corresponding to new bonding would be seen. Growth procedures can be modified to load the wafers at low temperatures ($<250°C$) to drive off absorbed species before rising the temperature and initiating growth. In either case, the original wafer surface is typically buried under a "sacrificial" silicon film in order to remove it from the active region of the device. Low defect concentrations on the order of $10/cm^2$ have been reported using this technique.

Although UHV-CVD occurs at low temperatures, it must be re-emphasized that it is a

surface reaction limited process. While that leads to lower growth rates than for systems which enhance the reaction on the surface, it does have a major implication with respect to crystal quality. The energy of a molecule striking the surface in UHV-CVD is too low to cause any damage to the lattice. Another low temperature technique for growing Si:Er, ECR-PECVD, uses energies in the range of 10-15 eV, which are very close to the predicted onset of point defects at 12 eV. The lack of a background of point defects in films grown in this reactor should help in the pumping efficiency of the erbium.

3.1 Description of System

This reactor consists of three basic parts; a gas manifold system, load lock and growth chamber. The gas manifold is further divided into the gas cabinets and a regulation/control system. The process gases used are SiH_4, GeH_4(15% in argon), B_2H_6(100 ppm in SiH_4), and either AsH_3 or PH_3 (in SiH_4or H_2 respectively). These gases are outside a class 100 clean room where the reactor is located and are piped to the control cabinet which sits beside the reactor. The control cabinet (see figure 3-2) was custom made by Applied Energy Systems (Malvern, PA), and contains further regulation, mass flow controllers (MFC's), purifilters, manual, check and pneumatic valves. The Nanochem filters are designed to reduce the water and oxygen content to below 1 ppb and are on all gas lines except the diborane (no filter is available for that gas). The all-metal MFC's are made by MKS Instruments (series 1459C) and only allow for a maximum flow for process gases of 10 standard cubic centimeters per minute (sccm) on every line except for the bubbler line. The SiH_4 and GeH_4 lines have by-pass valves around the MFC's for faster purging. Hydrogen dilution of the dopant lines was incorporated to have finer control over the doping concentration. This is accomplished by inserting hydrogen between two MFC's on both doping lines. By balancing the settings of the downstream MFC and an excess venting MFC, the dilution can be controlled down to 0.1% of the minimum flow without dilution.

Lag time in gas switching has been minimized to obtain abrupt interfaces by design. On the downstream side of the MFC's, the gas lines are split into two lines, named 'reactor' and 'by-pass', which empty into two trunk lines. All of the 'reactor' lines go to the trunk line that is connected to the upstream side of the growth chamber, while the 'by-pass' lines go to

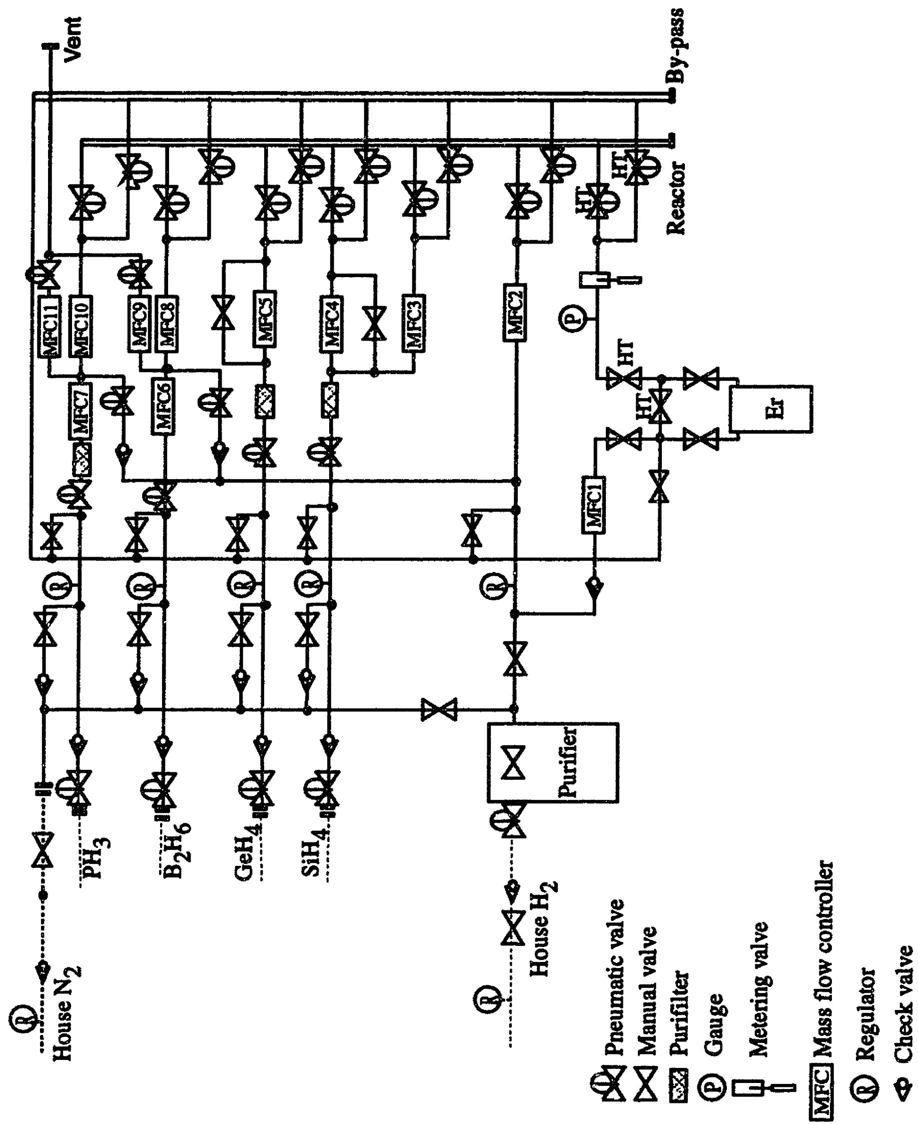

Figure 3-2: Diagram of the gas lines used for the UHV-CVD reactor.

the line attached just above the process turbomolecular (turbo) pump. For each process gas line, the pneumatic valves on the split lines are wired together such that when one valve is closed, the other simultaneously opens. Since both of the split lines have the same pressure on the downstream side, no large transient spikes of gas flow occur when switching in a gas from by-pass to the reactor. An additional SiH_4 line was added to ensure rapid switching between two different compositions of $Si_{1-x}Ge_x$. This is accomplished by setting up a second silane flow in the by-pass line for a desired composition while another composition is being grown. To initiate the new growth, the first silane line is switched out of the reactor while the second is simultaneously switched in. This avoids resetting the silane flow during growth with the resulting gradation of the $Si_{1-x}Ge_x$ alloy. Finally, the proximity of the valves and MFC's helps to shorten the switching times.

The erbium source used in the reactor is an organometallic compound which is bubbled through a hydrogen line. The bubbler is capable of heating the source to 300° C with control of ±1°. High temperature valves are downstream from the bubbler so that the gas line can be heated to prevent condensation of the erbium. The hydrogen MFC for the bubbler is able to flow 500 sccm for higher erbium incorporation. Temperature fluctuations in the bubbler have the ability to create large changes in the precursor's vapor pressure. To prevent this from affecting the concentration in the film, a needle valve was placed in-line downstream of the bubbler. The pressure drop across this valve dampens the oscillations.

The load lock is pumped by a Balzers TPU 330 liters/sec turbo pump, backed by an Alcatel mechanical pump. Conflat fittings are used everywhere except for the load lock door and pressure gauge fittings, which have a rubber o-rings. The base pressure is 1×10^{-7} torr and is achieved after 8 hours of pumping. An activated alumina trap is located between the two pumps to prevent oil backstreaming. A pirani and cold cathode pressure gauge are dedicated for the load lock. Transfer of the sample into the growth chamber is accomplished with the use of a magnetic transfer arm.

Growth occurs in a hot-walled reactor, as shown in figure 3-3. A three-zone furnace, made by Mellon, heats a 130 mm inner diameter quartz tube. This size of tube is necessary for processing 4 inch wafers, but quartz to metal seals are not practical for these dimensions. As a result, a coupling assembly using viton o-rings was used. Each end of the tube has a vacuum in a

small area outside an 'interior' o-ring created by a small Alcatel mechanical pump. This should significantly reduce the leak rate into the system through these o-rings. All other fittings are UHV-compatible conflats. The chamber has a ion gauge and capacitance manometer to measure pressure from 1 torr to vacuum. A thermistor gauge, which can measure from about atmosphere to 1 mtorr can be exposed to the chamber depending on the valving. Partial pressures of gases can be determined from a Leybold-Inficon residual gas analyzer (RGA). The RGA can detect fragments up to 200 amu/charge and partial pressures as low as 10^{-13}torr. The pumps on the chamber include Leybold's S60A mechanical pump, WA500 roots pump, and a Balzer's 510 liters/sec turbo pump. They are valved so that the mechanical and roots pump can either back the turbo pump or directly pump on the chamber. A stainless steel trap sits between the two pumps to prevent the mechanical pump from backstreaming. All pumps have fomblin oil to prevent a reaction with the process gases. The base pressure of the growth chamber at room temperature is 8×10^{-9} torr, rising to 2×10^{-8} torr at 850° C. The partial pressure of water and oxygen are usually in the low 10^{-10} torr range at $600°C$.

A calibration of the furnace temperature has been done to accurately know the growth temperature. A type-K thermocouple was mounted in contact with a silicon wafer which was then loaded into the system. A specially designed UHV electrical feedthrough flange allowed for temperature measurement at pressures of 10^{-8} torr (baseline) and 10^{-3} torr under the flow of hydrogen to mimic growth conditions. No appreciable temperature difference between these conditions was seen, however, which is reasonable due to the lack of heat transfer to gas at these low concentrations. Data points were taken at $50°C$ intervals after allowing for the temperature reading to stabilize. As can be seen in Figure 3-4, the wafer temperature was consistently some $50°C$ cooler than the furnace setting.

3.2 Safety Features

Since such toxic and pyrophoric gases are used in this system, safety is a critical concern. Because most of the process gases can ignite if large flow rates occur, limiting orifices are on all cylinders. High pressure pneumatic valves are at the outlets of all the cylinders which will close upon the detection of a leak. The MDA unit, which monitors for leaks, has sensing points in the

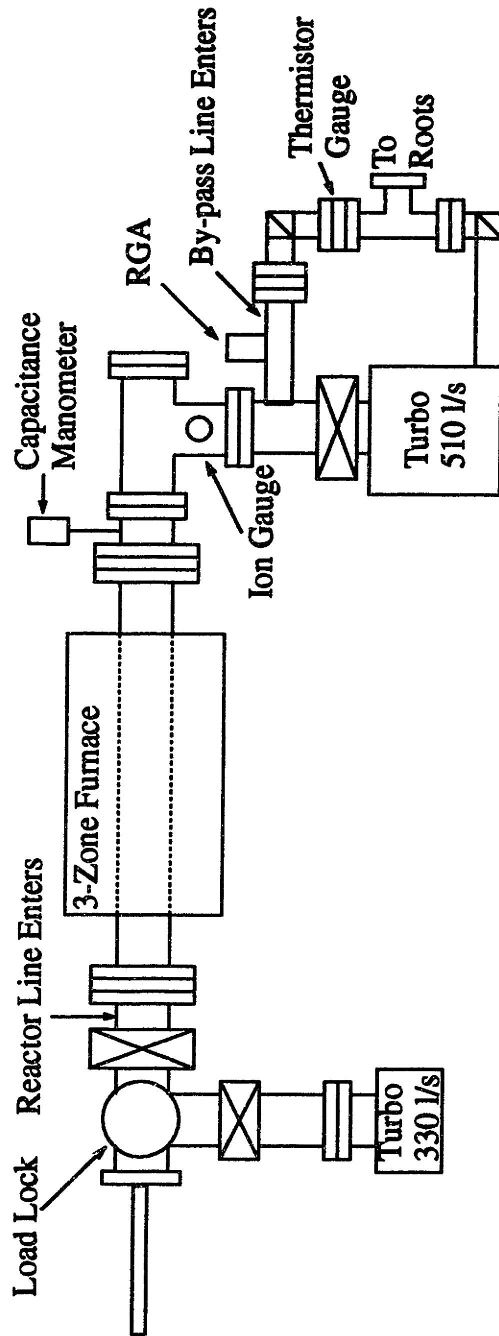

Figure 3-3: Diagram of the UHV-CVD reactor.

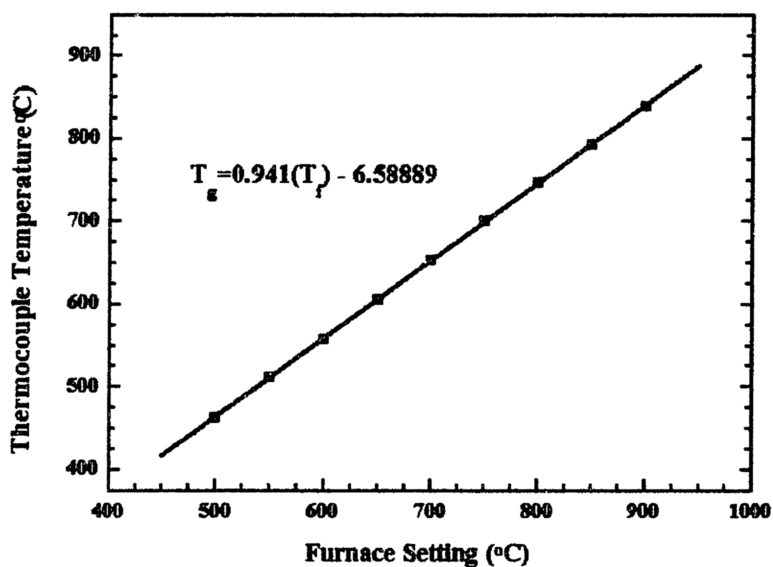

Figure 3-4: Growth temperature calibration based on the temperature reported by the furnace thermocouples.

gas cabinet, gas manifold, at both ends of the quartz tube and outside the exhaust system. An extensive interlock system has been built into the control cabinet as well. Besides leak detection, exhaust failure and overpressure will automatically shut off all gases. Additionally, the gate valve above the turbo closes with overpressure to protect it from a possible catastrophic tube failure. Two emergency shut-off switches control the gas manifold and the reactor equipment. The RGA is also continuously used for monitoring the system itself for leaks. Any sign of increasing partial pressures of nitrogen and oxygen result in a full system leak check.

3.3 Summary

UHV-CVD is a growth process which relies on low partial pressures of oxidizing species and a clean substrate surface to allow maintain the stability of an oxide-free surface and allow for epitaxy at low temperatures ($520°C$ and above). Since diffusion and precipitation are thermally activated processes, these low temperatures effectively quench the movement of erbium in the lattice which results in metastable concentrations. A UHV-CVD reactor was specifically designed and built for this thesis to allow for the growth of Si:Er and $Si_{1-x}Ge_x$:Er films. Quick switching of gases and low operating pressures, which result in a gas residence time on the order of a few seconds, are used to enable the films to have abrupt interfaces.

Chapter 4

Silicon-Germanium Heterostructures

4.1 Introduction

The use of $Si/Si_{1-x}Ge_x$ double heterostructures for erbium-doped LED's offers the same advantages that the AlGaAs/GaAs system gave to the III-V LED's; electrical and optical confinement. Unlike that system, however, significant lattice mismatch exists between the substrate (Si) and the SiGe alloy. This imposes constraints on the device structure and processing in order to avoid the strain relieving mechanisms which can severely degrade material quality. These advantages and disadvantages, as well as experimental results of $Si_{1-x}Ge_x$ films grown by UHV-CVD, will be discussed in this chapter.

4.2 Band Structure and Electrical Confinement

Silicon's indirect bandgap of 1.12eV is based upon the transition from the "Δ-like" conduction band minimum to the valence band maximum. Even though germanium is very similar to silicon in structure and chemistry, it's smaller bandgap of 0.77 eV results from a different conduction band minimum, along the L direction. This has important effects in the magnitude the unstrained bandgap as a function of germanium mole fraction. As seen in figure 4-1, the bandgap gradually decreases with increasing germanium composition until approximately 85%, at which point the bandgap starts to fall sharply. This break is due to a transition of the conduction-band minimum from one that is silicon-like (i.e. along the Δ-direction) to one that

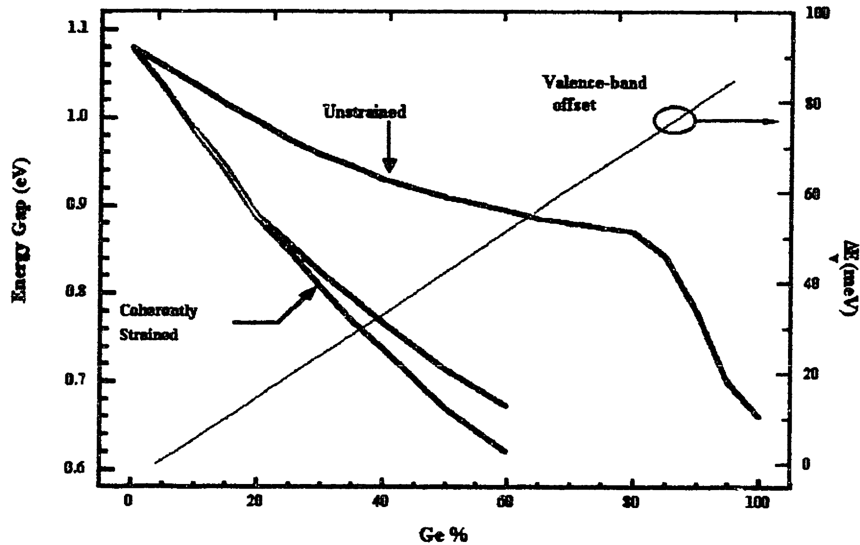

Figure 4-1: Theoretical bandgap and valence band offset for strained $Si_{1-x}Ge_x$ on Si.

is germanium-like (along the L-direction).

The first systematic studies of the strained bandgap of SiGe alloys grown on silicon[58][59] predicted an additional decrease of bandgap energy with respect to silicon due to the effects of strain on the valence and conduction bands. Both hydrostatic and biaxial strain are present in SiGe pseudomorphic growth, each altering the band structure differently. The hydrostatic strain is just a normalized volume change, and serves to only shift the band states. The biaxial strain, also sometimes called uniaxial, is caused by the difference of strain between directions parallel to the growth interface and those perpendicular to it. SiGe alloys are in compression along the growth interface due to the larger equilibrium lattice constant, which therefore causes a dilation in lattice normal to the interface. Because of the directional nature of this strain, band states can be split by it although the average energy of this states will not be changed. The result of this interaction is a further decrease in the bandgap. This can also be seen in figure 4-1, where the uncertainty in the modeling parameters creates a region of possible bandgap energies.

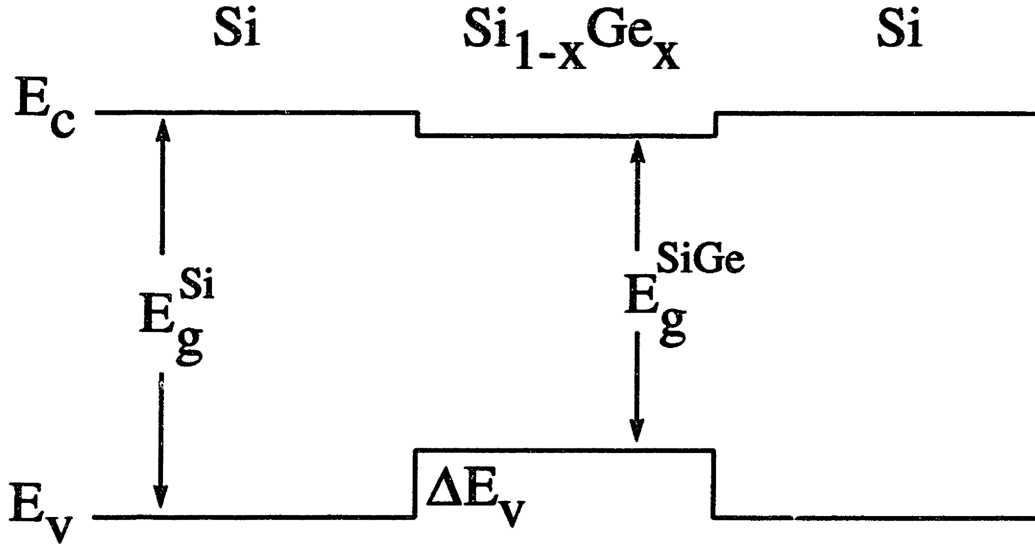

Figure 4-2: Model of the band structure of strained $Si_{1-x}Ge_x$ on Si.

It is also critical to know the band offsets in this system since they can have a great influence on the excitation and de-excitation processes of the erbium-doped $Si_{1-x}Ge_x$LED's. Both theoretical models and experimental evidence[63][62] show that the difference in bandgap is dominated by valence band offset. This offset has been predicted by Van de Walle[59] as;

$$\Delta E_v = 0.85x \tag{4.1}$$

where ΔE_v is the valence band offset in eV and x is the mole fraction of Ge. The direction of the conduction band offset is still uncertain although recent experiments suggests that the conduction band is lower in SiGe (type-I). In either case, it is known that the offset is very small (less than 20 meV). A model of this is shown in figure 4-2.

Optical confinement in the $Si/Si_{1-x}Ge_x$ system has not been as widely studied as electrical confinement. Soref [60] modeled the system for waveguides by assuming a linear dependence of the index on the germanium content for concentrations up to 20% of

$$n_{Si_{1-x}Ge_x} = n_{Si} + 0.18x \tag{4.2}$$

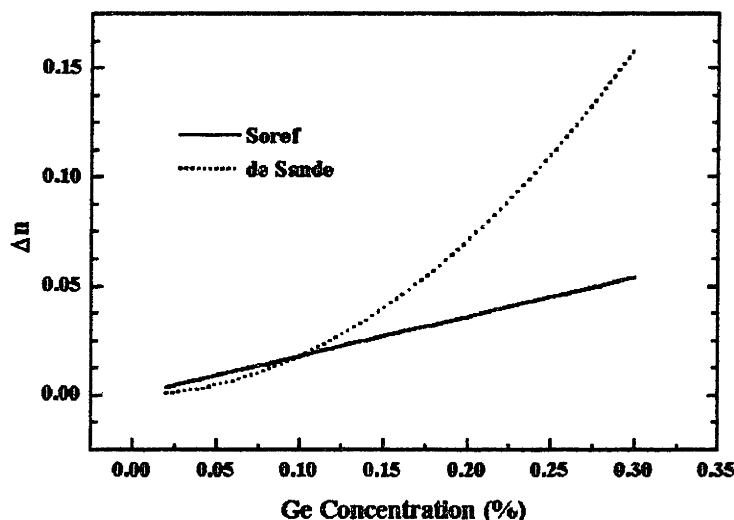

Figure 4-3: Index difference between strained $Si_{1-x}Ge_x$ and Si. The curve labeled Soref is a model based on a red-shift effect while the de Sande curve is based on an empirical fit to data.

with no explicit wavelength dependence. This model predicts rather moderate index contrast even for large germanium content. Recent ellipsometry studies show much different behavior which has been empirically fit by de Sande [61] to

$$n_{\mathrm{Si}_{1-x}Ge_x}(\lambda, x) = n_{\mathrm{Si}}(\lambda) + (1.16 - 0.26)x^2 \tag{4.3}$$

for germanium concentrations up to 30%. The index contrast at 1.55 μm has been plotted for both of these relationships in figure 4-3. The experimental data clearly shows a larger index difference (Δn) as the germanium content increases, and reaches 10^{-1} for x = 30 %. This compares favorably to the index difference of 1-5x10^{-2} in the III-V alloys typically used in LED applications.

4.3 Growth Morphology

Pseudomorphic growth of $Si_{1-x}Ge_x$ on Si introduces strain into the epilayer. For compositions of interest in this work ($x < 0.3$), the mismatch caused by the difference in lattice parameters is below 1.2%. The presence of strain has profound effects upon the film morphology. At low thicknesses, the strain energy stored in the film is low and planar growth is possible. As the $Si_{1-x}Ge_x$ film grows, however, the strain energy increases to the point above which relaxation becomes favorable. This has been found to occur by two mechanisms, the introduction of misfit dislocations or surface roughening. Both of these events have severe implications to device properties so a brief outline of this area will be given. At low strains (<1%), the introduction of misfit dislocations is favored at the thickness where the 'formation energy' of the defect is lower then the strain energy. This is called the critical thickness and it is solely based on thermodynamic arguments. Metastable films exceeding the critical thickness can be grown at lower temperatures due to the kinetics of dislocation introduction at the interface. Figure 4-4 shows a plot of critical thickness for different growth temperatures. Once the film starts the relaxation process, locally varying strain fields at the top of the film cause spatial variations in the growth rate, ultimately resulting in a characteristic cross-hatch pattern. Threading segments of the misfit dislocation, which penetrate through the active device region, can easily reach densities on the order of $10^7/cm^3$. At higher strains, the films roughen before the introduction of dislocations. Tersoff[67] has modeled this process and found that the barrier to roughening scales as ε^{-4}, where ε is strain. Build-up of stress occurs in the troughs created by the roughening and misfit dislocations will finally nucleate. The driving force for this relaxation is the elastic deformation which can take place at free surfaces. The surface morphology of a film which relaxed by this mechanism is shown in figure 4-5.

4.4 Film Quality

The quality of the films and interfaces was measured by two techniques; photoluminescence (PL) and x-ray diffraction rocking curves. Photoluminescence is sensitive to radiative defects such as excitonic emission, dislocations and some clusters of contaminants (e.g. carbon, oxygen and metals). Small shifts in excitonic emission, caused by strain, have been used to determine

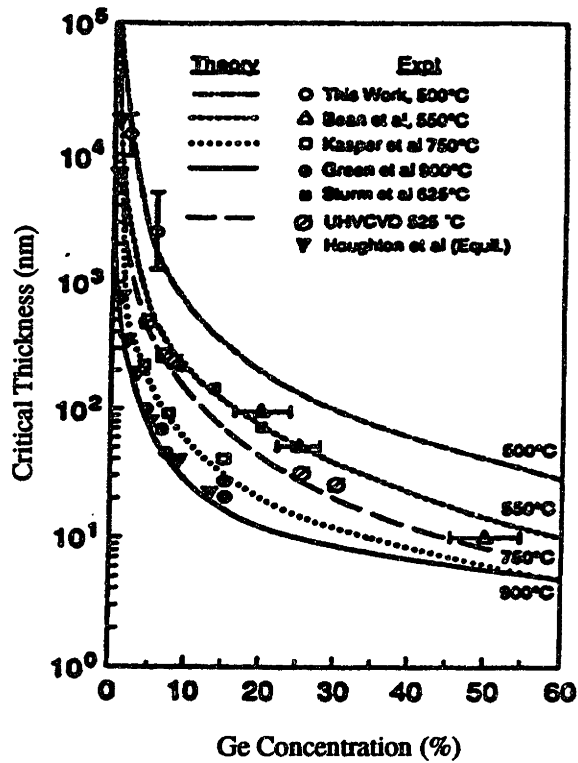

Figure 4-4: Critical thickness in the $Si_{1-x}Ge_x$ system as a function of the growth temperature.

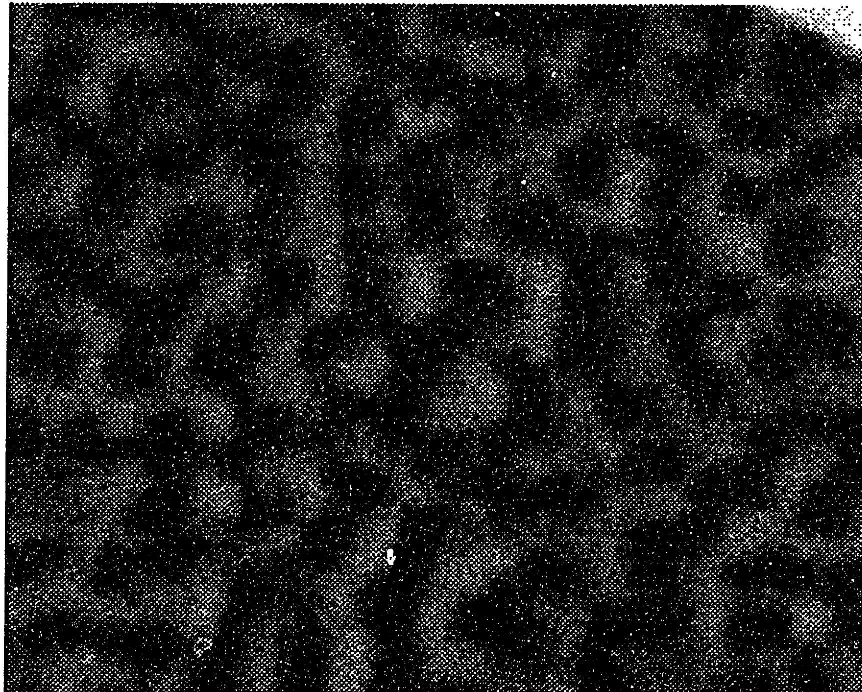

Figure 4-5: SEM image of a $Si_{0.7}Ge_{0.3}$ film which relaxed by roughening.

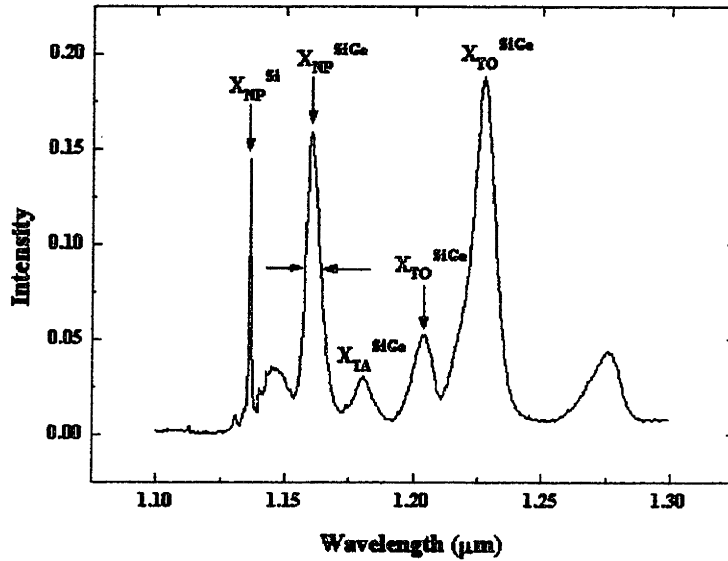

Figure 4-6: Photoluminescence taken at 4 K of a multiple quantum well structure grown at 560°C. The sample consisted of 30 periods of $Si_{0.75}Ge_{0.25}/Si$ layers.

the composition in coherent SiGe and III-V films. The width of peaks also gives information about the unformity and interfacial quality of the films. A common figure of merit is the full width at half maximun (FWHM) of the no-phonon peak of the strained alloy. A PL spectrum of a 30 period $Si_{0.75}Ge_{0.25}/Si$ quantum well growth showing this feature is in figure 4-6. The thickness of the $Si_{0.75}Ge_{0.25}$ films is 40 Å with the silicon spacer layers approximately 100 Å thick. The FWHM of this sample was 5.9 meV, only slightly wider than the lower limit of approximately 5 meV caused by alloy scattering. This peak width is comparable to reported values from MBE and other CVD grown films. As the silane flow was constricted over the last 5 quantum wells during the growth, the 5.9 meV reported for this sample should also overestimate the interfacial roughening of the system due to the different composition and thicknesses of the last 5 layers.

X-ray diffraction rocking curves from samples with only a single $Si_{1-x}Ge_x$ layer were also used to qualitatively determine the interfacial quality. Figure 4-7 shows rocking curves of the

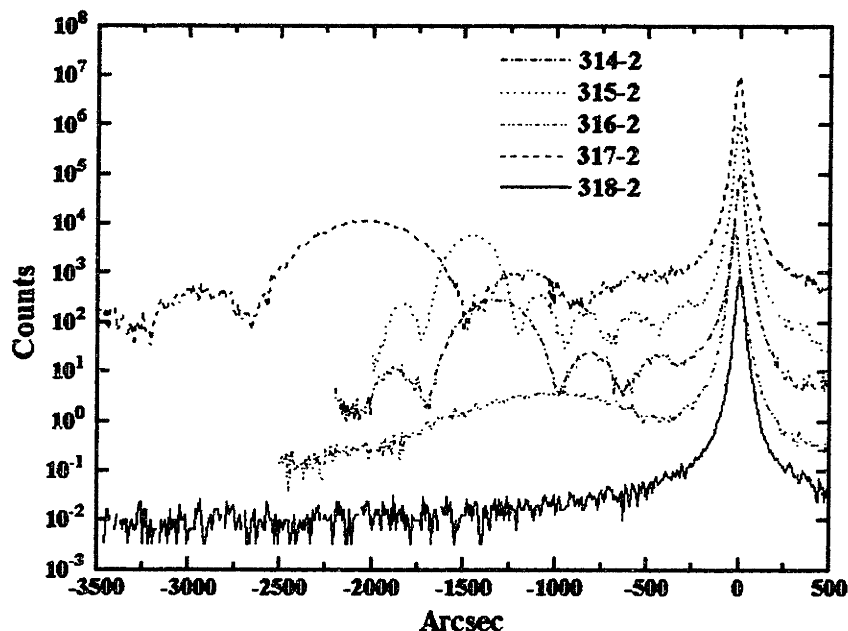

Figure 4-7: X-ray diffraction rocking curves of $Si_{1-x}Ge_x$ films.

(400) Si peak for five samples grown for growth rate calibration. Three of the five films grown showed Pendellösung fringes between the sharp substrate peak at the origin and the broad strained film peak shifted to the left due to compressive strain. The fringes are a result of a 'beating' effect from reflections at the top and bottom interfaces and are indicative of high film quality. The two films which did not show these fringes (the third and fifth films grown in the series) were deposited in the second growth run of the day, in between the growth of high quality films. As the compositions and thicknesses were similar in most of these runs, it is probable that the poorer quality interfaces were caused by contamination such as germane outgassing from the previous run or elevated partial pressures of water or oxygen due to the additional transfers through the load lock. This situation could be avoided by lengthening the interval between runs and depositing a thicker silicon layer on the tube before the second growth.

4.5 Growth Rates

Calibration of film composition and growth rate of $Si_{1-x}Ge_x$ were made at 530°and 560°C, which covers the temperature range of interest for erbium doping of $Si_{1-x}Ge_x$. In all growths, 20 sccm of silane was flowed with varying amounts of germane. Samples were of two kinds, multilayers of different thicknesses and compositions or a single film with a uniform composition. Energy dispersive spectroscopy (EDS), measured at 5 keV, was used to quantify composition in single layer films with thicknesses greater than 5000 Å so that the x-ray generation volume was entirely inside the film. Single layer strained films were also grown and analyzed by double crystal x-ray diffraction.

Analysis of the multilayer films was done by Rutherford backscattering (RBS). A 2 MeV beam of alpha particles (He^{++}), incident approximately 10° from the surface normal to avoid channeling, was used to determine composition and thickness. An annular detector was used for all data collection. Calibration of the energy per channel, using a silicon sample with a gold monolayer, was done before each session of analysis. The raw data was then simulated by RUMP to finally determine the sample structure.

The incorporation of germanium into the film was linear with respect to germane flow, which is commonly observed for these systems (figure 4-8). The behavior of the growth rate does not follow theory for growth at these temperatures however. Below approximately 600°C, growth rates of silicon from numerous groups have followed an activation rate of approximately 46 kcal/mol, which agrees with the activation energy for hydrogen desorption from silicon[65] reported to be 47 kcal/mol. The hydrogen can come from the dissociation of the hydride SiH_4, but if excess hydrogen is present, it will be the dominant source through the following:

$$H_2(g) \rightleftharpoons 2H(a).$$

The addition of germanium to the growth surface alters the desorption energy due to a decrease in bond strength between Si-H and Ge-H of 40 kJ/mol[66]. Since the desorption energy of hydrogen is reduced, more active sites are available on the surface for the attachment of silane and germane molecules. This additional active surface sites account for the initial increase in growth rate with the addition of germane. At higher germanium concentrations

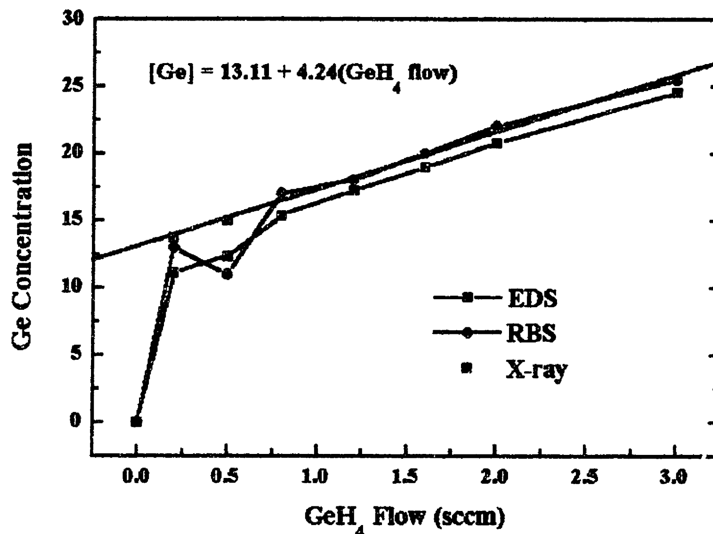

Figure 4-8: Germanium concentration as a function of GeH_4 flow at 530°C with 20 sccm SiH_4 used for all growth runs.

(>15-25%), however, the growth rate typically falls off again. This has been attributed to a reduction in the sticking coefficient of silane and germane on the more 'germanium-rich' surface. Some of the data presented here (see figure 4-9 and 4-10) does not show a decrease in growth rate at higher germanium fractions. This is believed to be an artifact of the measurement technique however. If films are grown just above the kinetic critical thickness and relaxation begins to occur, growth rates increase due to the reduction of strain on the surface. This was the case in the films analyzed by RBS with the three highest germanium fractions, where thicknesses ranged from 3000 to 7000 Å. Measurement of growth rate would therefore be dependent on the thickness of the film and would bias the data to higher values. As the critical thickness is lower for higher germanium fractions, those films are the most susceptible to this error. When films were grown below the critical thickness and analyzed by x-ray diffraction, the predicted behavior was observed.

A point that needs to be stressed when comparing data from different UHV-CVD reactors is that the furnace temperature, measured by thermocouples outside the tube, can be far from the

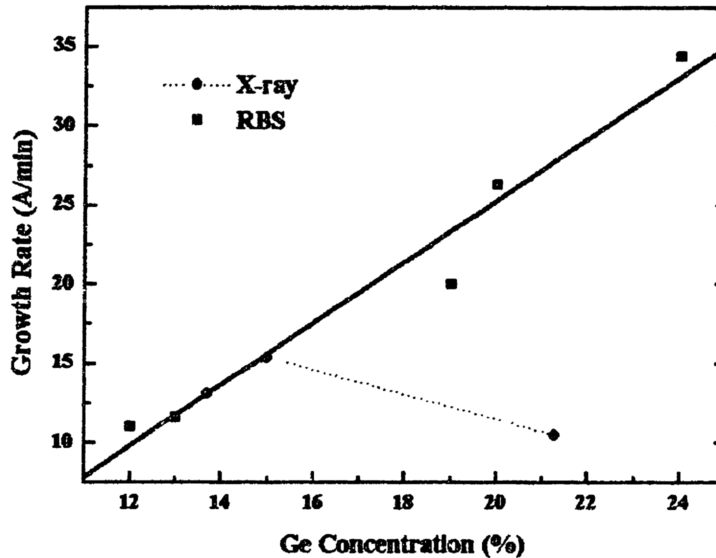

Figure 4-9: Growth rate calibration for $Si_{1-x}Ge_x$ at 530°C.

actual growth temperature. Due to the complexity of UHV-compatible electrical feedthroughs in quartz tubes, it is extremely difficult to calibrate the growth temperature with a thermocouple. As a result, several groups either use optical pyrometers or rely on the furnace thermocouples to determine the growth temperature. Errors as large as 50°C would (and did) occur in this system if similar techniques were used.

4.6 Summary

The $Si/Si_{1-x}Ge_x$ system offers two major advantages for the improvement of quantum efficiency of erbium luminescence; electrical and optical confinement. Figures of merit for these confinements in the composition range studied in this work are 85-100 meV for electrical confinement (valence-band offset) and 5×10^{-2} to 1×10^{-1} for the difference in refraction index.

Growth of $Si/Si_{1-x}Ge_x$ films was done to calibrate the UHV-CVD reactor and check the film quality. Growth rates were determined at 530°C and 560°C and, in general, match the trends and values reported in literature. Film quality was checked by x-ray diffraction and

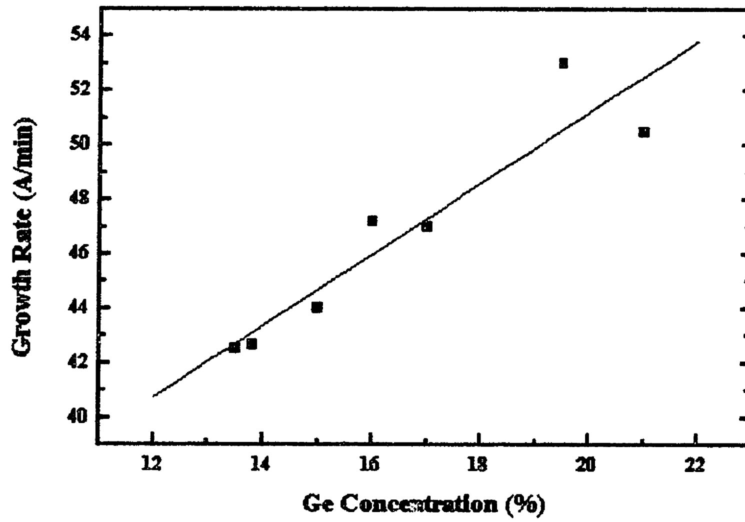

Figure 4-10: Growth rate calibration for $Si_{1-x}Ge_x$at $560°C$. The line is a linear best fit to the data.

photoluminescence. Pendellösung fringes were observed in single layers of $Si_{1-x}Ge_x$, indicating planar interfaces. The FWHM of the no-phonon line in a MQW structure, a measure of thickness and composition flucuations, was 5.9 meV which is comparable with the best MBE and CVD results. The thickness of the $Si_{1-x}Ge_x$ quantum wells was 40 Å even without optimizing the growth time or gas switching procedure, which demonstrates the control of the reactor.

Chapter 5

Growth of Erbium-Doped Films

5.1 Erbium in Silicon

Typical MOCVD almost universally occurs in a cold wall system in which the precursor only cracks on the a single hot substrate. In this unique hot-wall MOCVD system, on the other hand, the precursor can collide several times with the walls or wafers, possibly cracking at any occurrence. Additionally, the precursor or it's fragments can be depleted by depositing on these surfaces before reaching the end of the wafers. To a large extent, precursor chemistry dictates at what location the precursor fragments, and the resulting species incorporated into the film. For this reason, selection of the precursor is crucial in film quality. Only one erbium precursor had been previously studied under conditions similar to this system, and the results showed that the precursor was leaving large amounts (20%) of carbon in the film[27].

5.1.1 Precursors

Three different organometallic erbium precursors have been used in this study. These precursors were selected because each contained erbium already bonded to ligands in the molecule. The first two used, tris(2,2,6,6-tetramethyl-3,5-heptanedionato) erbium(III) [$Er(tmhd)_3$] and tris(1,1,1,2,2,3,3-heptafluoro-7,7-dimethyl-4,6-octanedionato) erbium (III) [$Er(fod)_3$], belong to the β-diketone family and have very similar structures. In both molecules, the erbium is bonded to six oxygen atoms, a complex which could be the optically active structure in CZ-Si. The difference between $Er(fod)_3$ and $Er(tmhd)_3$ is the replacement of one group of $C(CH_3)_3$ with

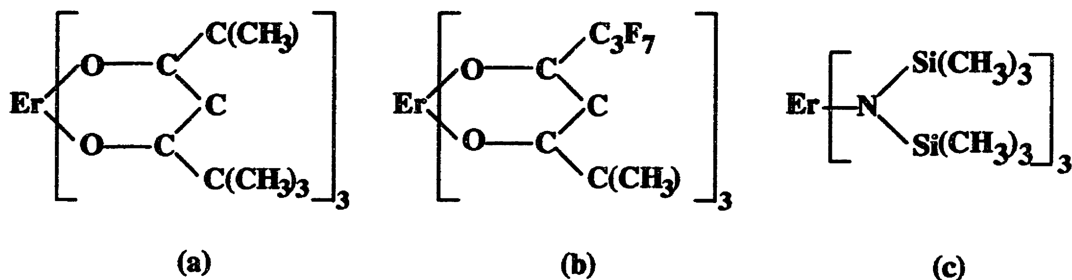

Figure 5-1: Structure of the three precursors used in this study; (a) Er(tmhd)$_3$, (b) Er(fod)$_3$, (c) Er(tmsa)$_3$.

Element	Atomic %
Si	19.4
Er	17.9
O	57.9
C	4.7

Table 5.1: Composition of film deposited by Er(tmsa)

C_3F_7 in Er(fod)$_3$.

This substitution has two effects on deposition. The vapor pressure of the Er(fod)$_3$ is higher due to the fluorinated group[68], which allows the bubbler temperature to be reduced for the same pressure. Since the gas lines from the bubbler to the reactor are heated with heating tapes to a temperature slightly above the bubbler, this reduction makes heating the lines easier. The other effect is that fluorine might also complex with erbium in the film. Studies done with Ba(fod)$_3$ have deposited BaF_2, showing that the fluorine can be 'mobile' enough in an MOCVD reactor to find the metal. The third precursor used in this research, tris(N,N-bis(trimethylsilyl)amido) erbium (III) [Er(tmsa)$_3$], radically differs in both the structure and composition. Erbium is directly bonded to 3 nitrogen atoms and no oxygen is in the molecule. Additionally, the number of carbon atoms has been reduced and it is found only in methyl groups. Thin films (40 Å) from this precursor have been deposited on silica and analyzed with auger electron spectroscopy (AES)[69]. The composition is shown in table 5.1. The author ascribed the carbon and oxygen to atmospheric contamination. The lack of nitrogen reported could be the result of decomposition at the growth temperature of 600°C.

While the reactor does have a dedicated erbium bubbler line, initial heating problems of the

line caused the precursor to condense out before it reached the reactor. Therefore, a temporary modification of precursor delivery was made to simplify the situation. Instead of using the bubbler, a second quartz boat containing typically one gram of precursor was loaded to sit just outside of the furnace, upstream of the wafers. The furnace temperature, heating tapes wrapped around the reactor tube, and boat position were crudely used to control the vaporization of the precursor. Only $Er(tmhd)_3$ was used for this procedure because of its tolerance to small exposures of the atmosphere which occured during loading. Unfortunately, this precursor was never tested in the bubbler due to the large cost of a dedicated bubbler and a previous report describing extremely high carbon incorporation problems. Because of the difference in delivery, some care should be taken in direct comparisons between it and the other two precursors. Since the growth time and amount of powder consumed per run for each precursor was approximately the same, however, the growth environments were similar.

5.1.2 Growth Procedure

The growth of erbium-doped material presented some unique problems which required adjustments from normal growth procedures. The gas line running from the bubbler into the reactor, which needed to be heated to above the bubbler temperature to avoid condensation was the creator of many of these problems. All but one valve was for high temperature use, the exception being there to ensure that no unwanted leak-by due to its superior valve sitting. The maximum operating temperature of this valve was rated at $190°C$, only 40° above the bubbler temperature used for some runs. Months of failure occurred before the necessary control of the heating tapes used to heat the gas lines was gained.

A buffer layer of silicon was grown at temperatures of 560-580$°C$ to take advantage of the higher growth rates. During this time the variable transformers controlling the heating tapes were turned up to begin heating the lines. After 90 minutes the furnace was cooled to the growth temperature. The first zone of the furnace, upstream of the wafers, was set 30-40$°C$ cooler than the growth temperature. This was a compromise between keeping a uniform temperature over the wafers and reducing the distance that the precursor would have to travel at high temperatures. As the furnace was stabilizing, the bubbler temperature turned up. While 50 sccm of hydrogen was following through the erbium line into the by-pass line, the bubbler was

opened up when it reached 100°C. The procedure for this is critical as a mistake can ruin the gas line. The downstream bubbler valve was opened first. The upstream valve was then opened simultaneous to closing a valve which forced hydrogen through the bubbler. This ensured that no excess pressure could build up in the bubbler and allow for backstreaming of the precursor into the unheated upstream gas lines. As the bubbler temperature neared to 5° of the setpoint, the hydrogen was switched into the reactor. Within 3 minutes, the bubbler was at temperature and the official time of the growth run was started. If an erbium-doped $Si_{1-x}Ge_x$film was being grown, the germane would be turned up to the required flow and switched into the reactor just before the hydrogen was to keep the films thickness below the critical thickness. During growth the pressure was constantly monitored on the capacitance manometer for any dramatic changes which could indicate blockage of the bubbler line. When the run was finished, the bubbler temperature would be turned down, but the hydrogen was kept following through it into the reactor after another 2-3 minutes. This was done it sweep out the remaining erbium in the gas phase, keeping the top of the bubbler and its valves free from condensation as it was cooled. The bubbler was then closed in reverse order to the opening procedure. A capping silicon layer was grown on top of the erbium-doped film to facilitate chemical analysis by moving the surface away from the erbium region.

The films doped with $Er(tmhd)_3$were deposited differently since the precursor had to be loaded directly into the reactor. The wafers were loaded into the reactor and a buffer layer was grown while a boat carrying the precursor was placed into the loadlock. When the pressure dropped to the mid-10^{-7} torr range, growth was interrupted and the precursor boat was transferred into the tube just upstream of the furnace. Heating tapes controlled by a variable transformer enabled for a limited control of the rate of precursor consumption.

5.1.3 Comparison of precursors

Luminescence

Due to the relative ease of measurement and the applicability to processes occurring in LEDs, photoluminescence was used as the principle tool to characterize the growths of all erbium-doped films. The system uses an Ar^+ laser as the excitation source incident upon the sample, which is located inside a helium cooled cryostat. Luminescence from the sample was passed

through a Spex 0.75 m spectrometer and collected by a nitrogen-cooled germanium pin detector. Standard lock-in techniques were used for data collection.

Spectra taken at 4 K for silicon doped with each of the precursors are shown in figure 5-2, and were offset for clarity with the intensities roughly normalized. The spectrum of the sample doped with $Er(tmhd)_3$ and grown at $560°C$ has only one distinct feature at 1.538 μm. Little luminescence was seen from samples as-grown by this precursor. The luminescence developed only after annealing under an argon atmosphere. Annealing at temperatures between $400°C$ and $800°C$ was done to optimize the luminescence. The best annealing schedule, $585°C$ for 150 minutes, increased the luminescence of erbium by 55 times. The spectrum in figure 5-2 is from this sample. Doping with $Er(fod)_3$ at growth temperatures of $560°C$ resulted in a much different spectrum, showing a large background and one sharp peak. As-grown samples had 30 times the luminescence of the as-grown $Er(tmhd)_3$ samples. Annealing at $590°C$ for 150 minutes increased the luminescence by a factor of 1.5 with the longer wavelength peak at 1.549 μm rising from the background. The shorter wavelength peak, located at 1.538 μm did not shift during the annealing process. Although the latter peak is close to erbium luminescence seen in several materials, the origin of the former peak is unknown. No photoluminescence spectrum from erbium-doped silicon had a sharp feature at this location. The final precursor, $Er(tmsa)_3$, had strong luminescence from samples without annealing. Two distinct peak are seen with a shoulder at longer wavelengths. Annealing at $590°C$ did not improve the luminescence for these samples. The spectrum showed in figure 5-2 was the first film grown by this precursor, as compared to the best samples doped with the other precursors.

The optimization of photoluminescence for Si:Er doped with $Er(tmhd)_3$ and $Er(fod)_3$ after annealing at $585°C$ is similar to the observed behavior of erbium implanted into semi-insulating polycrystalline silicon (SIPOS)[78]. In that case the improvement was cited to be a combination of defect annealing and an increase of optical active erbium through ligand diffusion. The difference in time and temperature between growth and annealing for CVD, 30 minutes longer and $25°C$ higher during the anneal, should be great enough to cause these effect as well. After annealing amorphous silicon deposited at $560°C$, the loss of optical power decreased by two orders of magnitude, indicating that defects could be reduced at these low temperatures. This would increase the minority carrier lifetime and allow for more efficienct pumping of the

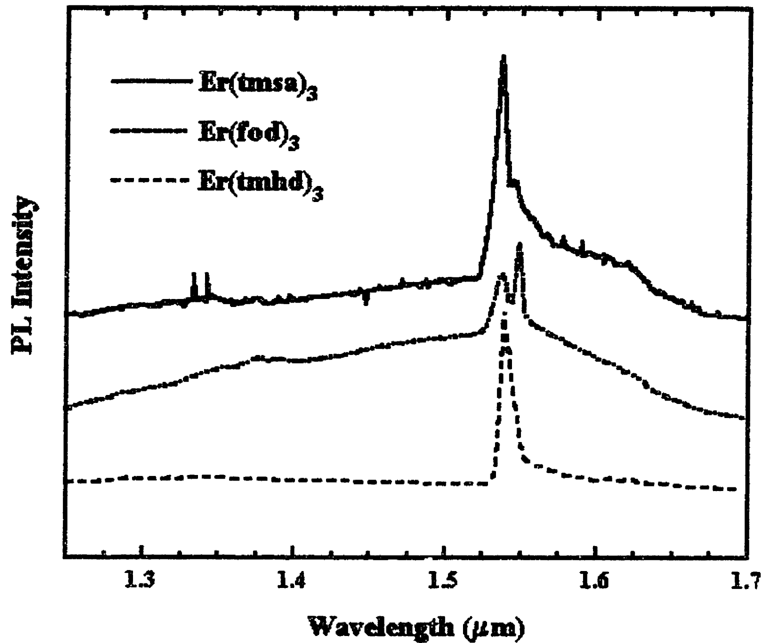

Figure 5-2: Photomuniescence at 4 K of Si:Er doped with three different precursors. All growths were done at 560°C.

erbium. Optical activity could also increase over the small difference of temperature between the annealing and growth conditions because this causes a difference in the oxygen diffusion length of a factor of 3. Since the higher quality material grown by Er(tmsa)$_3$ did not show any improvement upon annealing, the role of defects is most likely the dominant factor for low luminescence in the Er(tmhd)$_3$ and Er(fod)$_3$ materials.

Film Composition

The composition of films grown by each of the precursors was determined by SIMS. Figure 5-3 shows the data from a sample doped with Er(tmhd)$_3$. The film had such high concentrations of oxygen and erbium that quantification of the composition was not possible due to the large deviation from the reference of standard silicon. Atomic percent of all elements were present which resulted in a non-silicon film being grown. This was also manifested by the deep colors

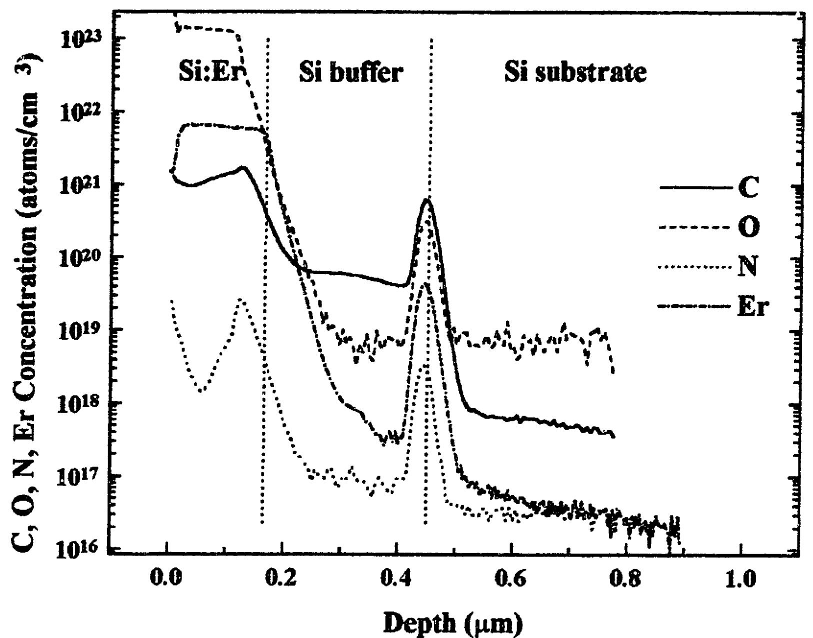

Figure 5-3: SIMS of Si:Er grown at 560°C using the precursor Er(tmhd)$_3$.

the wafers had after deposition which were indicative of a large change in the index of refraction. SIMS of a film doped by Er(fod)$_3$ is shown in figure 5-4, and reveals much lower incorporation of all species in the precursor. Films grown with this precursor, while looking 'silicon-like', did have something resembling soot on them after deposition. SIMS from samples grown with Er(tmsa)$_3$ showed less oxygen incorporation than the Er(fod)$_3$ samples, but a full discussion of the results of SIMS on samples doped with Er(tmsa)$_3$ will be postponed until chapter 6.

Film Quality

A more quantitative measure of the quality of the films was made through the use of glancing x-ray diffraction. This measurement is different from a typical $\theta - 2\theta$ scan in that the incident angle of the x-rays is held constant at a shallow angle. The detector is moved through 2θ to determine the presence of separate phases, polycrystalline structure, or strain. This technique

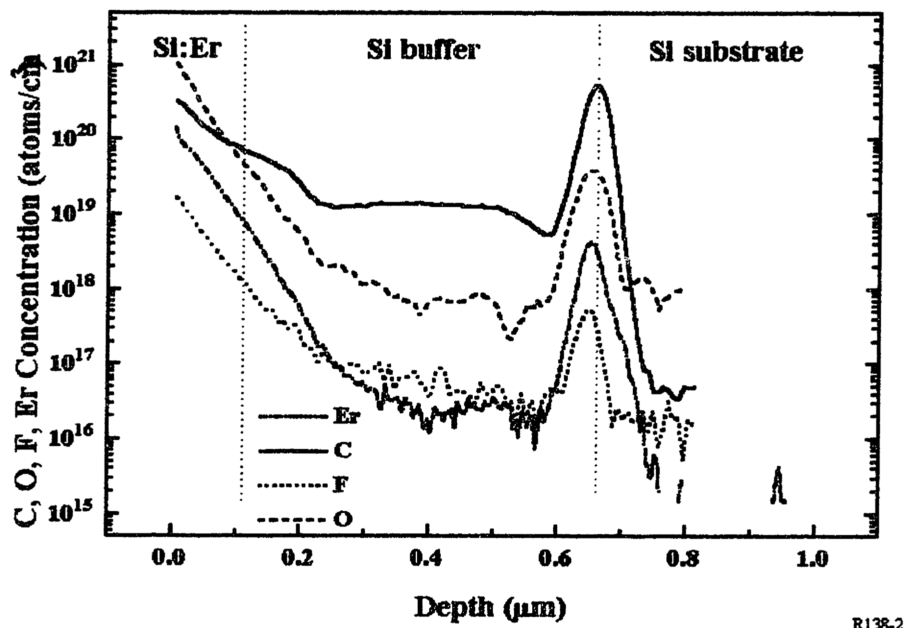

Figure 5-4: SIMS of Si:Er grown at 560°C with the precursor Er(fod)$_3$.

is very sensitive for thin films, although the resolution for small strains is not comparable to rocking curves due to the extra crystal axis in the latter. To ensure that the x-rays were not penetrating too deeply into the substrate, a series of scans were taken at different incident angles to determine which features were due to the substrate and which by the film. An incidence angle of 0.5° was found to give the best results for analysis of the films. Samples from the same films that underwent SIMS analysis were examined with this method. The results are shown in figure 5-5, with a few of the many peaks identified. The $Er(tmhd)_3$ sample exhibits diffraction from several silicon planes, indicating polycrystalline structure, as well as several peaks from Er_2O_3 and SiO_2. The scan of the $Er(fod)_3$-doped sample also reveals polycrystalline silicon and SiO_2, although no Er_2O_3 phase was found. This is reasonable based on the reduction in erbium concentration by two orders of magnitude. In contrast to these two samples, the $Er(tmsa)_3$-doped sample showed no peaks that were not present in the silicon reference, even though the erbium concentration was higher than in the $Er(fod)_3$ sample by 8 times. This is clear evidence that the decomposition of the precursor is the governing factor in crystal quality.

The decomposition pathway of $Er(tmhd)_3$ was studied to understand the mechanism for the degradation of epitaxy. Due to the similarities of structure to the $Er(fod)_3$, some of the results might to applicable to it as well. The experiment was conducted in a molecular beam mass spectrometer (MBMS) with much more capability to detect high mass to charge particles than the RGA on the UHV-CVD reactor. A quartz bubbler filled with $Er(tmhd)_3$ was placed in a small furnace. Helium was used as a carrier gas to drive the precursor from the bubbler, and through another furnace with a temperature which could be varied from 300° to $800°C$, mimicing the CVD reactor chamber. A small vacuum of 10^{-2} torr in the system was obtained through the use of a mechanical pump. The precursor and fragments then passed through an orifice where it was cooled and skimmed to form a molecular beam. This then went to the triple quadrupole mass spectrometer which ionized the molecules before detection. An ionization potential of 22 eV was used to minimize fragmentation in the MBMS which would otherwise obscure the thermal decomposition pathway. The triple quadrupole mass spectrometer was capable of detecting species with a mass to charge ratio (m/z) of up to 700. Due to the large number of possible fragments and ionization states for each m/z ratio, the analysis of the data was particularly difficult. General trends could be observed however. It was clear that

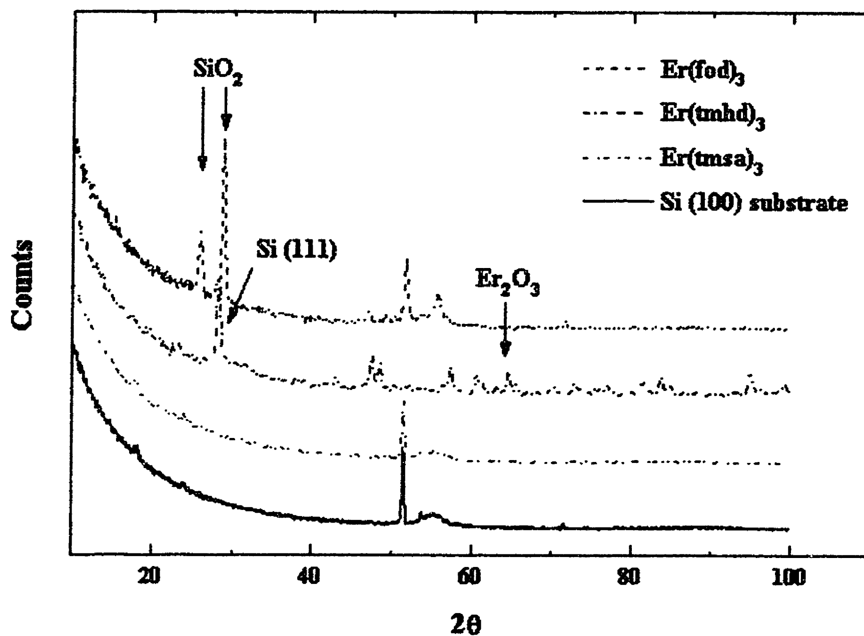

Figure 5-5: Glancing angle x-ray diffraction of Si:Er doped with three different precursors. All growth were at $560°C$. A scan from a silicon substrate is included for reference.

methyl groups and individual ligand groups were present in the beam. Large intensities from fragments of the ligand, such as $[(CH_3)_3CCOC\text{-}C\text{-}]^+$ and $[(CH_3)_3CCO]^+$among others, were also seen. These fragments, which would not be present in the decomposition of the much simpler $Er(tmsa)_3$ molecule, would be highly reactive and able to poison the growth surface.

Due to the superior performance of the superior performance of $Er(tmsa)_3$, research on the β-diketones was discontinued. The rest of the data presented in this thesis was done using $Er(tmsa)_3$ only. Once the selection of a precursor was made, studies on uniformity, growth and the physics of the excitation/de-excitation were undertaken.

5.1.4 Uniformity of Luminescence

In order to develop an understanding of incorporation processes occurring during growth, the intensity of luminescence from erbium and other features was monitored as a function of position in the reactor. Growth runs typically used three wafers spaced approximately 0.75 cm apart in the boat. The orientation of the wafer with respect to the boat was recorded and scribed on the back of samples broken from the wafer after growth. Photoluminescence was done on all samples from a growth in the same day so that variations in the PL setup could be eliminated. The results from Si:Er grown at 560°C with 60 sccm $H_2/Er(tmsa)_3$ flow is shown in figure 5-6. Pieces from the center of each wafer were measured at 4 K with 0.2 W of laser power. The absorption depth of 488 nm light in silicon is approximately 1 μm, so carrier generation occurs throughout the erbium-doped region and into the substrate. The peak at 1.14 μm is luminescence from a bound exciton at a shallow dopant level in the substrate. The intensity of this peak serves as a measure of film quality since carriers generated in the epilayer can diffuse into the substrate if the their lifetime is long enough to permit it. This lifetime is dependent not only upon imperfections in the film but also on the concentration of erbium which serves as a recombination center. As can be seen in the figure, the intensity of this peak increases slightly in going from the first to second wafer, but then precipitously falls in the last wafer. The erbium luminescence quickly falls by 40 % from the first to the second wafer but then only loses another 11% in going to the final wafer. Two other pieces of information can be seen in this plot. The first is that the background signal increases the further back the wafer was positioned. The second thing to notice is the pair of peaks located near 1.61 μm in the third

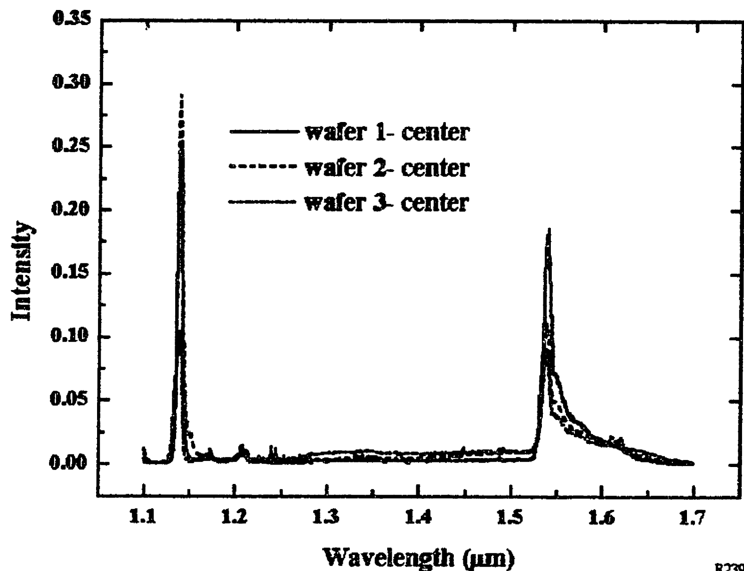

Figure 5-6: Photoluminescence at 4 K of Si:Er from three sample scribed from the center of wafers in the same growth run.

wafer. These peaks have been identified as the P-line, which is a carbon-oxygen defect pair. Typically this defect shows a single peak at 1.616 μm, whereas in this case it is split into two peaks at 1.609 μm and 1.623 μm. At higher temperatures the two peaks do merge into one centered at 1.616 μm. This peak can form in virgin silicon if it is annealed between 450-550°C due the pairing of carbon and oxygen already in the wafer. Since the luminescence from the P-line in the samples is clearly non-uniform, and does not even appear in the first two wafers at 4 K, this source can be neglected.

The same trends are evident when samples taken from different locations on the same wafer are examined. Figure 5-7 shows photoluminescence spectra from the third wafer in figure 5-6. Samples from the top, center, and a position in between were scanned under the same conditions previously reported. In this comparison, the bound exciton line falls continuously with a corresponding increase in the background signal. The P-line increases in intensity linearly from the edge, where it is not evident at this pump power, to the center (see figure 5-8). This is an interesting trend. If the source of carbon was traveling in from the edge either in the gas

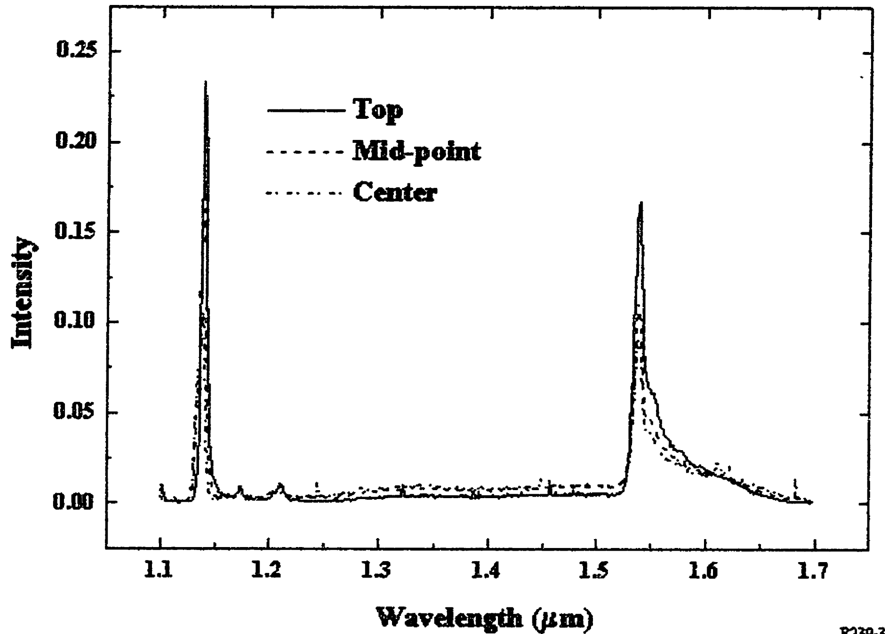

Figure 5-7: Photoluminescence at 4 K from three different samples from the last substrate in the growth run. The samples were scribed from the center, top and a point mid-way in between.

phase or on the surface, the intensity of the P-line, which is proportional to its concentration, would have an opposite trend. On the other hand, an increase in the concentration of 'free' carbon as it traveled toward the center of the wafer would be consistent with the data. This could mean that a gaseous species (possibly CH_3) is breaking apart after several collisions with the wafer, or that a molecular adatom diffusing on the surface was liberating carbon at some point. Since diffusion should be far more isotropic than gas flow under these circumstances, the surface diffusion mechanism is unreasonable.

A variation of photoluminescence can be more clearly understood with the aid of figure 5-8. The intensity of the bound exciton (BE) peak drops sharply in the last wafer of the growth run (wafer #3). This drop in intensity is correlated to the linear increase in intensity of the C-O defect (P-line) as seen in figure 5-8 (b). This is supported by the fact that the second wafer, which did not show the P-line at this temperature and power, had a BE peak intensity that

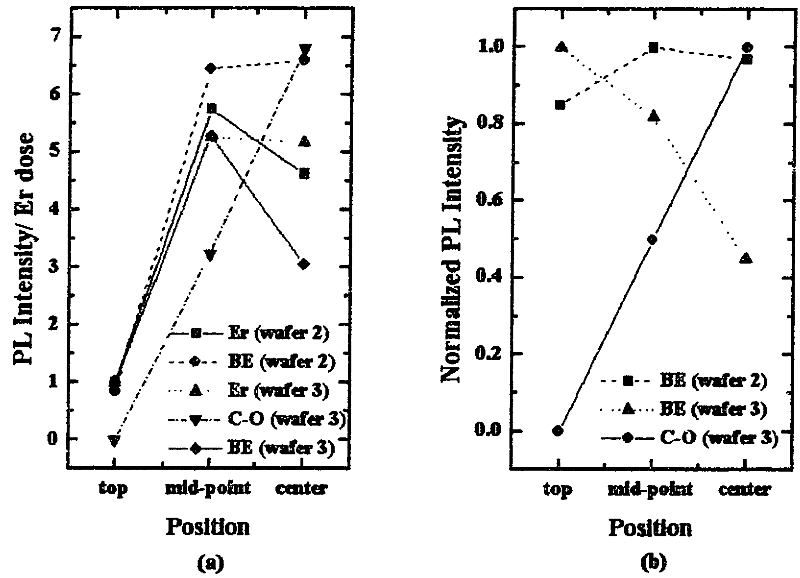

Figure 5-8: Dependence of PL intensity at 4 K as a function of the position across the wafer and from wafer to wafer. In (a), the intensities were divided by the erbium dose at that location. This shows that the liminescence efficiency of erbium is increasing closer to the center of the wafer. In (b), the relationship between the bound excition (BE) line and the C-O defect (C-O) line is shown. No C-O line was observed in the second wafer at this power and temperature.

was not a strong function of position. Errors bars for these points are less than 2% since the signal strength was high. The simultaneous increase of the C-O lines with the decrease of the BE line indicates that either the C-O defect is outcompetiting the shallow dopants (the origin of BE line) for excitons or that a degregation in crystal structure, associated with the increase of carbon, reduces the amount of excitons available. The variation in erbium luminescence is replotted in figure 5-8 (a), where the luminescence has been renormalized to the dose of erbium across the wafer. The doses were determine by SIMS from the second wafer in another growth run. As the growth conditions for both runs were identical, however, only a slight error will be introduced in the use of the SIMS data. That data showed a decrease in the erbium dose by a factor of 7 from the edge to the mid-point followed be a much smaller decrease in going to the center (factor of 1.06). As can be seen, the efficiency of erbium luminescence increases in going toward the center of the wafer. The rise the erbium efficiency, coupled with the increase the the intensity of carbon-oxygen detects, closer to the center of the wafer strongly suggests that the fragmentation of the precursor is enhancing the luminescence of erbium. This fragmentation would create the P-line defect in a pattern as seen in figure 5-8 (b) and would also increase the ligand concentration in the film. A richer ligand environment increases the luminescence of erbium as reported by Priolo[10]. This effect will be discussed in greater detail in chapter 6.

The roll-off of erbium luminescence across the surface of a wafer was used to generate an upper bound for the sticking coefficient of the erbium fragment. Several assumptions were made for this model. The trajectories of the erbium-carrying species were assumed to be unaffected by collisions with other gas molecules. As the mean free path (λ_{mfp}) is long at the growth pressure, this will not adversely affect the results. An average entrance angle between wafers was used to calculate the number of molecule-wafer collisions that would occur from the edge to the center of the wafer. Since the molecule could also stick to the backside of the previous wafer, only every other collision could result in erbium in the film of interest. For this simple model, the total number of collisons from the edge to the center was 21. This number is a lower bound only as interactions in the gas phase will decrease the mean-free path, with a corresponding increase the residence time between the wafers. The exiting angle of the fragments are also random which again increases the residence time and number of collisons. Flux coming from the opposite side of the wafer has been neglected. The model also assumes that there is only one

	Normalized PL ratio	**s**
wafer #2, center	0.684	1.79x10^{-2}
wafer #2, mid-point	0.891	1.00x10^{-2}
wafer #3, center	0.760	1.30x10^{-2}
wafer #3, mid-point	0.816	1.83x10^{-2}

Table 5.2: Calculated sticking coefficients as a function of position on the wafer

sticking coefficient for erbium and that the optical activity does not change across the wafer. Since the molecules are most likely fragmenting at these collisions, this assumption is not totally valid. This error tends to underestimate the sticking coefficient as the optical activity should be higher at the center than the edge (see discussion in chapter 6). Data from samples which were plotted in figures 5-6 and figure 5-6 were used to calculate the sticking coefficient across the second and third wafers. No calculation for the first wafer was attempted since the flux at the surface should be nearly unifrom. The sticking coefficient, s, can be found by

$$(1-s)^n = \frac{[Er]_x}{[Er]_{edge}}, \tag{5.1}$$

where n is the number of collisions and $[Er]_x$ and $[Er]_{edge}$ are the erbium concentrations at the point of measurement and the edge respectively. The term on right was approximated by the photoluminescent intensity normalized to the intensity at the edge of the wafer. The calculated values for the sticking coefficient are shown in table 5.2.

These numbers are approximately one order of magnitude higher than those of silane or germane which is reasonable considering the difference nonuniformity between the two groups.

5.1.5 Glancing Angle X-ray Diffraction

X-ray diffraction was used as a definitive test for the theory that the crystal structure was degrading as a function of the position of the wafer. Figure 5-9 shows glancing angle x-ray diffraction scans of five Si:Er samples all grown at 560°C. They are identified by the growth run number (e.g. R239), followed by the wafer number of that run. Five peaks have been identified, three of which are present in reference silicon and are labeled by S. The two other peaks arise from diffraction of other silicon planes, indicating poorer quality films. The two films which were the first wafers in their respective runs only have the three substrate peaks.

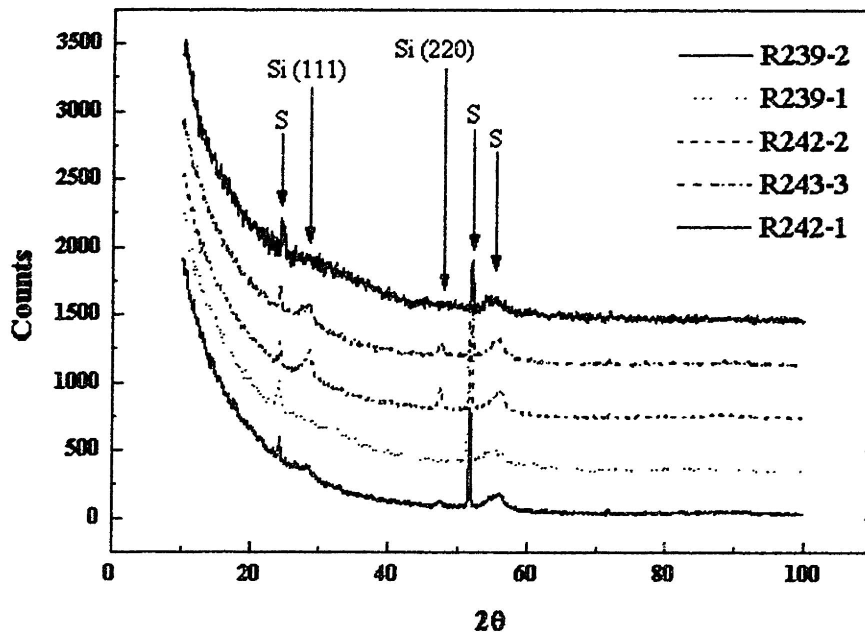

Figure 5-9: Glancing angle x-ray diffractions scans of Si:Er from samples scribed from substrates in different positions over several runs.

The other films, located further back during the runs, show the substrate peaks as well as the Si (111) and Si (220) peaks. This confirms that the first wafer has the highest quality structure.

5.1.6 Electrical Activity

The electrical activity of erbium in silicon has been reported to be of both donor and acceptor type. The confusion is caused by the added electrical activity of defects caused during the incorporation of the erbium. More recent studies have been converging on donor behavior for erbium though. Zheng[36] has reported n-type behavior with a carrier concentration approximately 50 times lower than that of the erbium concentration. The carrier concentration was also shifted closer to the surface than the erbium distribution. This was attributed to ligand outdiffusion and to possible interaction with implantation defects. Other groups have also observed similar reductions in carrier concentration[64] in ion-implanted material. No reports of

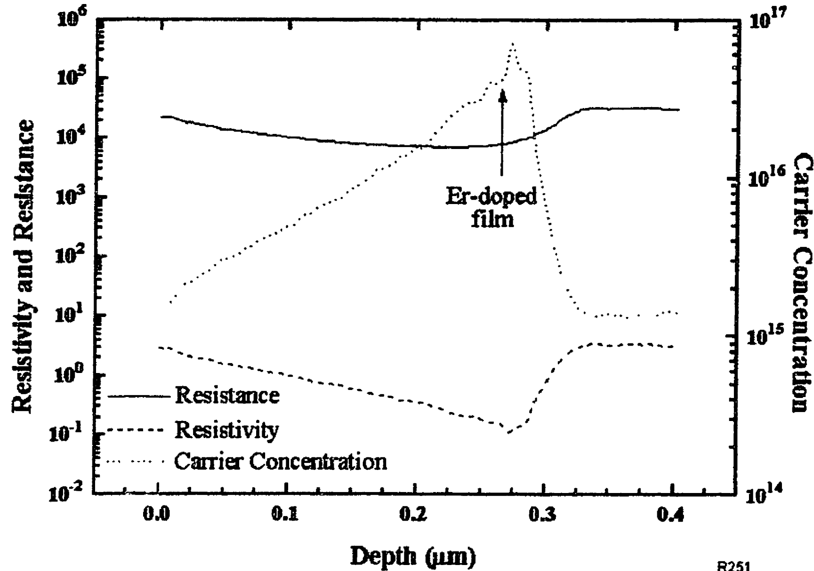

Figure 5-10: Spreading resistance of Si:Er with an undoped Si capping layer. The erbium concentration was determined to be $3\text{x}10^{20}/cm^3$ by RBS.

any electrical behavior of erbium-doped silicon made by any method but ion implantation have been published.

Spreading resistance measurements from two films are shown below in figures 5-10 and 5-11. In both samples the erbium-doped film showed n-type behavior with approximately 0.03% and 0.28%, respectively, of the erbium concentration having donor behavior. Although enough measurements have not been done to know if this difference is meaningful yet, it would be consistent with other data. Specifically, the sample with 0.28% electrically active erbium was scribed from the third wafer (furthermost back in the reactor) where the ligand/erbium ratio should be highest. The sample with 0.03% electrically active has taken from the second wafer in another growth run, with a lower ligand/erbium ratio. If this is the case, co-doping with boron to make erbium films intrinsic will only be successful in a limited range in the reactor. The lower donor activity of the CVD samples as compared to the implanted samples is not understood.

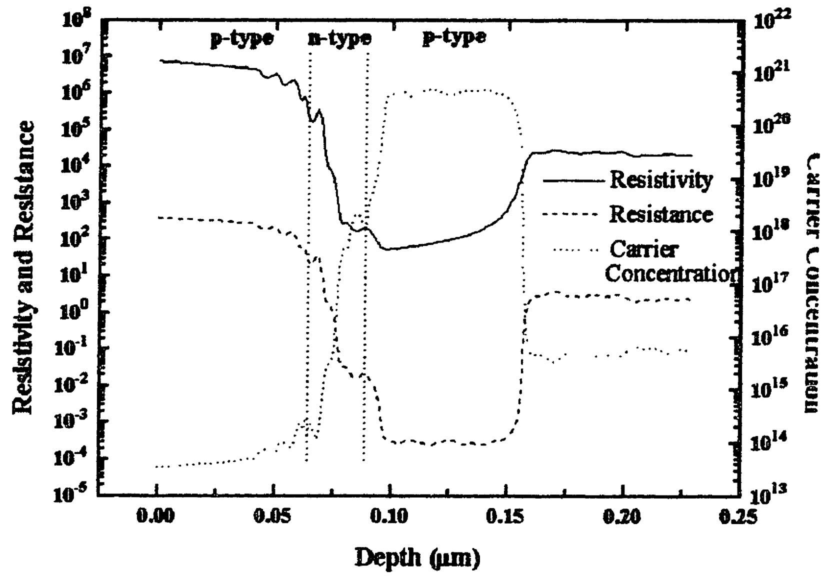

Figure 5-11: Spreading resistance of a Si:Er film grow on top of an epi-p^+ layer. An undoped capping layer is also present. The erbium concentration is 7x$10^{20}/cm^3$.

5.2 Erbium in $Si_{1-x}Ge_x$

5.2.1 Luminescence

The photoluminescence of erbium in $Si_{1-x}Ge_x$ is similar to that already shown for silicon. Figure 5-12 shows the PL of a series of $Si/Si_{1-x}Ge_x$(Er) double heterostructure growth runs. The maximum intensity came from a sample doped with an erbium concentration of $3x10^{18}/cm^3$, the highest concentration found in any of the second wafers in growth runs. Because it was hard to determine erbium concentration below $10^{18}/cm^3$ in RBS, the correlation of intensity to concentration is not entirely clear however. The sample with the best resolution of satellite erbium peaks also had the lowest concentration ($<10^{18}/cm^3$). Not coincidently, the structure of this film had the lowest channeling yield in RBS which indicates higher quality material. Cross-sectional transmission electron microscopy (XTEM) was also done on this sample and is shown in figure 5-13. The quality of the $Si_{1-x}Ge_x$ film and the Si capping layer have no defects within the sensitivity of the measurement (i.e. $<10^6/cm^2$). It is not yet possible to decouple the effects of concentration and structure which are leading to the sharper luminescence. As the distance between the erbium centers at a concentration of $3x10^{18}/cm^3$ is well over 100 Å, broadening by exchange interaction is not a factor since it operates on much smaller distances. Other mechansims, such as dipole interaction, could still allow for boardening though.

Increased temperature quenching of erbium luminescence in smaller bandgap materials has been reported in the $In_{1-x}Ga_xP$ system[70][71]. A model for this system was proposed in the the erbium-related state in the bandgap was tied to the vacuum level. As the conduction band in higher indium alloys moved nearer to that state, the activation energy needed for thermalization decreased making quenching easier. As earlier work comparing IV, III-V, and II-VI materials by Favennec[72] also showed temperature quenching of erbium luminescence was a stong function of bandgap, a concern in the $Si_{1-x}Ge_x$ system was that significantly less room temperature light would be detected. At the germanium concentrations examined in this study (x<0.20), this was not the case. Indeed, the sample with the highest room temperature intensity was a $Si_{0.9}Ge_{0.1}$:Er film. The spectra taken at room temperature is shown in figure 5-14. This is only the second report of room temperature luminescence from SiGe alloys[73], the first coming from relaxed $Si_{0.87}Ge_{0.13}$ films which were implanted with erbium. Quenching

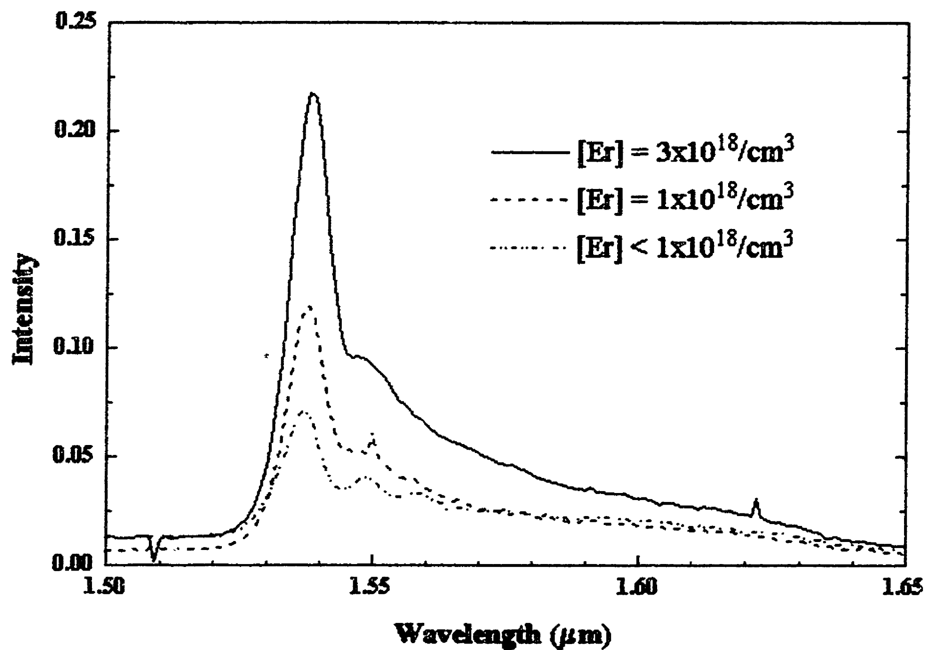

Figure 5-12: PL at 4 K of $Si_{1-x}Ge_x$ grown at 530°C. The increasity increases with increasing erbium concentration upto $3\times10^{18}/cm^3$, the highest value measured in the second wafer of a growht run.

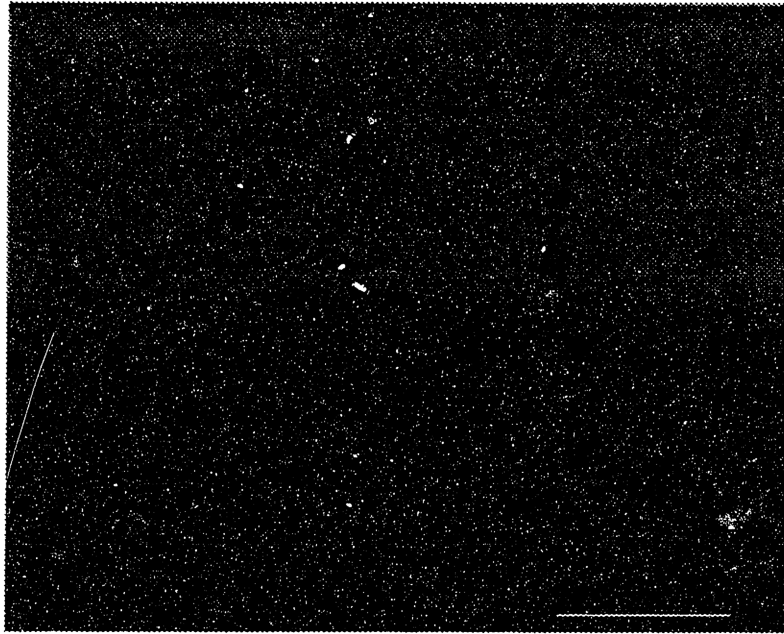

Figure 5-13: XTEM of $Si_{0.9}Ge_{0.1}$:Er. The erbium-doped region is the dark area, with a lighter silicon capping layer above it. This was taken under a weak beam (220) condition in an attempt to reveal any defects. None could be seen though. The space bar is 100 nm.

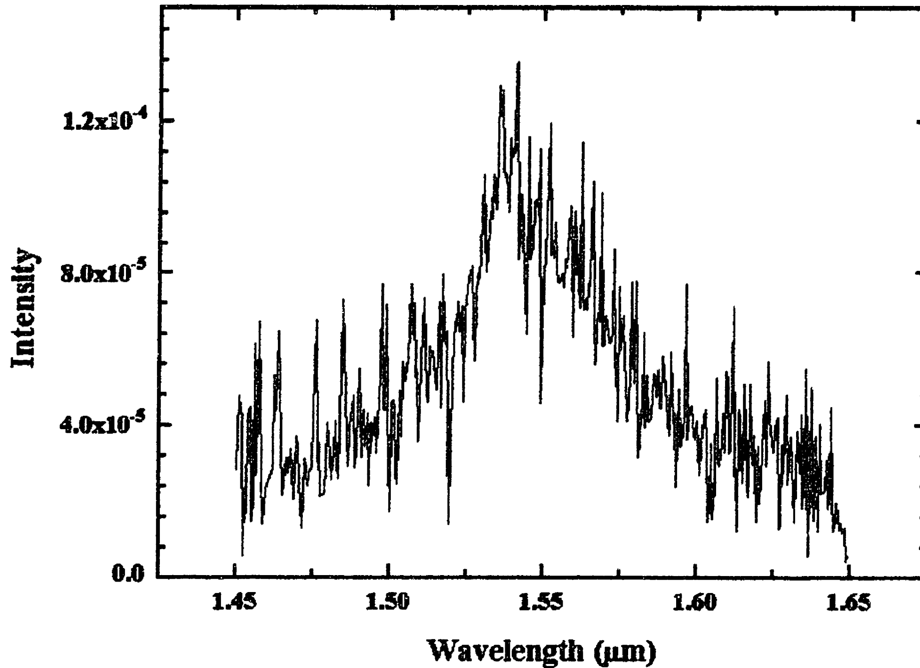

Figure 5-14: Room temperature photoluminescence of $Si_{1-x}Ge_x$:Er.

will be discussed more fully in a latter section.

5.2.2 Lattice Position of Er

The lattice position of erbium is important in determining the type of crystal field splitting. Several groups have used RBS channeling to measure the concentration of erbium on lattice sites as compared to interstitial sites. Gillin[74] examined erbium implanted silicon (with no oxygen co-implant) and found that erbium was distributed on the both sites. More recent work in silicon tends to find erbium only in interstitial sites. No RBS work has ever examined erbium in SiGe alloys. Due to the difference in the lattice with increasing germanium content, it is unclear how erbium would behave in this system. This technique is based on the comparison of spectra from random and channeled scans. When the sample is aligned with the beam so that large 'channels' are co-linear to it, few alpha particles are backscattered and the intensity

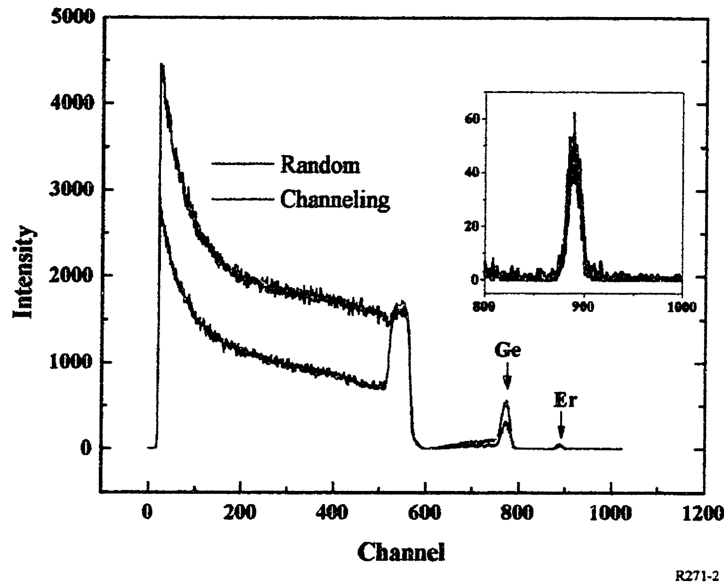

Figure 5-15: RBS channeling and random spectra of $Si_{1-x}Ge_x$:Er grown at $530°C$. The inset is of the erbium peak.

goes down. Atoms sitting in interstitial sites would still backscatter, however, so the ratio of the channeling yield to the random yield gives the relative proportions of the concentration is substitutional and interstitial sites.

Figure 5-15 shows a comparison of the random and channeling scans. The capping silicon layer, located near channel 500, shows no channeling and is the result of polysilicon growth on top of the erbium-doped $Si_{1-x}Ge_x$ layer. This film also shows poor quality ($\chi_{min} = 50\%$) although it is much better than the capping layer. The inset of the figure focuses on the erbium peak. Since there is no difference between the two scans, 100% of erbium is in an interstitial site. This has also been seen in erbium-doped silicon and agrees with most theoretical models.

5.2.3 Segregation of Ge

The segregation of germanium in the MBE growth of SiGe alloys has been widely reported [75][76][77]. Due to the strain involved with incorporation, germanium finds it energetically

favorable to sit on the surface. If the surface mobility of germanium adatoms is reduced, however, incorporation will occur because the germanium becomes buried before it can move to another surface site. Under typical CVD conditions, the surface is mostly covered with hydrogen which blocks germanium motion and prevents segregation. Figure 5-16 shows a RBS scan from a run which occured under such conditions (R353). This was a $Si/Si_{1-x}Ge_x$ double heterostructure run which was intended to duplicate an erbium run as much as possible without the actual presence of erbium. The hydrogen flow which normally was sent through the bubbler when doping with erbium was simply directed into the reactor so that the growth pressure (and partial pressures) would be nearly identical for both types of runs. The germane flow rate was slightly higher than normal so the height of the germanium peak should not be compared with the erbium runs. Both the top (right) and bottom (left) surfaces of the undoped $Si_{1-x}Ge_x$ film are vertical in the scan which means that no segregation had taken place. On runs where the erbium precursor was flowing, however, a shoulder to the right of the main germanium peak is seen, clear evidence of nonuniform germanium incorporation. The germanium concentration in this region typically reached a steady state value between 1 and 1.5%, with a layer thickness between 1500 Å and 4000 Å. Assuming that this layer had been grown for the entire time the germane had been flowing through the reactor, the growth rate would be approximately 20 times the expected rate. The erbium in these films was found only in the high germanium concentration regions.

This behavior is consistant with germanium segregation. Figure 5-17 shows that the maximum germanium concentration (in the high germanium concentration film) is related to an effective dose of germanium in the region with low germanium concentration. This indicates that germanium is being pushed ahead of the lower [Ge] film and is incorporated into the higher [Ge] film. Also seen in figure 5-17 is the dependence of the peak erbium concentration on the effective dose of germanium in the film with low germanium concentration. The behavior would seem to suggest that the segregation is inhibited by the presence of erbium, but as the phenomenom is only seen under erbium doping, that relationship is not causal. The behavior could also be intrepreted in another way. Less erbium is incorporated into $Si_{1-x}Ge_x$ films which have a higher concentration of germanium. As the incorporation of both germanium and erbium would increase the compressive strain in the film, the reduced incorporation of erbium

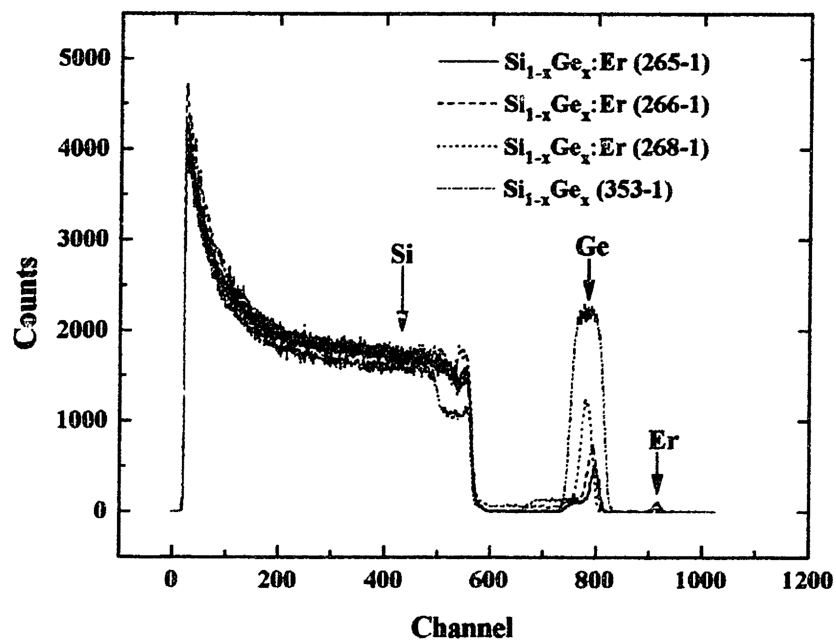

Figure 5-16: RBS spectra of $Si_{1-x}Ge_x$ growth runs with and without erbium doping. All films were grown at $540°C$ and the same pressure.

at higher germanium fraction could simply be due minimization of strain energy at the surface. Figure 5-18 shows the strong correlation between the maximum counts (which is proportional to concentration) of germanium and erbium. The slope of the linear fit is -0.25, meaning that 4 germanium atoms introduce the equivalent amount of strain as one erbium 'atom', although a cluster might be more accurate. The number is larger than one for two reasons; bonding and size. Germanium wants to form tetrahedral bonds just as silicon does, while erbium does not. The size of the germanium atom is also 1.2 times smaller than erbium which means that less strain is created if germanium is incorporated. As seen in the distribution coefficients of isovalent impurities in silicon (Ge and Sn), the effect of size on incorporation is not linear, but increases by an order of magnitude going down one element in the column (size difference<1.2x). Since erbium is not isovalent in silicon, the size effect on incorporation might be mitigated, but the trend is correct. These factors lead to an increased effective solubility of germanium, or put another way, a lower penalty for incorporation.

The finding that the incorporation of germanium and erbium is competitive has far-reaching implications in this research. As can be seen in figure 5-18, as the germanium concentration increases the incorporation of erbium is hindered. Above 18% germanium, RBS could not even detect erbium, which means that the erbium concentration is below $10^{18}/cm^3$. Since erbium concentrations close to $10^{20}/cm^3$ are required for useful optical devices, the germanium fraction cannot be arbitrarily set, and should be approximately 10% or below. This limitation places further constraints on the electrical and optical confinements that are achievable in this system. Finally, it should also be noted that competitive incorporation can occur in other systems where two species which introduce the same sign of strain are being incorporated into the film. As this effect is already operative for strains estimated to be 1% or lower in the $Si_{1-x}Ge_x$:Er system, it is quite possible that it could have significant impact in other important material systems.

The direct cause of the germanium segregation is not well understood however. Any model which fits the segregation must also include the increased growth rate. As all films shown in figures 5-16 and 5-17 were grown at the same temperature and gas flows, the difference in germanium incorporation is remarkable. The segregation could not be fit to the erbium concentration, bubbler temperature, or the duration of the preheating of the gas lines. As these are the only 'erbium' parameters controlled in the experiments, modeling of segregation was

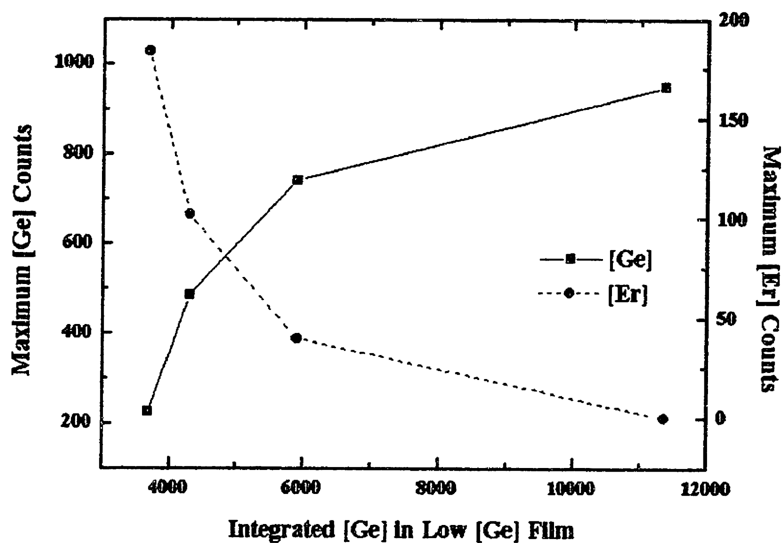

Figure 5-17: Dependence of peak germanium and erbium concentrations on the integrated area of germanium in the low content $Si_{1-x}Ge_x$ film. Integration was carried out over channels, not depth.

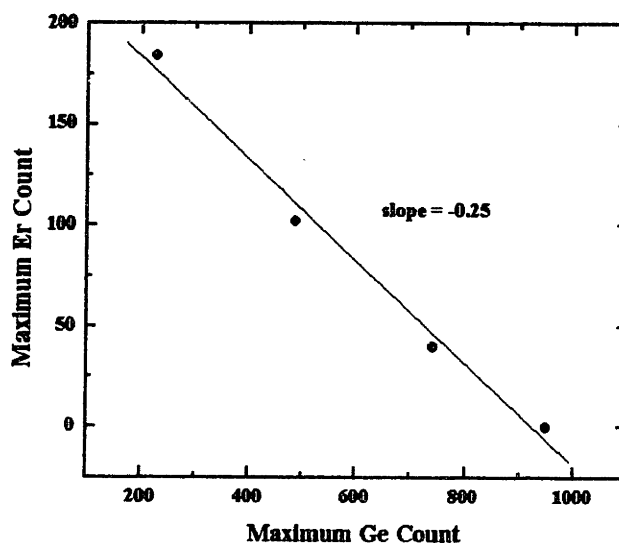

Figure 5-18: Correlation of erbium concentration to the germanium concentration in the segregated $Si_{1-x}Ge_x$ film.

unsuccessful. A plausible mechanism which explains both the segregation and the increased growth rate is a reduction of surface hydrogen. Since hydrogen desorption is the limiting step in growth at these low temperatures, growth rates would increase if the coverage of hydrogen was decreased. The elimination of surface hydrogen would also allow for more mobile germanium with segregation ensuing. Future experiments will be need to determine whether this is occurring or not, and what would be the cause of it.

5.3 Summary

Three different precursors were used as the metallorganic source of erbium to determine which one would give the strongest luminescence and best crystal structure. Si:Er films which had $Er(tmsa)_3$ as the source showed ten times the luminescence at 4 K as films doped with the other two precursors. Crystal structure of the films was determined by glancing angle x-ray diffraction and also revealed that the $Er(tmsa)_3$ films were superior to the $Er(tmhd)_3$ and $Er(fod)_3$-doped films. This was most clearly seen in the additional phases and polycrystalline structure of the

latter while the former and no different features than the substrate itself. Work was therefore only continued on the $Er(tmsa)_3$ source for these reasons.

Inter- and intrawafer variation in the photoluminescence within an order of magnitude has been observed at 4 K. The luminescence was strongest on the first wafer and the edges of other wafers and slowly dropped in the interior of the wafers. This roll-off in luminescence did not closely follow the erbium concentration, however, since the concentration dropped nearly an order of magnitude more than the luminescence over the same distance across the wafer. After the luminescence was normalized to the erbium concentration, however, it was observed that the efficiency of the erbium was actually increasing from the edge to the center of the wafer. Photoluminescence measurements at 4 K also show the development of a C-O complex (at 1.61 μm) near the center of downstream wafers, which corresponds to the fragmentation and incorporation of carbon containing species with increased collisions between the wafers. The increase of erbium luminescence efficiency with precursor fragmentation can be attributed to the change in the local environment of the erbium, and this will be more fully discussed in the next chapter.

Growth of the first $Si/Si_{1-x}Ge_x$ double heterostructures has been achieved. It was shown through RBS channeling measurements that 100% of the erbium is located in interstitial sites. Signs of segregation were also seen in RBS, with a thick film of low concentration of germanium (1-1.5%) followed by a higher germanium concentration film in which erbium was incorporated. Although the cause of the segregation could not be determined, a competitive incorporation mechanism (mediated by strain) between germanium and erbium was clearly seen. It was found that 4 germanium atoms had a strain equivalence of one erbium atom.

Chapter 6

Excitation and De-excitation of Erbium in Si and $Si_{1-x}Ge_x$

This chapter discusses the interaction between the local environment of erbium and the resulting optical behavior. Previous work in SPE of Si:Er by Priolo *et al.*[10] has shown that erbium luminescence can be increased by increasing the the ratio of oxygen concentration to erbium concentration, with an optimum ratio of 10:1. Temperature quenching in films with high ligand to erbium ratios was also significantly reduced by as much as an order of magnitude. Based on results showing passivation of damage-related deep level defects and an increase in the concentration of an erbium-related level, the mechanism of improvement with increasing oxygen was reported to be an increase in pumping efficiency. Results from CVD grown material will also show that the ligand environment is not constant for all films in the same growth run and that the ratio of ligand to erbium is critical in governing the luminescence intensity.

6.1 Optically Active Sites

Due to the large concentration of possible ligands, the local environment of optically active erbium in CVD grown material is not as clear as in ion implanted material. In order to understand where the luminescence is coming from, comparisons of high resolution photoluminescence between the CVD grown and FZ-Si ion implanted with various ligands were made. The scans were all taken at 4 K with an instrument resolution of 4 Å. Figure 6-1 shows scans taken on Si:Er and

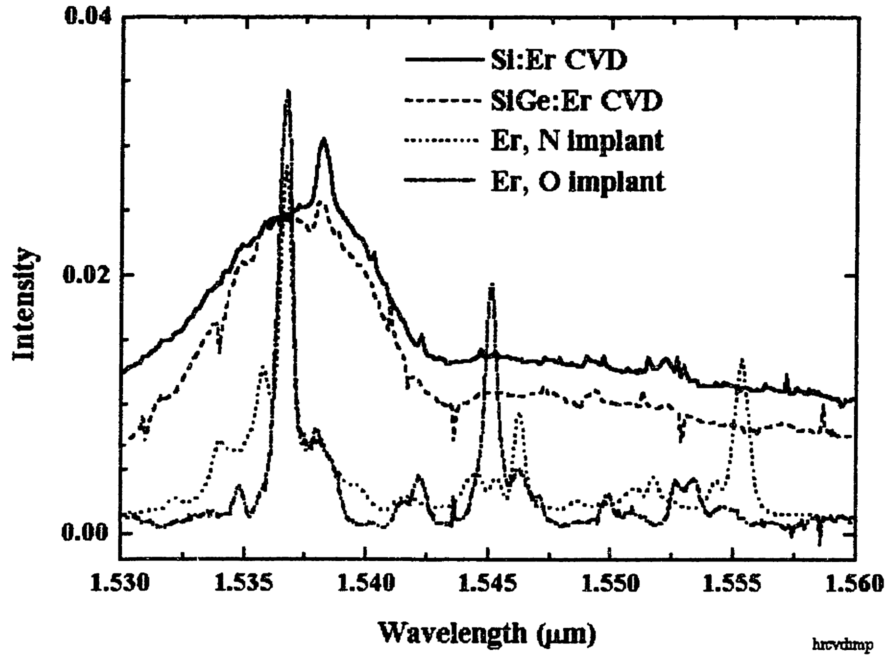

Figure 6-1: High-resolution photoluminescence measurements at 4 K of Si:Er and $Si_{1-x}Ge_x$:Er samples. Spectra from float zone silicon implanted with Er/O and Er/N are shown for comparison.

$Si_{1-x}Ge_x$:Er grown by CVD, as well as Er/O and Er/F implants. The erbium concentrations in the CVD samples were $4\times10^{20}/cm^3$ and $1\times10^{18}/cm^3$ for the Si:Er and $Si_{1-x}Ge_x$ samples respectively. The implanted samples both had an erbium concentration of $5\times10^{17}/cm^3$. Both CVD samples have a broad peak with a sharp feature at 1.5382 μm, with the $Si_{1-x}Ge_x$ sample also showing smaller peaks at 1.537 μm, 1.5361μm, and 1.5349 μm. The Er/N implanted sample has an intense peak at 1.5367 μm with smaller lines at 1.5358 μm, 1.5341 μm, and 1.5381 μm. The spectra from the Er/O also has peaks at 1.5367 μm and 1.5380 μm, but the differences in higher and lower energy peaks can clearly be seen. Unfortunately, no Er/C FZ-Si sample was on-hand to see if that ligand field was operating in the CVD samples, although it is known that the most intense peak for Er/C is at 1.5368 μm.

The two orders of magnitude difference in erbium concentration in the CVD samples makes

a fair comparison of photoluminescence structure between them difficult. Either strain effects or erbium-erbium interactions could effect luminescence at higher erbium concentrations. Nevertheless, comparisons to implanted samples should be valid as the spectra of both CVD grown materials are generally similar. The lines in the implanted samples have been reported to come from different centers due to the number and differences in energy level splittings[5]. It it not required, therefore, that the dominant peak in the CVD sample match the dominant peak in an implanted sample. Ligand environments which exist in small populations in one method could be favored in the other. The major peak in CVD samples at 1.5382 μm falls on top of smaller peaks of the implanted samples, particularly the Er/N implant. A shorter wavelength peak of 1.5349 μm is similar to an Er/O peak however. The fact that the CVD spectra are dominated by a broad peak indicates that there are far more different environments around the erbium than in the implanted samples, so it should not be surprising if erbium is complexing with any ligand around it. The sharp feature in the high resolution spectra could signify that one of these clusters is more optically active then, or that one cluster is likely to be formed. It is not possible at this time to distinguish between these.

Another approach to understanding the local environment of erbium in CVD-grown films is by chemical analysis. Samples from the first and second wafers of the same run ($Si_{1-x}Ge_x$:Er) were examined by SIMS. Strong differences in the composition can be seen. Figure6-2 shows the SIMS results of a $Si_{1-x}Ge_x$:Er sample with strong luminescence at 4 K. This sample was grown at 540°C with the upstream zone at 515°C. SIMS of the second wafer of this run is shown in figure 6-3. The erbium concentration has fallen by over two orders of magnitude by the second wafer. The ratios of erbium to ligands has also changed dramatically and is summarized in table 6.1. Also included in the table is a Si:Er sample grown by ECR-PECVD which also used $Er(tmsa)_3$ as the precursor. The ratio of nitrogen to erbium incorporated into the upstream-most wafer in UHV-CVD and the ECR-PECVD film is exactly the ratio in the precursor (3:1), meaning that the core erbium-ligand bond is surviving up to at least 540°C for some time. The carbon-erbium ratio is slightly carbon poorer in both films when compared to the precursor. The sample prepared by ECR-PECVD does have a much larger oxygen to erbium ratio (14.7 times) however, which is due either to contamination of the precursor or etching of the quartz used to confine the plasma. SIMS does show peak in the oxygen in the erbium-doped region in

	Wafer #1	Wafer #2	ECR-PECVD
$[Er]_{peak}$	$4.2\times10^{20}/cm^3$	$1\times10^{18}/cm^3$	$2\times10^{19}/cm^3$
$\frac{[N]_{peak}}{[Er]_{peak}}$	3	41.6	3
$\frac{[O]_{peak}}{[Er]_{peak}}$	0.17	7	2.5
$\frac{[C]_{peak}}{[Er]_{peak}}$	17	375	15

Table 6.1: Comparison of the ratio between erbium and possible ligands. Data from a sample grown with the same precursor by ECR-PECVD is also included

the first UHV-CVD film, also possibly indicating that the precursor contained a small amount of water. The oxygen would be quickly incorporated in the presence of erbium and silicon and be depleted as it travels down the tube since it does not appear in the second film. In light of the high resolution photoluminescence measurements showing broad emission, however, it is clear that there must be more to the story. If the theory that most (if not all) of the erbium is bonded to 3 nitrogen atoms is accepted, then next-nearest interactions must be creating the difference in the local environment which broadens the emission. The next-nearest neighbor could be oxygen, carbon or silicon.

In contrast to the first wafer, the second wafer does not have concentration ratios remotely resembling the precursor. The carbon-erbium ratio increases from 17 in the first wafer to 375 in the second wafer and the nitrogen-erbium ratio increases from 3 to 42. This clearly indicates that the precursor is breaking apart as it travels through the reactor. It can be inferred that the precursor is breaking in at least two places. The erbium-nitrogen bond must be breaking with the nitrogen fragment more easily incorporated into the film. Additionally, either the nitrogen-silicon or silicon-methyl bond is breaking (or both) which releases large amounts of carbon into the system. Again, the carbon fragment must be more readily incorporated into the film than the erbium to account for the large increase in the ratio. This could be expected based on the size and chemistry of carbon relative to erbium.

The trend of decreasing crystalline quality the further downstream the wafer cannot be directly associated with the concentration of ligands as those are actually decreasing downstream. It is consistent with an increase of precursor fragments. While the ligands are still bonded to erbium they are not able to block active surface sites and disrupt epitaxy. Smaller hydrocarbon will poison these sites however.

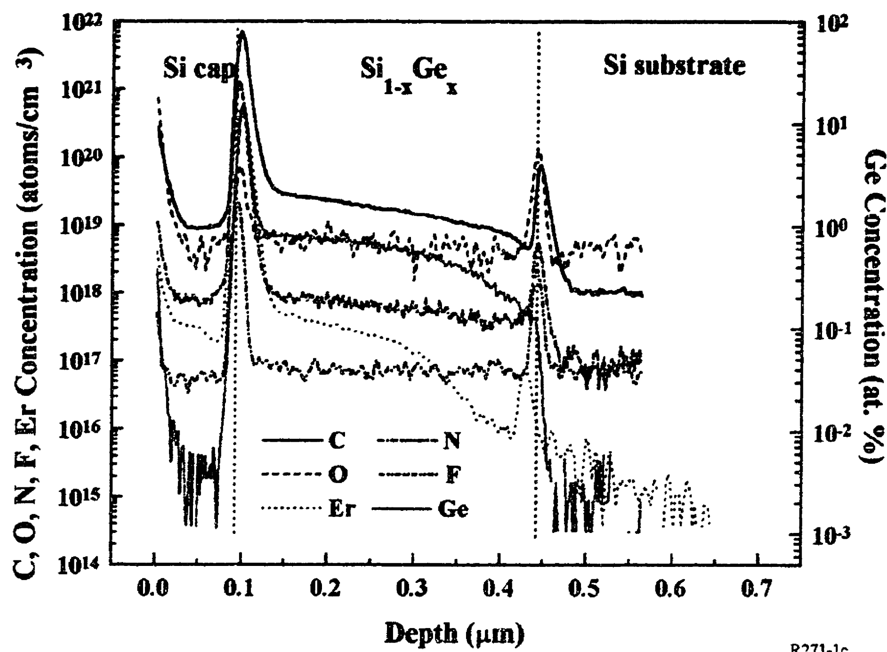

Figure 6-2: SIMS of $Si_{1-x}Ge_x$:Er grown at 540°C. Besides the species in the precursor, oxygen and fluorine were also monitored since they could be contaminants.

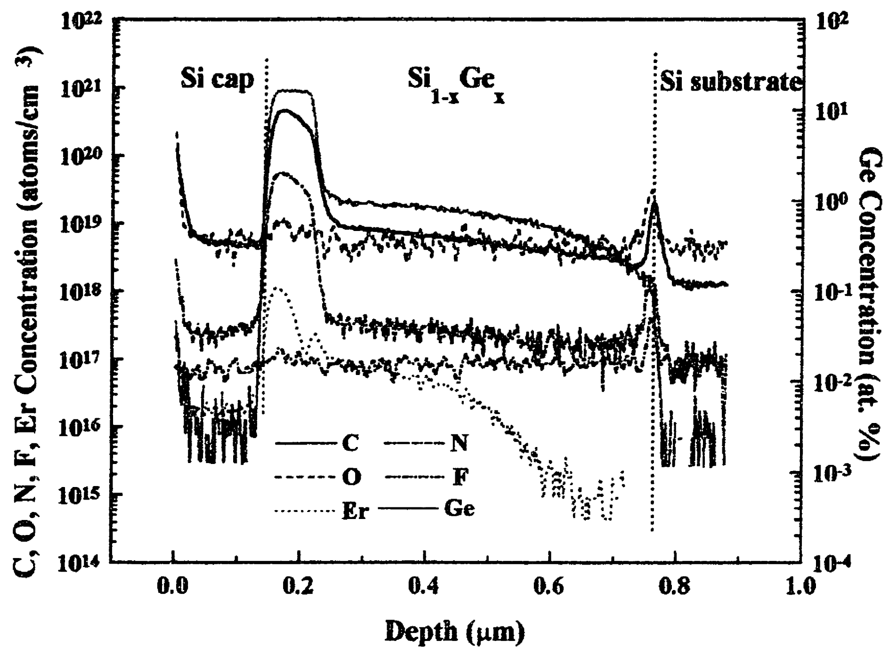

Figure 6-3: SIMS of $Si_{1-x}Ge_x$:Er. This sample was scribed from the wafer directly located behind the wafer (during growth) for which SIMS was reported above.

6.2 Quantum Efficiencies

The low internal quantum efficiency (η_i) of erbium hampers the ability to get a reasonable amount of power out even at low temperatures. Contributions to the internal quantum efficiency can by broken up into two factors according to

$$\eta_i = \eta_{pump} \cdot \eta_{rad}, \tag{6.1}$$

where η_{pump} is the pumping efficiency, and η_{rad} is the radiative efficiency of the erbium. The former factor is governed by issues such as crystal quality and dopant concentration since both provide pathways to redirect excitons away from the erbium. The radiative efficiency is more closely related to the local environment around the erbium since this affects how quickly energy can be transferred away from a erbium center relaxing by non-radiative means. More insight can be gained by making the dependencies of the factors in eq 6.1 more explicit[14];

$$\eta_i = \frac{1}{(1+\frac{\tau_{ex}}{\tau_{cp}})} \cdot \frac{1}{(1+\frac{\tau_{sp}}{\tau_{bt}})} \tag{6.2}$$

where τ_{cp}, τ_{ex}, τ_{sp},and τ_{bt} are the lifetimes for electron-exciton Auger recombination, erbium Auger excitation, spontaneous emission of erbium and non-radiative backtransfer from the erbium. Since the terms in eq. 6.2 are strong functions of temperature and power, η_i can vary by over three orders of magnitude for the same sample depending upon the measurement conditions. The internal quantum efficiencies of erbium-doped $Si_{1-x}Ge_x$ have been measured at for 4 K by measuring the output power with a Newport power meter. Several corrections due to optical losses in the system had to be made to arrive at correct input power (P_{in}) and output power (P_{out}) values. The excitation power reaching the sample was only 30% of the laser power due to losses at a filter, two mirrors, and the cryostat windows. Reflection of the incident light at the silicon surface has also been taken into account. Corrections to P_{out} include losses at the cryostat windows, lenses and a notch filter designed to let light only at 1.54 μm into the power meter. These losses reduced the output power by a factor of 95. Measurements were taken at laser powers ranging from 0.1 to 1.5 W. The internal quantum efficiency decreased over this range from 1.2×10^{-5} to 1.8×10^{-6}. This number neglects the fact that only 4.2% of the light generated inside of the silicon is within the critical angle of the

silicon/air interface and can escape to be detected. If this is also included in the calculation, the internal quantum efficiencies range from 2.9×10^{-4} to 4.3×10^{-5}. By referencing the voltage on the germanium pin photodetector to the power output, a estimate of quantum efficiencies of erbium-doped silicon could be make by comparing the PL intensity. The Si:Er sample with the most intense luminescence was calculated to have a η_i of 2.3×10^{-4} at the lowest power (0.1W) and 5.9×10^{-5} at the highest power (1.5W).

These quantum efficienices are very low compared to III-V materials, but it is important to put them into context. Palm[14] reports a η_i of 2×10^{-5} at 1.6 W and 4 K for silicon implanted with erbium at 4.5 MeV. A forward biased LED which was fabricated from very similar material had an internal quantum efficiency of 4×10^{-4} at 100 K[36]. The improvement in η_i, made more impressive in light of the increased temperature, is due not to material quality but to a more efficient excitation process in electroluminescence. When the implantation energy was reduced to 400 keV using the same processing steps in LED fabrication, the quantum efficiency increased by a factor of 2.5[36]. Franzò[17] reports values for η_i for SPE regrown LED's in forward and reverse bias of 1.5×10^{-5} and 1.5×10^{-4} respectively, at room temperature. Extrapolating back to 77 K, these values become 3×10^{-4} and 5×10^{-4}. Although the η_i of the CVD samples is comparable to these values at lower temperatures, thermal quenching makes the samples less than competitive with the SPE samples.

The intensity of erbium luminescence as a function of power is proportional to the internal quantum efficiency by

$$I(p) = \frac{\eta_i}{hv}p, \tag{6.3}$$

where $I(p)$ is the intensity, and p is the pump power. As already discussed, η_i is comprised of a pumping and radiative efficiency factors. Figure 6-4 shows the raw power dependence data for a Si:Er and $Si_{1-x}Ge_x$:Er sample with the highest erbium luminescence. Although the $Si_{1-x}Ge_x$:Er sample has a higher initial slope, and hence higher η_i, than the Si:Er sample, this finding was not consistant with all $Si_{1-x}Ge_x$:Er samples. Differences in the quality and thickness of the capping silicon layer can contribute to the variation in slopes as nonradiative defects could reduce the power actually reaching the erbium-doped film. It is therefore not possible to determine if the electrical confinement effect in $Si_{1-x}Ge_x$ is improving the internal

quantum efficiency. As the thinnest $Si_{1-x}Ge_x$:Er film grown is 250 Å thick, it is possible that the local confinement of the exciton to the erbium is a bulk-like process and no confinement would be seen. Thinner films should be grown to more clearly see the onset the confinement effects. Figure 6-5 shows the normalized power dependence of CVD grown Si:Er and $Si_{1-x}Ge_x$:Er. A silicon sample implanted with erbium at 400 keV is also included. The most striking feature is that the implanted sample is already saturated at 0.1 W while the CVD samples cannot be saturated even at 1.5 W. One possible explanation for this would that higher erbium concentrations in CVD films simply cannot be pumped hard enough to be saturated. As several of the CVD samples shown in the plot have erbium concentrations within a factor of two of the implanted sample, however, effects from erbium concentrations cannot be the source of the difference. Since the environment of the erbium is not the same throughout the sample, the ability of the erbium to luminesces is unequal and a comparison based on the erbium concentrations is not strictly fair. An estimate of the optically active fraction of erbium in silicon implanted with erbium has been made by Zheng[12] when the sample was in saturation by

$$P_{out} = \frac{N_{Er}^{opt} \cdot hc}{\tau_{sp}} \tag{6.4}$$

where P_{out} is the output power of erbium luminescence, N_{Er}^{opt} is the number of optically active erbium and τ_{sp} is the radiative lifetime of erbium. For Si:Er implanted at 400 keV, an LED had an estimated optically active percentage of 7.4% of the total erbium present. Since the CVD samples could not be saturated, this calculation cannot be done. However, the effective optical cross-section and the optically active fraction are figures of merit for the same process, as can be seen in eq. 6.5, where $\sigma_{o,i}$ is the effective optical cross-section (discussed later) of erbium in environment i. It is therefore not critical (or even possible with simple measurements) to distingish between the two.

$$P_{out} \propto \sum N_{Er,i}^{opt} \cdot \sigma_{o,i} \tag{6.5}$$

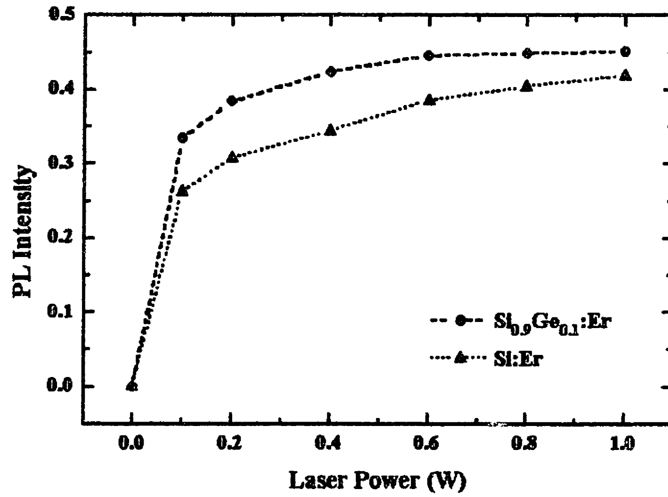

Figure 6-4: Raw power dependence dependence of the Si:Er and $Si_{1-x}Ge_x$:Er samples with the highest 4 K luminescence.

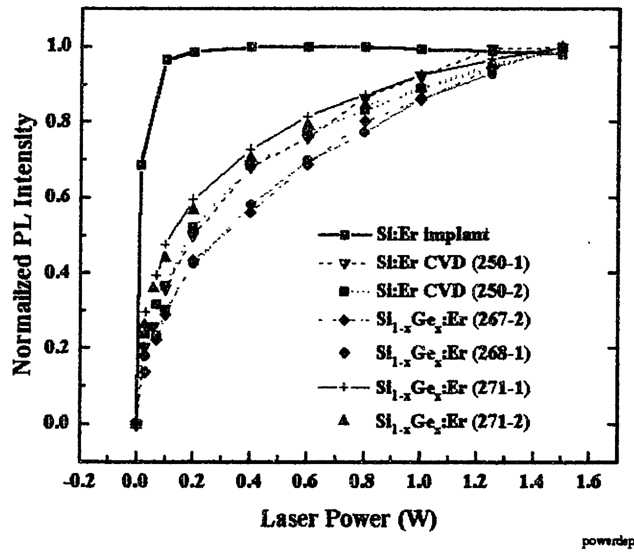

Figure 6-5: Normalized PL dependence of erbium luminescence at 4 K of implanted and CVD-grown material.

6.3 Lifetime Measurements

In order to better understand the differences in power dependence between the implanted and CVD grown materials, lifetime measurements of the erbium luminescence were taken as a function of power and temperature. Data collection was similar to photoluminescence with the exception that a faster InGaAs detector with a notch filter for 1.54 μm was used instead of the Ge detector. The signal from the detector, together with a triggering signal from the chopper, was sent to an oscilloscope were it was averaged over 256 points. Response time of the system was approximately 10 μs. The falltime of the luminescence was fit to either a single or double exponential decay to extract the lifetimes of the decay processes. Raw data taken at 4 K for an implanted sample, a Si:Er CVD sample and a $Si_{1-x}Ge_x$:Er CVD sample are shown in below in figures 6-6, 6-7, and 6-8. It is important to note that excitation of the erbium after the pump light is chopped can be neglected. The minority carrier lifetime is estimated to be below 1 μs based on capture by erbium if a trapping cross-section of $10^{-16}/cm^2$ and a thermal velocity for electrons of 10^6 cm/s are assumed. Excitons trapped near erbium have a lifetime of only 4 μs[14] which is not resolvable in the system.

There is a clear difference in the fall time between the implanted and CVD samples. Both CVD samples have a fast initial decay, as seen by the vertical drop in intensity when the pump light effectively turned off by the chopper. This sharp decrease require the use of a double-exponential fit to model the data. The decay curves for the implanted sample were fit by both a single-exponential fit and double-exponential fit. No improvement in fitting was observed in going to the double- exponential model at 4 K, so only data for the single-exponential will be reported. Figure 6-9 shows the lifetimes extracted from the fitting for the different pump powers. The error bars on the lifetime caused by the fitting are approximately ±10%. Some of these measurements were done twice to check the repeatibility of the system. The values were within 5% and the trends were identical.

The long lifetime in all samples was near 1 ms, which represents the spontaneous lifetime (τ_{sp}) seen in figure 1-1. This lifetime is statistically significantly smaller in both the CVD samples as compared to the implanted sample. The only explanation is that the oscillator strength of the $4f$ transition is stronger due to different crystal field splitting in the CVD samples. The shorter lifetime seen in the CVD sample is indicative of a non-radiative backtransfer process

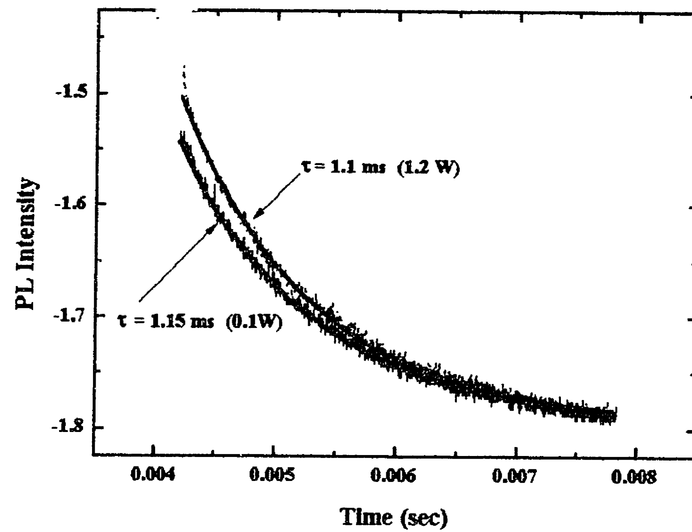

Figure 6-6: PL decay curves at 4 K of Si implanted with erbium at 400 keV. Fits to the curves are shown.

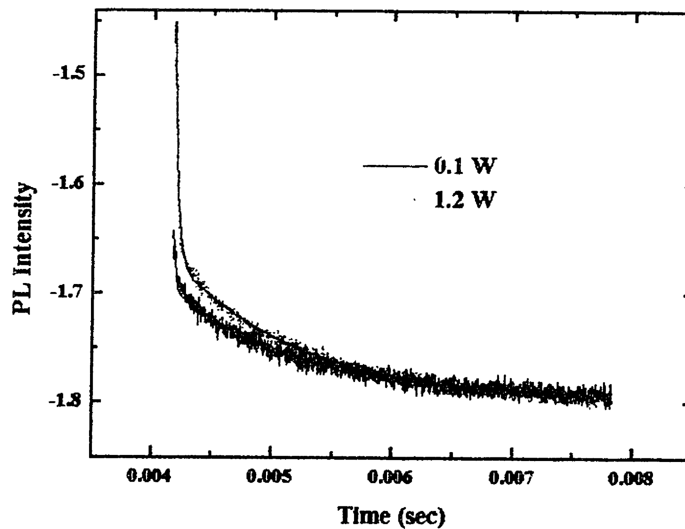

Figure 6-7: PL decay curves at 4 K of Si:Er grown by CVD at 560°C. A double exponential equation was used to fit the data (as shown).

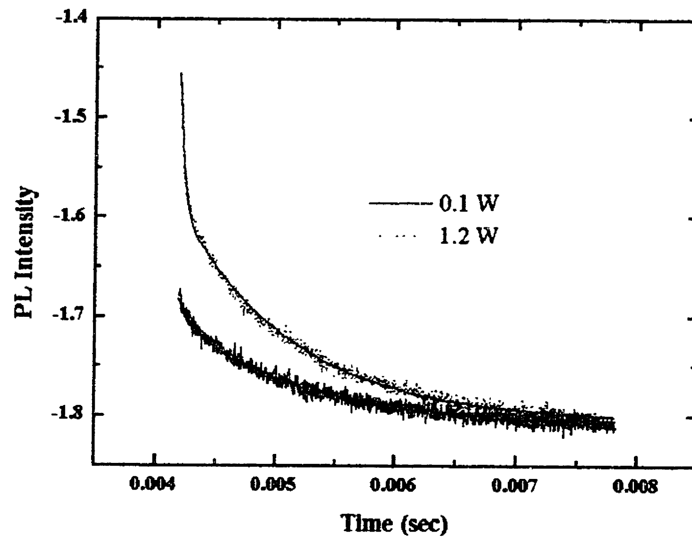

Figure 6-8: PL decay curves at 4 K of $Si_{0.92}Ge_{0.08}$:Er grown by CVD at 560°C. A double exponential equation was used to fit the data.

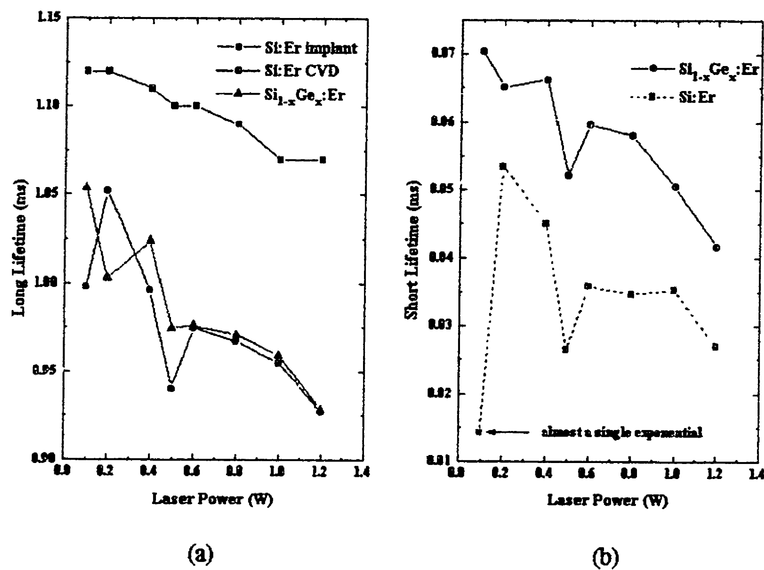

Figure 6-9: PL decay lifetimes at 4 K of implanted and CVD grown material; (a) long lifetimes, (b) short lifetimes.

with a lifetime τ_{bt}. It cannot be a reduced pumping efficiency as this would not generate a smaller lifetime.

Some information about the backtransfer process can be inferred from the difference between the Si:Er and $Si_{0.9}Ge_{0.1}$:Er samples. The effect of Auger backtransfer on lifetime can be expressed as

$$\frac{1}{\tau_{bt}} = c_A n \tag{6.6}$$

where τ_{bt} is the backtransfer lifetime, c_A is the auger coefficient and n is the carrier concentration. At 4 K there are no thermally generated free carriers in Si or $Si_{1-x}Ge_x$, and n is not changed to the first order between these cases. However, the interaction of the pump light with the material is different due to the differences in the absorption coefficient, α. At 488 nm, silicon has an α of $5.07\text{x}10^3/cm$ while $Si_{0.9}Ge_{0.1}$ has an estimated value of $3\text{x}10^4/cm$. Taking into account the thickness of both films and the exponential nature of the absorption process (Beers Law), the $Si_{0.9}Ge_{0.1}$ should have approximately 1.3 times the number of free carriers of the silicon and a corresponding reduction of 77% of τ_{bt}. Since τ_{bt} in the $Si_{0.9}Ge_{0.1}$:Er film is actually larger, the Auger process cannot be invoked to account for the difference.

6.4 Effective Optical Cross-Section

The effective optical cross-section of erbium (σ_o) is defined in the equation

$$\sigma_o = \frac{\Phi_{out}}{\Phi_{in}} N_{Er}, \tag{6.7}$$

where Φ_{in} and Φ_{out} are the incident and emitted photon fluxes, and N_{Er} is the areal density of erbium. The photon fluxes can be easily calculated from the data collected from the quantum efficiency measurements by dividing the power by the appropriate photon energy. This calculation was carried out on samples from the same wafers for which SIMS was shown. These were the first and second wafers of an erbium-doped double heterostructure growth run. Because the erbium concentration decreased by more than two orders of magnitude while the PL intensity actually slightly rose from the first to second wafers, σ_o for the second wafer was greater than two orders of magnitude larger than the first wafer. These values are summarized in table 6.2,

	Complex	N_{Er}(cm^3)	Ligand:Er ratio	σ_o(cm^2)
Si:Er implant	Er/O	5x10^{17}	4	2.2x10^{-18}
$Si_{0.9}Ge_{0.1}$:Er (wafer #1)	Er/N?	4x10^{20}	3	9.4x10^{-19}
$Si_{0.9}Ge_{0.1}$:Er (wafer #2)	Er/?	1x10^{18}	400	4.5x10^{-16}

Table 6.2: Effective Optical Cross-Section of Erbium. The data was taken at 1.5W

and show an almost linear dependence of σ_o with ligand to erbium ratio. This result is surprising for the CVD samples since the precursor had clearly dissociated by the time it reached the second wafer. Since the crystal quality was decreasing in wafers further downstream, it might be expected the defects would compete with erbium complexes for the capture of excitons and thereby reduce the effective optical cross-section. It is clear, however, the the effect of increasing the ligand to erbium ratio through the fragmentation process outweighs the degregation in the film structure. The large ratios of concentrations of ligands to erbium shown in table 6.1 for the second wafer could indicate that the erbium is either forming more optically active centers, or more efficient ones after the precursor breaks down. This implies that the 'pure' erbium-nitrogen center found in the precursor is not the most efficient and that better results could be found with another precursor.

As equation which describes the effective optical cross-section (eq. 6.7) can be directly converted into a definition of quantum efficiency (eq. 6.3), the larger optical cross-section should lead to a larger quantum efficiency for the CVD material., as previously reported. The difference in the internal quantum efficiency between the CVD and implanted material was only a factor of 2, however, instead of the larger difference seen in the optical cross-section. This discrepancy is due to the different implantation conditions in the reference samples. The implanted sample used as a comparison for quantum efficiency was implanted at 4.5 MeV and had a higher dose, while the implanted sample used for the effective optical cross-section was implanted at 400 keV. As the 4.5 MeV samples are known to have a far higher quantum efficiency at 4 K, even after normalizing to erbium concentration, the discrepancy in the comparison between CVD and implanted is following the expected behavior.

6.5 Temperature Quenching

The decrease of luminescence with respect to temperature was measured for implanted and CVD grown samples. The laser power was 1 W for all measurements. Figure 6-10 shows the photoluminescence intensity plotted against temperature so that the differences between the samples could be seen more easily. Palm[13] has analyzed the implanted sample and found two backtransfer regimes, as previously discussed, demarcated by the breaking point at close to 100 K. These two regimes are not clearly seen in the CVD samples, which suffer from an initial fast roll-off in luminescence at low temperatures. The reason for this is not understood. Photoluminescence lifetime measurements show a fast lifetime in the turn-off in the CVD samples which is not present in the implanted sample until higher temperature are reached. This is characteristic of a backtransfer process, but no experiments have been done to discover the origin yet. The higher temperature quenching is not as severe in the CVD samples as in the implanted samples. Data close to room temperature is difficult to get for the CVD samples, however, because of interference with the P line. The normal growth temperature is ideal for the formation of this defect and even low concentrations will emit light at high temperatures or powers. The peak broadens with increasing temperature until it finally overlaps with the erbium peak. Annealing has been done to remove the defect but a reduction of intensity of the erbium is also observed.

This same data is plotted against inverse temperature to determine the activation energies of the quenching processes. The implanted sample, co-doped with oxygen, showed an activation energy near 150 meV as previously reported. The CVD-grown Si:Er and $Si_{0.9}Ge_{0.1}$:Er samples had activation energies for quenching of 80 meV and 70 meV respectively. Silicon implanted with erbium and nitrogen and regrown by SPE had an activation energy identical to erbium/oxygen implants[37], namely 150 meV, so the difference in activation energies between the samples is unknown.

The importance of the small energy difference in thermal quenching between the Si and $Si_{1-x}Ge_x$ samples on the physics of de-excitation can be understood with some knowledge of the band structure in the $Si_{0.9}Ge_{0.1}$ sample. The valence band offset in the Si/$Si_{0.9}Ge_{0.1}$ double heterostructure is 85 meV. Studies in the III-V materials doped with erbium showed that the erbium level in the bandgap was tied to the vacuum level. When alloying was done in those

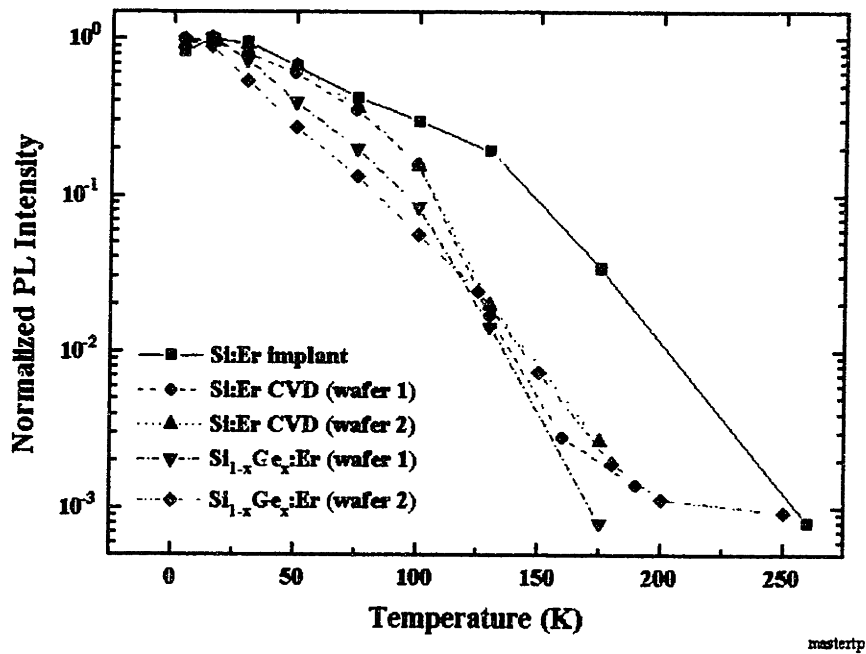

Figure 6-10: Normalized temperature dependence of erbium luminescence in Si:Er and $Si_{1-x}Ge_x$:Er. The pump power was 1.0 W for all measurements.

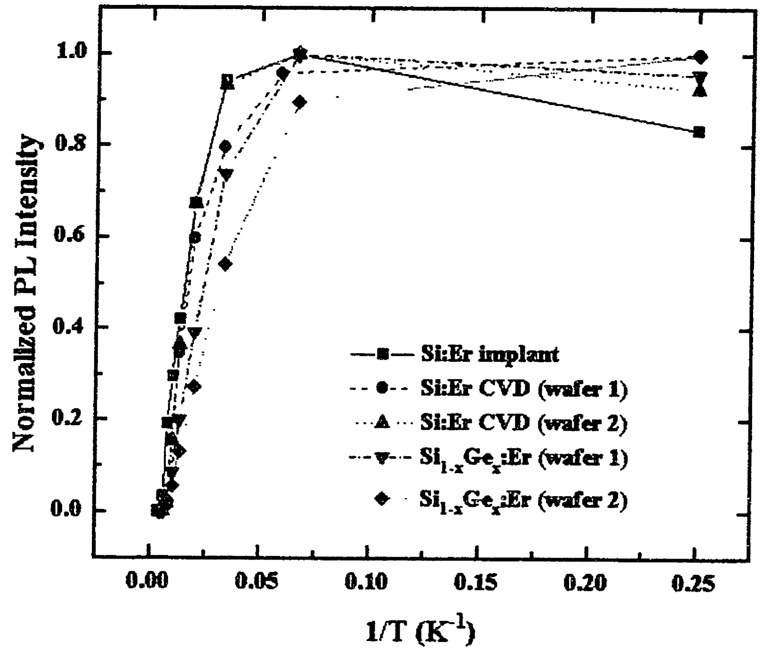

Figure 6-11: Temperature dependence of erbium luminescence plotted against recipirical temperature.

systems, the activation energy would shift by the offset in the conduction band (this was because the de-excitation of erbium was not phonon-mediated, but only required the thermalization of a carrier from the erbium state into the conduction band). If the limiting process in the multiple phonon non-radiative backtransfer process is the phonon participation, the activation energy should decrease by the valence band offset. Clearly that is not the case since the difference between the two samples is only 10 meV, with an error of approximately 30 meV. If, on the other hand, the limiting step was the thermalization from the state into the conduction band, the activation energy would remain constant or change by a small amount depending on whether the $E_c - 0.15$ state was tied to the vacuum level or conduction band. Because of scatter in the data, no attempt can be made to answer which of these two options is correct.

The temperature quenching of an erbium-doped silicon sample made by ECR-PECVD was also compared to UHV-CVD grown samples. Both techniques used $Er(tmsa)_3$ as the precursor,

but growth in the PECVD system occurred at $430°C$. The photoluminescence intensity only fell by a factor of 40 from 4 K to room temperature, but a large background present even from low temperatures. Table 6.1 lists the reported ligand ratios for this sample. Just like the first sample in the UHV-CVD run, the PECVD sample has maintained the 3:1 ratio of nitrogen to erbium. However, the sample also has a high concentration of oxygen which might be the reason for the reduced quenching. Previous studies have shown that increasing the oxygen to erbium ratio is effective in increasing the onset temperature of luminescence quenching.

6.6 Summary

Fundamental understanding of the excitation and de-excitation of erbium in CVD-grown films has been achieved. Although the UHV-MOCVD growth was designed to incorporate high concentrations of erbium with large effective optical cross-section, problems due to precursor fragmentation have arisen. The wafer located further upstream (closest to the gas inlet) does reach erbium concentrations above $10^{20}/cm^3$, but the erbium is ligand-starved and, as such, has a low effective optical cross-section of 9.4×10^{-19} cm^2. Wafers located downstream have a higher ligand to erbium ratio and effective optical cross-section (4.5×10^{-16} cm^2), but the erbium concentration is reduced by over two orders of magnitude. More work will be needed to determine if this problem is inherent in hot-wall MOCVD growth.

Erbium-doped films grown by CVD could not be saturated at the highest laser power of 1.5 W while silicon implanted with erbium was already saturated at 0.1 W. As the intensity of erbium luminescence at 4 K was greater in the CVD films and since the erbium concentration was similar in some CVD and implanted samples, the difference in saturation must be caused by greater optical activity, or larger optical cross-section. Corresponding to the larger effective optical cross-section was an increase in the internal quantum efficiency of CVD-grown samples over the implanted samples.

The temperature dependence of the intensity of erbium luminescence clearly showed that the quenching mechanisms in CVD-grown films were different from implanted samples. The CVD films exhibited a faster loss of intensity at low temperatures (4 to 150 K) than implanted samples, but the trend was reversed above 150 K. The activation energy for temperature quench-

ing of Si:Er and $Si_{0.9}Ge_{0.1}$ were 70 and 80 meV respectively with error bars of approximately 30 meV, as compared to an activation energy of 150 meV for the implanted material. The difference in activation energy between the Si and $Si_{0.9}Ge_{0.1}$ samples could not be attributed to differences in the band structure as that would favor the $Si_{0.9}Ge_{0.1}$sample having a lower activation energy. Lifetime measurements of the decay of the luminescence of erbium were taken at 4 K to gain some insight into the difference in quenching among the samples. A short, nonradiative lifetime component was observed in Si:Er and $Si_{0.9}Ge_{0.1}$:Er grown by CVD but not in the implanted sample, although it too showed the onset of the short lifetime at 15-30 K. A significant difference of the short lifetime component between the Si and $Si_{0.9}Ge_{0.1}$ sample was modeled by assuming an Auger backtrasfer process which was a function of the bandgap. This model predicted a short lifetime in the $Si_{0.9}Ge_{0.1}$ sample which was 77% that in the Si sample. As the short lifetime was actually long in the $Si_{0.9}Ge_{0.1}$ sample, a bandgap dependent Auger process was ruled out. Deep level transient spectroscopy (DLTS) work should be done to determine if defect states in the bandgap might be responsible for this behavior.

Chapter 7

Achievements and Future Work

In an effort to improve the quantum efficiency and output power of erbium-doped silicon-based materials, a low temperature, low damage growth method has been explored. A hot-walled UHV-MOCVD reactor was constructed for the growth of Si:Er and $Si_{1-x}Ge_x$:Er films at temperatures approximately 200-300°C below the maximum temperature used in the implantation process. Calibration of growth rates and concentrations were made at several temperatures before erbium-doped films were grown. The quality of undoped films were found to be comparable to the best competing grow techniques. The FWHM of the $Si_{1-x}Ge_x$ quantum well structure (5.9 meV) and Pendellösung fringes in x-ray diffraction rocking curves were presented as evidence of this.

Most of the goals set at the beginning of the thesis for erbium have been achieved. Metastable erbium concentrations as high as $2\times10^{21}/cm^3$ have been obtained in high quality material. The CVD- grown films have shown a higher quantum efficiency and effective optical cross-section than the best implanted samples at 4 K, as well as marginally higher luminescence at room temperature. The world's first Si/$Si_{1-x}Ge_x$:Er double heterostructure has also been grown, which is the first step on the road for potential laser and LED applications. Throughout these growths, fundamental knowledge about the novel hot-wall MOCVD process has been gained which can be applied to other fields as well.

This work represents only an initial attempt to use CVD to produce device quality material, however, and has created more questions than it has answered. Although high quality erbium-doped films have been grown, the potential benefits expected from this technique have not yet

been realized. Indeed, they may never be without better control of the environment around erbium. This work clearly showed that none of the precursors studied provided the optimum conditions for erbium luminescence. A concerted effort has to made, therefore, in designing the precursor structure to achieve high ratios of ligand to erbium and yet maintain crystal quality. Based on the experiences with the three precursors in this study, some guidelines can be offered for what the precursor should look like. Complicated structures as found in the β-diketone family must be avoided due to the fragmentation and incorporation of inordinate amounts of oxygen and carbon. Unfortunately, these same fragments, which destroy film quality and minority carrier lifetime, increase the optical activity of erbium. This places a narrow window around the decomposition process for how much fragmentation is acceptable. Precursors with larger ligand coordination might increase this window since the undecomposed molecule would provide a more optically active erbium. This could be counter-productive with respect to a simpler molecule structure however.

There are two ways of avoiding going to more complex molecules to increase the ligand to erbium ratio. One would be to introduce oxygen or nitrogen into the gas stream in a form amenable to incorporation into the film. Since oxygen and silane react vigorously to form SiO_2 (sand), it would be wiser to concentrate on nitrogen in the short-term. Two possible sources for this would be to use nitrogen as the carrier gas for the precursor, or to dilute germane in nitrogen instead of argon. Both of these could be done at little additional cost. Another alternative would be to use a second precursor, which would decompose to yield a high concentration of ligands. In this way each molecule could be optimized for different purposes. The second precursor could be placed in a separate bubbler (very expensive) or pre-mixed with the erbium precursor if the chemistry allowed for it.

Although gaining control of the environment of erbium is the single most crucial step in improving the luminescence, device design can also be important in getting more light from erbium. The recent results in reversed-biased LEDs must be seriously considered as temperature quenching is not significant in these devices. Growth of devices of this type is straight-forward in CVD and offers several advantages over the SPE process. The erbium-doped films can be counter doped with boron to make thick, intrinsic films. This increases the volume which is able to be pumped since only erbium centers located in the depletion region can effectively give

off light. This factor alone could increase the EL by an order of magnitude since the depletion region is only approximately 100 Å in the SPE devices. As previously alluded to, the addition of germanium to build in a potential could also make a reversed-biased diode more practical is it could reduce the applied voltage needed to drive the device.

These issues pertain only to the light emitting devices, however, but a larger view is necessary if erbium is to be relevant in optoelectronics. Work on integration issues with waveguides and detectors needs to be accomplished needs to be done to test system-wide power requirements for erbium devices. The detector will be the limiting factor since absorption at 1.54 μm is difficult in silicon based materials ($Si_{1-x}Ge_x$ or $Si_{1-x-y}Ge_xC_y$). If erbium cannot provide the power at the detector necessary for 'error-free' operation, then other light emitters will have to be considered. The easiest of things to check is other rare-earths capable of emitting at shorter wavelengths. There are problems in this approach due to the de-excitation mechanism though. The larger the energy given off in the $4f$ transition, the more susceptible the center is to temperature quenching. This susceptibility is caused by a reduction in the number of phonons required to assist an electron into the rare-earth related defect state because more energy is supplied by the nonradiative decay. This might be avoided if reversed-biased excitation is used since temperature quenching is not as major an issue as in forward-biasing.

Bibliography

[1] P. Singer, Semiconductor International **5**, 88 (1996).

[2] H. Ennen, J. Schneider, G. Pomrenke, and A. Axmann, Appl. Phys. Lett. **43** 943 (1983).

[3] F.Y.G. Ren, J. Michel, Q. Sun-Paduano, B. Zheng, H. Kitagawa, D.C. Jacobson, J.M. Poate, and L.C. Kimerling, Mater. Res. Soc. Symp. Proc. **301**, 87 (1993).

[4] P.N. Favennec, H. L'Haridon, D. Moutonnet, M. Salvi and M. Gauneau, Jpn. J. Appl. Phys. **29**, L524 (1990).

[5] J. Michel, J.L. Benton, R.F. Ferrante, D.C. Jacobson, D.J. Eaglesham, E.A. Fitzgerald, Y.H. Xie, J.M. Poate, and L.C. Kimerling, J. Appl. Phys. **70**, 2672 (1991).

[6] H. Przybylinska, G. Hendorfer, M. Bruckner, L. Palmetshofer, and W. Jantsch, Appl. Phys. Lett. **66**, 490 (1995).

[7] A. Terrasi, G. Franzò, S. Coffa, F. Priolo, F. D'Acapito and S. Mobilio, Appl. Phys. Lett., **70**, 1712 (1997).

[8] D.L. Adler, D.C. Jacobson, D.J. Eaglesham, M.A. Marcus, J.L. Benton, J.M. Poate, and P.H. Citrin, Appl. Phys. Lett. **61**, 2181 (1992).

[9] L. Assali, F. Gan, and L.C. Kimerling, to be published.

[10] F. Priolo, G. Franzo, S. Coffa, A. Polman, S. Libertino, R. Barklie, and D. Carey, J. Appl. Phys. **78**, 3874 (1995).

[11] J.L. Benton, J. Michel, L.C. Kimerling, D.C. Jacobson, Y.H. Xie, D.J. Eaglesham, E.A. Fitzgerald, and J.M. Poate, J. Appl. Phys. **70**, 2667 (1991).

[12] B. Zheng, Ph.D. Thesis, Mass. Institute Tech. (1996).

[13] J. Palm, B. Zheng, F. Gan, J. Michel and L.C. Kimerling, to be published.

[14] J. Palm, F. Gan, B. Zheng, J. Michel, and L.C. Kimerling, Phys. Rev. B **54**, 17603 (1996).

[15] P.G. Kik, M.J.A. de Dood, K. Kikoin, and A. Polman, Appl. Phys. Lett. **70**, 1721 (1997).

[16] A. Taguchi, K. Takahei, and Y. Horikoshi, J. Appl. Phys. **76**, 7288 (1994).

[17] G. Franzò, S. Coffa, F. Priolo, and C. Spinella, J. Appl. Phys. **81**, 2784 (1997).

[18] Y.H. Xie, E.A. Fitzgerald, and Y.J. Mii, J. Appl. Phys. **70**, 3223 (1991).

[19] D.J. Eaglesham, J. Michel, E.A. Fitzgerald, D.C. Jacobson, J.M. Poate, J.L. Benton, A. Polman, Y.H. Xie, and L.C. Kimerling, Appl. Phys. Lett. **58**, 2797 (1991).

[20] Y.S. Tang, Z. Jingping, K.C. Heasman, and B.J. Sealy, Solid State Comm. **72**, 991 (1989).

[21] A. Polman, J.S. Custer, E. Snoeks, and G.N. van den Hoven, Appl. Phys. Lett. **62** 507 (1993).

[22] J.S. Custer, A. Polman, and H.M. van Pinxteren, J. Appl. Phys. **75**, 2809 (1994).

[23] P. Liu, J.P. Zhang, R.J. Wilson, G. Curello, S.S. Rao, and P.L.F. Hemment, Appl. Phys. Lett. **66**, 3158 (1995).

[24] H. Efeoglu, J.H. Evans, T.E. Jackman, B. Hamilton, D.C. Houghton, J.M. Langer, A.R. Peaker, D. Perovic, I. Poole, N. Ravel, P. Hamment, and C.W. Chan, Semicond. Sci. Technol. **8**, 236 (1993).

[25] R. Serna, M. Lohmeier, P.M. Zagwijn, E. Vlieg, and A. Polman, Appl. Phys. Lett. **66**, 1385 (1995).

[26] K. Miyashita, Y. Shiraki, D.C. Houghton, and S. Fukatsu, Appl. Phys. Lett. **67**, 235 (1995).

[27] D.B. Beach, R.T. Collins, F.K. Legoues, and J.O. Chu, Mat. Res. Soc. Symp. Proc. **282**, 397 (1992).

[28] J.L. Rogers, P.S. Andry, W.J. Varhue, E. Adams, M. Lavoie, and P.B. Klein, J. Appl. Phys. **78**, 6241 (1995).

[29] M. Matsuoka and S. Tohno, J. Appl. Phys. **78**, 2751 (1995).

[30] N.A. Sobolev, O.V. Alexandrov, B.N. Gresserov, G.M. Gusinskii, V.O. Naidenov, E.I. Shick, V.I. Stepanov, Yu. V. Vyzhigin, L.F. Chepik, and E.P. Troshina, Solid State Phenom. **32-33**, 83 (1993).

[31] A. Thilderkvist, J. Michel, S.-T. Ngiam, L.C. Kimerling, and K. Kolenbrander, Mat. Res. Soc. Symp. Proc. **405**, (1996).

[32] K. Nakashima, Mat. Res. Soc. Symp. Proc. **301**, 61 (1993).

[33] H.K. Kim, C.C. Li, X.M. Fang, J. Solomon, G. Nykolak, and P.C. Becker, Mat. Res. Soc. Symp. Proc. **301**, 55 (1993).

[34] N.A. Sobolev, M.S. Bresler, O.B. Gusev, E.I. Shek, M.I. Makoviichuk, and E.O. Parshin, Semicond. **28**, 1100 (1994).

[35] X. Duan, J. Palm, B. Zheng, M. Morse, J. Michel, and L.C. Kimerling, Mat. Res. Soc. Symp. Proc. **442**, 249 (1997).

[36] B. Zheng, J. Michel, F.Y.G. Ren, L.C. Kimerling, D.C. Jacobson, and J.M.Poate, Appl. Phys. Lett. **64**, 2842 (1994).

[37] S. Coffa, F. Priolo, G. Franzò, V. Bellani, A. Carnera, and C. Spinella, Phys. Rev. B **48**, 11782 (1993).

[38] G. Franzò, F. Priolo, S. Coffa, A. Polman, A. Carnera, Appl. Phys. Lett. **64**, 2235 (1994).

[39] R. Serna, J.H. Shin, M. Lohmeier, E. Vlieg, A. Polman, and P.F.A. Alkemade, J. Appl. Phys. **79**, 2658 (1996).

[40] M. Tamura and T. Suzuki, Nucl. Instrum. Methods B **39**, 318 (1989).

[41] J. Stimmer, A. Reittinger, G. Absteiter, H. Holzbrecher, and C. Buchal, Mat. Res. Soc. Symp. Proc., to be published.

[42] J. Stimmer, A. Reittinger, J.F. Nutzel, G. Absteiter, H. Holzbrecher, and C. Buchal, Appl. Phys. Lett., to be published.

[43] M. Matsuoka and S.-i. Tohno, J. Vac. Sci. Technol. A, **13**, 305 (1995).

[44] M. Matsuoka and S.-i. Tohno, Appl. Phys. Lett., **66**, 1862 (1995).

[45] P.S. Andry, W.J. Varhue, F. Ladipo, K. Ahmed, E. Adams, M. Lavoie, P.B. Klein, R. Hengehold, and J. Hunter, J. Appl. Phys., to be published

[46] M.T. Morse, B. Zheng, J. Palm, X. Duan, and L.C. Kimerling, Mat. Res. Soc Symp Proc., to be published.

[47] D.L. Smith, *Thin-Film Deposition* (McGraw-Hill, New York, 1994).

[48] J.L. Rogers, P.S. Andry, W.J. Varhue, P. McGaughnea, E. Adams and R. Kontra, Appl. Phys. Lett. **67**, 971 (1995).

[49] H. Ennen, G. Pomrenke, A.Axmann, K. Eisele, W. Haydl, and J. Schneider, Appl. Phys. Lett. **46**, 381 (1985).

[50] B.S. Meyerson, F.K. LeGoues, T.N. Nguyen, D.L. Harame, Appl. Phys. Lett. **50**, 113 (1987).

[51] B.S.Meyerson,K .J. Uram, F. K. LeGoues, Appl. Phys. Lett. **53**, 2555 (1988).

[52] J.J. Lander and J. Morrison, J. Appl. Phys. **33**, 2080 (1962).

[53] G. Ghidini and F.W. Smith, J. Electrochem. Soc. **131**, 2924 (1984).

[54] F.W. Smith and G. Ghidini, J. Electrochem. Soc. **129**, 1300 (1982).

[55] H. M'saad, Ph.D. Thesis, Mass. Institute Tech. (1994).

[56] B.S. Meyerson, E. Ganin, D.A. Smith, T.N. Nguyen, J. Electrochem. Soc.**133** 1232 (1986).

[57] S.M. Sze, *VLSI Technology* (McGraw-Hill, New York, 1988).

[58] R. People, J.C. Bean, Appl. Phys. Lett. **48**, 538 (1986).

[59] C. Van de Walle, R.M. Martin, Phys. Rev. B **34**, 5621 (1986).

[60] R.A. Soref, F. Namavar, J.P. Lorenzo, Optics Letters **15**, 270 (1990).

[61] J.C.G. de Sande, A. Rodríguez, T Rodríguez, Appl. Phys. Lett. **67**, 3402 (1995).

[62] P.M. Garone, V. Venkateraman, J.C. Sturm, IEEE Elect. Dev. Lett. **12**, 230 (1991).

[63] S.P. Voinigescu, K. Iniewski, R. Lisak, C.A. Salma, J.-P. Noél, D.C. Houghton, Solid-State Electronics **37**, 1491 (1994).

[64] S. Libertino, S. Coffa, G. Franzó, and F. Priolo, J. Appl. Phys. **78**, 3867 (1995).

[65] M. Liehr, C.M. Greenlief, E. Kaxiras, and M. Offenberg, Appl. Phys. Lett. **56**, 629 (1990).

[66] D.J. Robbins, J.L. Glasper, A.G. Cullis, and W.Y. Leong, J. Appl. Phys. **69**, 3729 (1991).

[67] J. Tersoff and F.K. LeGoues, Phys. Rev. B **72**, 3570 (1994).

[68] R.E. Sievers and J.E. Sadlowski, Science **201**, 217 (1978).

[69] A.C. Greenwald, W.S. Rees, and U.W. Lay, Mat. Res. Soc. Symp. Proc. **301**, 21 (1993).

[70] A.J. Neuhalfen, and B.W. Wessels, Appl. Phys. Lett. **59**, 2317 (1991).

[71] A.J. Neuhalfen, and B.W. Wessels, Appl. Phys. Lett. **60**, 2657 (1992).

[72] P.N. Favennec, H. L'Haridon, M. Salvi, D. Moutonnet, Y. Le Guillou, Electron. Lett. **25**, 718 (1989).

[73] S.-J. Chang, D.K. Nayak, and Y. Shiraki, Jpn. J. Appl. Phys. **34**, 5633 (1995).

[74] W.P. Gillin, Z. Jingping, and B.J. Sealy, Solid State Comm. **77**, 907 (1991).

[75] D.E. Jesson, S.J. Pennycook, J.-M. Baribeau, D.C. Houghton, Thin Solid Films **222**, 98 (1992).

[76] N. Ohtani, S.M. Mokler, M.H. Xie, J. Zhang, B.A. Joyce, Surface Science **284**, 305 (1993).

[77] M. Copel, R.M. Tromp, APL **58**, 2648 (1991).

[78] S. Lombardo, S.U. Campisano, G.N. van den Hoven, A. Cacciato, and A. Polman, Appl. Phys. Lett. **63**, 1942 (1993).

THESIS PROCESSING SLIP

FIXED FIELD: ill. ______ name ______

index ______ biblio ______

► COPIES: (Archives) Aero Dewey Eng Hum

Lindgren Music Rotch (Science)

TITLE VARIES: ►☐ ______

NAME VARIES: ►☐ ______

IMPRINT: (COPYRIGHT) ______

► COLLATION: 116l

► ADD. DEGREE: ______ ► DEPT.: ______

SUPERVISORS: ______

NOTES:

cat'r: date:

page: J171

► DEPT: Mat Sci & E

► YEAR: 1997 ► DEGREE: Ph.D.

► NAME: MORSE, Michael Ty